NOVA SCHOOL OF SCIENCE & TECHNOLOGY

DEPARTMENT OF CHEMISTRY

IN-SITU ELECTROPOLYMERIZATION FOR SMART LABEL APPLICATIONS

ELIN HOWARD

BSc in Materials Science and Engineering

DOCTORATE IN CHEMISTRY

NOVA University Lisbon
February, 2024

NOVA SCHOOL OF SCIENCE & TECHNOLOGY

DEPARTMENT OF CHEMISTRY

IN-SITU ELECTROPOLYMERIZATION FOR SMART LABEL APPLICATIONS

ELIN HOWARD

BSc in Materials Science and Engineering

Adviser: António Jorge Dias Parola
Full Professor, NOVA School of Science and Technology, NOVA University Lisbon

Co-advisers: César António Tonicha Laia
Assistant Professor, NOVA School of Science and Technology, NOVA University Lisbon

Carlos Alberto Pinheiro Baptista
Chief Technology Officer, Ynvisible

Examination Committee

Chair: João Carlos dos Santos Silva e Pereira Lima
Full Professor, NOVA School of Science and Technology, NOVA University Lisbon

Rapporteurs: Marco Schott
Expert Group Manager Electrochromic Systems, Fraunhofer Institute for Silicate Research ISC, Fraunhofer R&D Center for Electromobility, Germany

Jorge Manuel Ferreira Morgado
Full Professor, Instituto Superior Técnico, University of Lisbon

Members: João Carlos dos Santos Silva e Pereira de Lima
Full Professor, NOVA School of Science and Technology, NOVA University Lisbon

Cristina Maria Grade Coto da Silva Cordas
Principal Researcher, HyLab – Green Hydrogen Collaborative Laboratory

Clara Isabel Barbosa Rodrigues Pereira
Assistant Researcher, Faculty of Sciences, University of Porto

DOCTORATE IN CHEMISTRY

NOVA University Lisbon
February, 2024

In-Situ Electropolymerization for Smart Label Applications

This document was created with the (pdf/Xe/Lua)LaTeX processor and the NOVAthesis template (v7.1.7) [1].

Acknowledgements

First and foremost I would like to express my deepest appreciation to my supervisors Professor Jorge Parola, and Professor César Laia for their help, support, and guidance over the past years. They have consistently provided clear direction, prompted thoughtful scientific discussions, and encouraged me throughout the process. I would also like to express my gratitude to the other staff, researchers, and students at the Cultural Heritage and Responsive Materials group for being so welcoming, kind, and supportive during my time in Portugal. Muito obrigada!

There are many people at Ynvisible that I want to acknowledge for supporting me throughout the Ph.D. process. I need to give a very special thanks to my industrial supervisor Dr. Carlos Pinheiro. He is the reason that I chose to pursue a Ph.D., and for that, I am extremely grateful. I would also like to give a special thank you to my co-worker Fábio Leite for his collaboration, friendship, and exquisite taste in laboratory music. Thanks to Florian Forsbach, Miriam Sousa, and Piotr Wierzchowiec for their daily input and support at the office in Freiburg. Thank you to Philip Holgersson for the fruitful technical discussions. Thank you to Lúcia Gomes and José Marques for their production support. Thank you to Marco Alexandre for his input on my designs. And, thank you to Inês Henriques and Ramin Heydarpour for supporting my personal and career development.

I would also like to acknowledge the CHARISMA 2020 innovative training network (ITN), and the funding from the European Union (Grant Number: 814299). This project has provided a unique opportunity to live, work, and collaborate with a network of universities and companies across Europe. I would like to thank all of the other Ph.D. students in the program for the collaboration, adventure, and discussions: Hamed Pourkheirollah, Matin Forouzmehr, Maria Angela Spirache, Alberto Trevisan, Sunil Behera, Diem Lee, and Gianvito Romano. I would also like to acknowledge all of the other advisors and researchers involved in organizing and administrating the project.

This work received financial support from PT national funds (FCT/MCTES, Fundação para a Ciência e Tecnologia and Ministério da Ciência, Tecnologia e Ensino Superior) through the projects UIDB/50006/2020 and UIDP/50006/2020.

Thanks to João M. Lourenço for providing the novaThesis LaTex template [1].

Thanks to Dr. Anna Österholm, Dr. Eric Shen, Dr. Graham Collier, and Dr. John Reynolds for first introducing me to the field of electrochromics and academic research, and encouraging me to pursue a Ph.D. program.

Thank you to my family! In particular, my parents Siv and Robert who have given me unconditional support throughout this process. And finally, thanks to all of the friends who have made sure that the past years were filled with laughter and joy.

Abstract

This body of work explores a recently emerging subset of electrochromic devices (ECDs): namely irreversible electrochromic indicators. In contrast to conventional ECDs which produce a reversible color change in response to an applied voltage, irreversible electrochromic indicators generate a single permanent color change in response to an applied voltage. This format of irreversible electrochromic indicator is envisioned for use in a broad range of applications including healthcare, food packaging, logistics, and authenticity labeling. The approach taken herein to produce irreversible electrochromic indicators is *in situ* electropolymerization, where a polymer film is deposited inside of a pre-assembled solid-state ECD.

An initial study investigates the influence of a gel polymer electrolyte (GPE), which is commonly employed in ECDs, on the electrodeposition process. Potential step methods, and cyclic voltammetry performed in a 3-electrode cell show that the addition of an ethylene oxide (EO)-propylene oxide (PO)-allyl glycidyl ether (AGE) matrix lowers the potential for film formation during electropolymerization of 3,4-ethylenedioxythiophene (EDOT) by 0.1 V, compared to a similar liquid electrolyte. Furthermore, in a device, the gel matrix improves the coloration efficiency and the homogeneity of the color change. Several variations of irreversible electrochromic indicators are then reported and characterized for a range of different monomer precursors. Higher coloration efficiencies and lower activation potentials are achieved by using oligomers of EDOT and thiophene - however, this comes at the expense of long-term stability. Then, fine-tuning of the indicator color states is demonstrated via electropolymerizing mixtures of EDOT, anthracene, and pyrene to form multichromic copolymers. The culmination of the developments for the irreversible indicators is their integration into a flexible smart label prototype designed for temperature sensing in cold-chain applications. Here, printed supercapacitors (SCs) and a chemical thermal sensor to control current flow upon temperature change are successfully used to trigger irreversible indicators in a flexible printed circuit.

The final embodiment of this work investigates *in situ* electropolymerization as a simple manufacturing technique for fully printed reversible electrochromic devices. In this case, poly(3,4-ethylenedioxythiophene) (PEDOT) indicators are produced which can

achieve 100,000 cycles with a modest loss in performance.

Keywords: Electrochromism, Electrochromic Devices, Irreversible Electrochromism, Irreversible Indicator, Smart Labels, *in situ* Electropolymerization, poly(3,4-ethylenedioxythiophene), poly(thiophene)

Resumo

Este trabalho explora um novo subconjunto de dispositivos electrocrómicos (ECDs): nomeadamente indicadores eletrocrómicos irreversíveis. Ao contrário de ECDs convencionais que produzem uma mudança de cor reversível em resposta à aplicação de um estímulo elétrico, os indicadores electrocrómicos irreversíveis geram uma mudança de cor permanente. Este novo tipo de indicador electrocrómico irreversível foi desenvolvido para uma ampla gama de aplicações, incluindo aplicações médicas, embalagem alimentar, logística e transporte e verificação de autenticidade de produtos. A abordagem adoptada neste trabalho para desenvolver indicadores electrómicos irreversíveis é a electropolimerização *in situ*, onde um filme polimérico é depositado dentro de um ECD de estado sólido.

Numa primeira abordagem foi investigado a influência de um gel electrólito polimérico (GPE), usado tipicamente em ECDs, no processo de electrodeposição. Métodos de cronoamperometria e voltametria cíclica realizados numa célula de 3 elétrodos mostram que a adição de uma matriz polímerica do polímero EO-PO-AGE reduz o potencial de formação do filme durante a electropolimerização de EDOT em 0,1 V em comparação com um eletrólito equivalente líquido. Além disso, em dispositivos, o gel eletrólito polimérico melhora a eficiência de coloração e a homogeneidade da mudança de cor. Diversas variações de indicadores electrocrómicos irreversíveis foram exploradas e caracterizadas para uma variedade de diferentes monómeros. Maiores eficiências de coloração e menores potenciais de ativação são alcançados usando oligómeros de EDOT e tiofeno, no entanto, tal ocorre às custas da estabilidade a longo prazo. Em seguida, o ajuste fino dos estados de cor do indicador é demonstrado através de misturas de electropolimerização de EDOT, antraceno e pireno para formar copolímeros multicrómicos. O desenvolvimento dos indicadores irreversíveis neste trabalho culmina na sua demonstração num trabalho de integração num protótipo flexível de uma etiqueta inteligente concebida para a detecção de temperatura em aplicações de transporte de frio. Neste demonstrador supercondensadores impressos e um sensor térmico químico foram usados com sucesso para ativar indicadores irreversíveis num circuito impresso flexível.

A concretização final deste trabalho explora a electrodeposição *in situ* como uma técnica simples de fabricação de dispositivos eletrocrómicos reversíveis impressos. Neste

trabalho, são produzidos indicadores PEDOT que podem atingir 100.000 ciclos com perda mínima de desempenho

---

Palavras-chave: Electrocromismo, Dispositivos Electrocrómicos, Eletrocromismo Irreversível, Indicador Irreversível, Etiqueta Inteligente, Eletropolimerização *in situ*, poli(3,4-etilenodioxitiofeno), poli(tiofeno)

Contents

List of Figures

List of Tables

Acronyms

ACN	acetonitrile *(pp. 49, 52, 53)*
AGE	allyl glycidyl ether *(pp. v, 39, 99)*
AZO	aluminum-doped zinc oxide *(p. 13)*
BFEE	boron trifluoride diethyl etherate *(p. 49)*
biEDOT	2,2'-bis(3,4-ethylenedioxythiophene) *(pp. 45–47, 56, 61, 64–66, 70, 75, 76, 82, 100)*
bithiophene	2,2-bithiophene *(pp. 45–48, 61, 64–66, 75, 76, 100)*
CE	coloration efficiency *(pp. 22, 23, 44, 46, 47, 56, 63, 76, 82, 99, 100)*
CV	cyclic voltammetry *(pp. 31, 32, 46, 50, 53, 57)*
DCM	dichloromethane *(pp. 52, 53)*
$\mathbf{E_a}$	activation potential *(pp. 44, 46, 56, 76, 82, 100)*
$\mathbf{E_g}$	band gap *(p. 6)*
EC	ethylene carbonate *(pp. 15, 16, 31, 40, 57, 70, 71, 82, 83, 96)*
ECD	electrochromic device *(pp. v, 4, 10–13, 18–23, 26, 30, 60, 86, 91, 96)*
ECP	electrochromic polymer *(pp. 7–9, 13, 14, 18, 19, 24, 25)*
EDOT	3,4-ethylenedioxythiophene *(pp. v, 5, 8, 9, 23, 24, 27, 30, 31, 33, 34, 39, 45–50, 52–56, 60–62, 64–66, 69, 70, 75, 76, 79, 80, 82, 86, 96, 97, 99, 100)*
EO	ethylene oxide *(pp. v, 39, 99)*
EPD	electrophoretic display *(p. 26)*
ESR	early stage researcher *(p. 27)*
FTO	fluorine-doped tin oxide *(p. 13)*
GPE	gel polymer electrolyte *(pp. v, 16, 27, 30, 40, 49, 50, 82, 83, 99)*

HALS hindered amine light stabilizer *(pp. 67, 69, 70)*
HDOR high-denisty oligomeric region *(p. 9)*
HOMO highest occupied molecular orbital *(p. 6)*

IoT internet of things *(pp. 1, 2, 74)*
IRO industrial research objective *(p. 27)*
ITN innovative training network *(pp. iii, 27, 75)*
ITO indium-doped tin oxide *(pp. 13, 14, 31, 36, 39, 40, 50, 53–55, 57, 58, 62, 64, 68, 70, 71, 82, 87, 90–92, 95, 99)*

LCD liquid crystal display *(p. 26)*
LED light emitting diode *(p. 26)*
LUMO lowest unoccupied molecular orbital *(p. 6)*

MCCP minimally coloring changing polymer *(p. 14)*
MW molecular weight *(p. 96)*

NFC near-field communication *(pp. 1, 4, 26, 74, 86)*

OCP open circuit potential *(p. 47)*

PC propylene carbonate *(pp. 15, 16, 31, 40, 49, 57, 70, 71, 82, 83, 92, 96)*
PEDOT poly(3,4-ethylenedioxythiophene) *(pp. v, 7, 14, 23, 31, 36, 40, 45, 54, 62, 86, 88–92, 94–96)*
PEDOT:PSS poly(3,4-ethylenedioxythiophene):polystyrene sulfonate *(p. 14)*
PEG poly(ethylene-glycol) *(p. 30)*
PEN poly(ethylene napthalate *(p. 13)*
PEO polyethylene-oxide *(pp. 16, 17)*
PET poly(ethylene terephthalate) *(pp. 13, 24, 31, 36, 39, 40, 50, 53, 57, 62, 64, 68, 70, 71, 75, 78, 82, 86, 87, 99)*
PMMA polymethyl methacrylate *(pp. 17, 49)*
PO propylene oxide *(pp. v, 39, 99)*
PPO polypropylene-oxide *(p. 17)*
PProDOT-Me$_2$ poly(2,2-dimethyl-3,4-propylenedioxythiophene) *(p. 30)*
ProDOT poly(3,4-propylenedioxythiophene) *(pp. 8, 86)*
PV photovoltaic *(p. 4)*
PVA polyvinyl alcohol *(p. 17)*
PVdF polyvinylidene fluoride *(pp. 17, 96)*

RFID radio frequency identification *(pp. 1, 4, 26, 74, 86)*

RH relative humidity *(p. 72)*

SC supercapacitor *(pp. v, 74–76, 78–83, 100)*
SPE solid polymer electrolyte *(pp. 16, 17)*

TBAP tetrabutylammonium perchlorate *(p. 53)*
TCO transparent conducting oxide *(pp. 13, 14)*
terthiophene 2,2:5,2-Terthiophene *(pp. 45–48, 56, 61, 64–66, 70, 75, 76, 80, 82, 100)*
TFT thin-film transistor *(p. 4)*

UV ultra violet *(pp. 17, 47, 50, 54)*

1

Introduction

1.1 Smart Labels and the Internet of Things

The internet of things (IoT) is a vision for embedding technologies into our devices that can collect, transfer, and convey information. This connected system of physical devices can monitor data through smart sensors and communicate with other devices via the internet [2]. The goal is to simplify day-to-day activities, improve efficiency, and create a world that is both interactive and responsive to the user [3], [4]. Broad adoption of IoT technologies promises to deliver a seamless human-machine interface. However, this vision depends on further technical innovation in several different fields.

One embodiment of the IoT with significant market potential is smart or intelligent labels. A smart label is a label that extends its functionality beyond a graphical print by embedding technologies that can track, transmit, and display information. Examples of these technologies include radio frequency identification (RFID) tags, near-field communication (NFC) tags, sensors, and displays. The demand for smart label technology cuts across many sectors including retail, healthcare, pharmaceuticals [5], cold chain [6], transportation, and logistics [7]. The ability to track an object throughout its commodity chain can lead to improvements in speed, efficiency, and product quality [3]. One market research report estimates the market size for smart labels to be approximately 13.47 billion USD in 2023 [8], with different market research reports estimating compound annual growth rates between 15.8 and 17.3 % [8]–[11].

Figure 1.1 illustrates how functionality can be introduced to a temperature and time-sensitive label through the addition of successive components. In the conventional embodiment, a graphical print simply conveys the environmental restrictions to the user. By adding elements such as a QR code, or an NFC tag, the user can scan the label to access dynamic information about the product. The key benefit here is that more information can be included than fits on the physical label, and the information can be updated over time. However, it requires that the user has a mobile device, and in some cases, the information may require an internet connection to access it.

Without electronics, smart labels primarily convey static information. By introducing

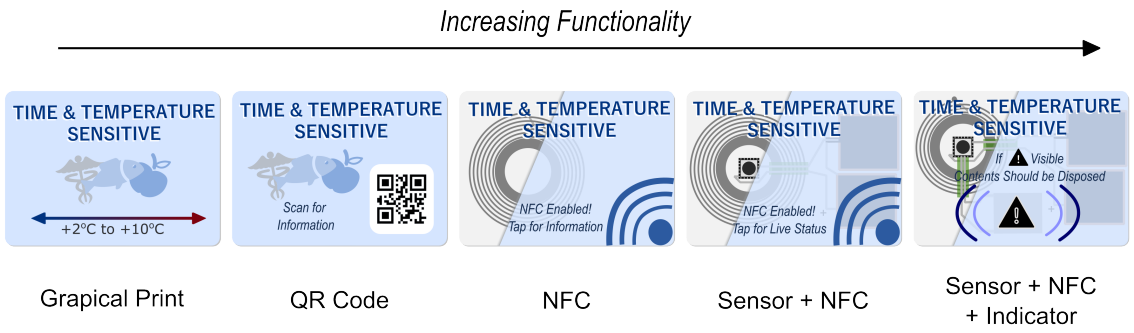

Figure 1.1: Schematic of labels for sensitive good tracking with increasing functionality.

electronic components, the smart labels can take on an active role, for example by monitoring the condition of the goods they are attached to [2]. In this case, the labels are used to track real-time changes in their local environments via sensors, and transmit that data via wireless communication. Types of sensors that can be integrated include temperature sensors, time sensors, mechanical sensors, chemical sensors, gas sensors, and biological sensors. Advanced smart labels can additionally include dynamic visual outputs, such as displays and indicators, to give visual alerts and information to the user without requiring intermediate data transfer technologies.

There are many applications where smart labels present a unique market opportunity. Some applications are summarized in Figure 1.2. In the food and beverage sector, smart labels can be used to track the freshness of products. In the healthcare and pharmaceutical sectors, smart labels can indicate the safety and status of medication. In the retail sector, smart labels can be used to dynamically change pricing based on real-time shopping analytics, or as anti-counterfeiting measures. In the supply chain, logistics, and transportation sectors, smart labels can track environmental conditions and alert breaches in them.

There is however a trade-off between functionality and cost. At the moment, connected and electronic smart labels are substantially more expensive than graphic print alternatives and are not yet economical to integrate for all the previously mentioned applications [12]. For the vision of the IoT and the subsection of smart labels to be successful, the electronic components should be low-cost, lightweight, thin, flexible, low-waste, and efficient. The field of organic and printed electronics has the potential to address many of these demands.

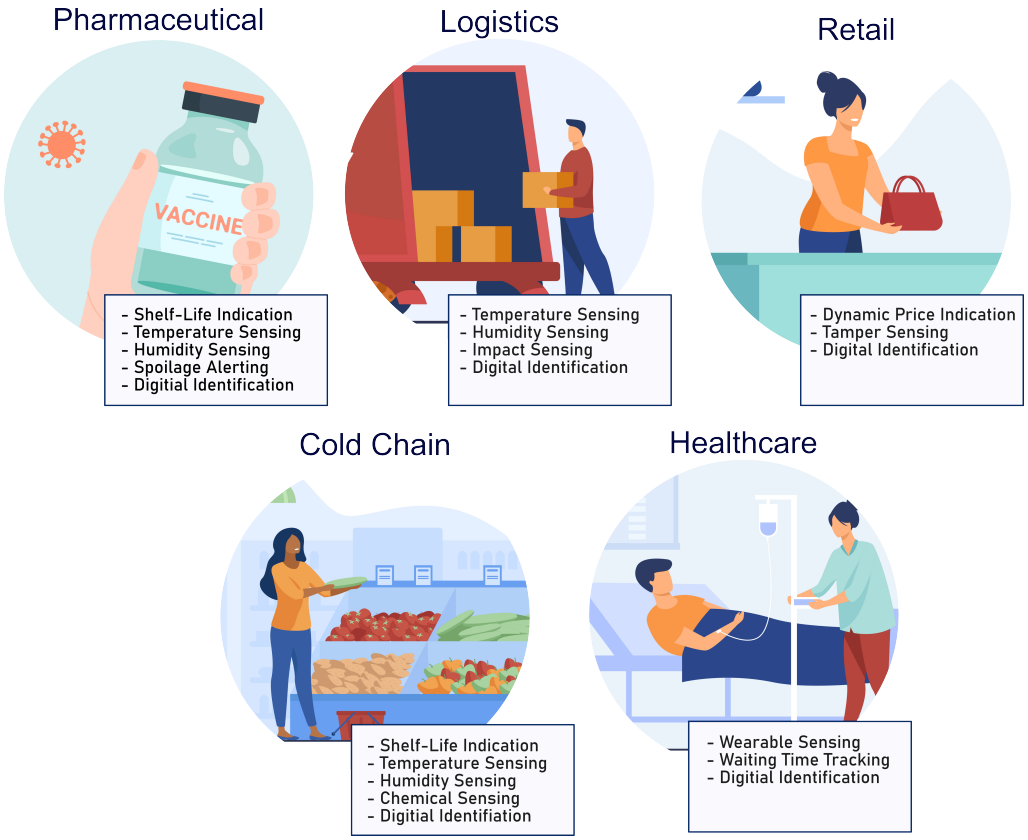

Figure 1.2: Schematic showing sectors where smart labels could be implemented. This schematic has been created using assets from Freepik.com.

1.2 Organic, Flexible and Printed Electronics

Over the past decades, the field of organic and printed electronics has emerged as an alternative to silicon-based conventional electronics manufacturing. Printing is a process where designs, texts, and images are deposited on substrates in the form of inks. Industrial printing techniques have the vital advantages of being high volume, high throughput, and low-cost. The process is also entirely additive, making the practice simple and low-waste.

Printing electronics is in principle analogous to conventional graphical printing. The key difference for printed electronics is that conductive, semiconductive, and dielectric inks are used to create active and passive elements. Many of the same printing techniques that are used in graphical paper printing can also be used in electronic printing. These include screen printing, gravure printing, offset printing, flexographic printing, and inkjet printing. The substrate can be carried in sheets, which is common for low volume, high precision work, or in a roll format, which is more common for high throughput manufacturing.

Screen printing has been widely used in the field of printed electronics [13]. A schematic demonstrating the principles of screen printing is shown in Figure 1.3a. A screen is stretched tightly across a frame and a pattern is removed from a polymer emulsion coating. The substrate is mounted below the screen, ink is added onto the

screen, and finally, a squeegee is pulled across the screen. This pushes the ink through openings in the screen, creating the desired pattern on the substrate. The properties of the printed layer are determined by many parameters in the process including the mesh count of the screen, the screen thickness, the screen tension, the squeegee pressure, the squeegee hardness, and the printing speed. Figure 1.3b shows rotary screen printing of silver ink onto flexible ECDs. Based on these techniques, researchers and industry have produced printed versions of many types of electronics including thin-film transistors (TFTs) [14], photovoltaics (PVs) [15], RFID tags [16], NFC tags, sensors [17]–[19], batteries [20]–[22], and displays [23], [24].

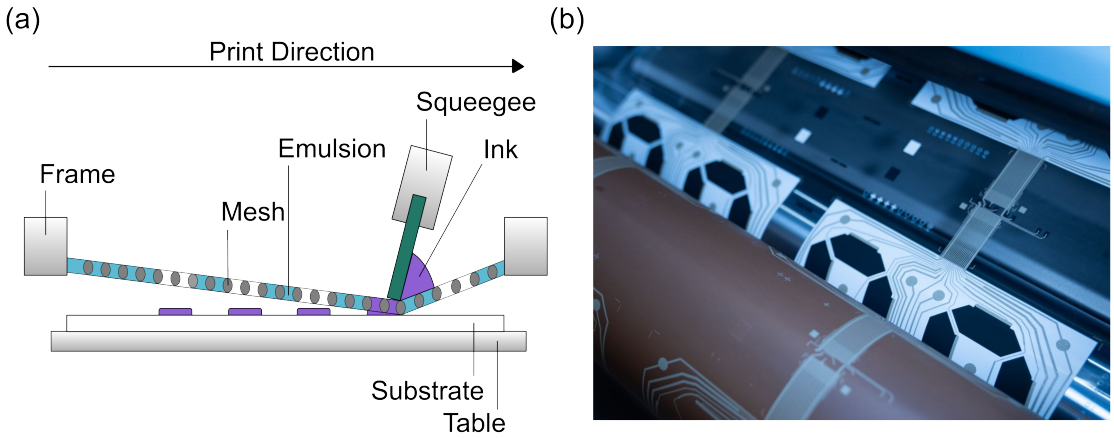

Figure 1.3: (a) Schematic showing the principles of screen printing, and (b) image of rotary screen printing of silver conductors onto a flexible display at Ynvisible Manufacturing in Linkoping, Sweden.

The development of functional inks is crucial for advancements in the field of printed electronics. Conductive inks are required to make electrical contacts and electrodes in components and are generally based on metals such as silver, gold, copper, and aluminum, carbon-based materials such as nanotubes or graphene, or conductive polymers [25]–[27]. Dielectric inks are required to insulate materials in the components or make capacitive elements and are typically composed of organic polymers, ceramics, or other insulating materials [25]. Semiconducting inks typically form the active layer of the electronics and are commonly formulated from metal oxides, carbon nanotubes, and conjugated polymer blends [25], [27], [28]. The rapid advancement in the field of printed electronics is evidenced by the number of companies that have developed commercial inks for this purpose [2]. Henkel, DuPont, AGFA, Heraeus, Saralon, Voltera, n-ink, Altana, Printed Electronics, INX, and SunChemical are just some examples of companies that now carry product lines for functional inks.

Despite these advancements, the performance and lifetime stability of printed and organic electronics components lag behind their non-printed silicon-based counterparts.

This is due to limitations in the electrical properties and environmental stability of the printable inks, as well as the resolution that can be achieved using high-volume printing lines [29]–[31]. The 9th Roadmap Whitepaper from the Organic and Printed Electronics Association, a leading industry association, also identifies manufacturing speed, limited item size, integrated hardware, and the limited number of approved materials as ongoing barriers to printed electronics [2]. The broad implementation of organic and printed electronics will require further research, development, and innovation to address these challenges.

1.3 Conjugated Polymers

1.3.1 Fundamental Concepts and Structure

Conjugated polymers are macromolecular systems defined by their backbones of alternating double and single bonds. The overlapping π orbitals create a system of delocalized electrons across the molecule, enabling them to conduct charge [32]. This makes them a fascinating material to study, as they have the potential to combine the electronic properties of metals and semiconductors, with the processing and mechanical properties of plastics. They have been a central feature of the developments in the field of printed and organic electronics, discussed in the previous section.

Research on conjugated polymers began in the 1950s and 1960s with poly(aniline) and poly(pyrrole), however, the field only received widespread attention when the 2000 Nobel Prize in Chemistry was awarded to Allan Heeger, Alan MacDiarmid, and Hideki Shirakawa for their work on halogen doped poly(acetylene) [33]–[36]. Since then, researchers have synthesized conjugated polymers based on many other monomer units and derivatives, including thiophenes, pyrroles, anilines, and EDOTs. Figure 1.4 shows the chemical structures of some common conjugated polymers.

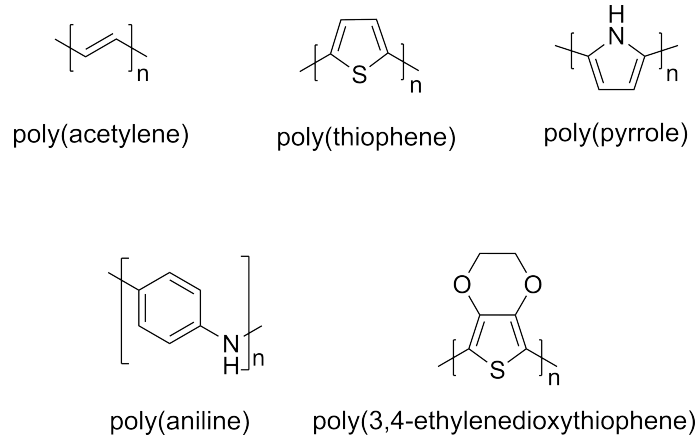

Figure 1.4: Chemical structure of some common conjugated polymers.

Molecular properties are determined primarily by the excitations that have the lowest energy difference. In the case of conjugated polymers, this is the interactions of the π

electrons, because the difference between the energy states of the occupied π and unoccupied $\pi*$ orbitals are significantly smaller than between the occupied σ and unoccupied $\sigma*$ orbitals [37]. The band gap of a conjugated polymer is the difference between the energy state of the highest occupied molecular orbital (HOMO) and the lowest unoccupied molecular orbital (LUMO), or the energy range where there are no molecular orbitals. The band gap (E_g) will determine the intrinsic electronic properties of the material.

The origin of a band gap in conjugated polymers can be understood by considering a series of oligiothiophenes with increasing length, see Figure 1.5a, and 1.5b. With each successive thiophene ring that is added to the system, there is further hybridization and more discrete energy levels are added to the system. Eventually, there will be enough energy levels that they coalesce into bands referred to as the valence band and the conduction band [38], [39]. While passive commodity polymers, such as polyethylene, have band gaps > 5 eV, conjugated polymers typically present band gaps between 1-3 eV.

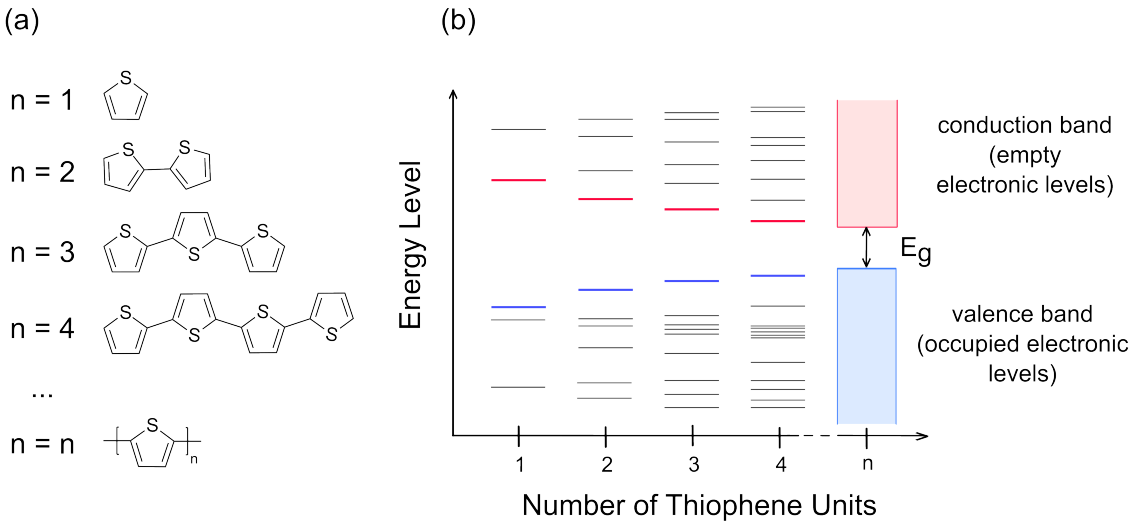

Figure 1.5: (a) Chemical structure of thiophene oligomers, (b) energy levels and band gap of thiophene oligomers with an increasing number of rings. Adapted from ref. [39].

1.3.2 Doping

Conjugation alone is not enough to make a polymer conductive. For a conjugated polymer to be conductive, there must be mobile charges in the system. The process of introducing charge, also referred to as 'doping', can be done electrochemically or chemically. Electron injection (reduction) will give an n-type semiconductor where electrons are the mobile charge carrier, and electron removal (oxidation) will give a p-type semiconductor where holes are the mobile charge carrier. Conjugated polymers, are typically p-type semiconductors that present higher conductivity upon oxidation [40].

The charging of the polymer chain leads to geometric reorganization. For aromatic structures, this can bring quinoid-like structure in the region of the charge, shortening the bonds between the monomer units as they take on more double bond-like character [41], [42]. For conjugated polymers, the oxidation process generally occurs in two steps. The removal of the first electron leads to the formation of a polaron, which is the combination of the charge and the local geometric distortion around the charge. Two polarons can become a single bipolaron if the energy that is gained in the reorganization of the chain is greater than the coulombic repulsion [43]. Figure 1.6a depicts the removal of electrons from a PEDOT chain to form polaronic and bipolaronic states. The energy levels of the polarons and bipolarons sit between the valence band and the conduction band, see Figure 1.6b [40].

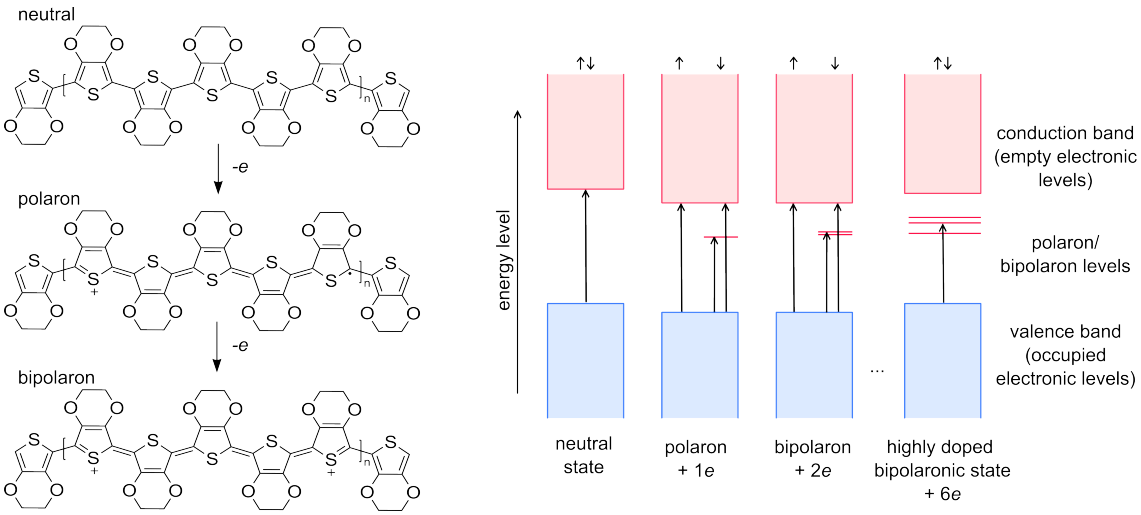

Figure 1.6: Neutral, polaronic, and bipolaronic states. Energy level diagram adapted from ref. [40].

1.3.3 Electrochromic Polymers

The unique bandgap and doping properties of conjugated polymers make them attractive for optoelectronic purposes, for example in electrochromics. Electrochromic polymers (ECPs) are polymers that exhibit a change in color in response to the application of an external bias. This behavior is a result of the introduction of new energy levels upon doping, which allows for lower-energy transitions.

Figure 1.7 shows spectroelectrochemical data for a PEDOT film. In the neutral state, PEDOT absorbs with a peak around 650 nm in the visible region [44]. As the film is electrochemically oxidized, the peak in the visible region decreases, and two new peaks in the infrared region appear, corresponding to the polaronic and bipolaronic states. This shift in the absorption spectra of PEDOT upon doping is observed by the viewer as a blue to transparent color change.

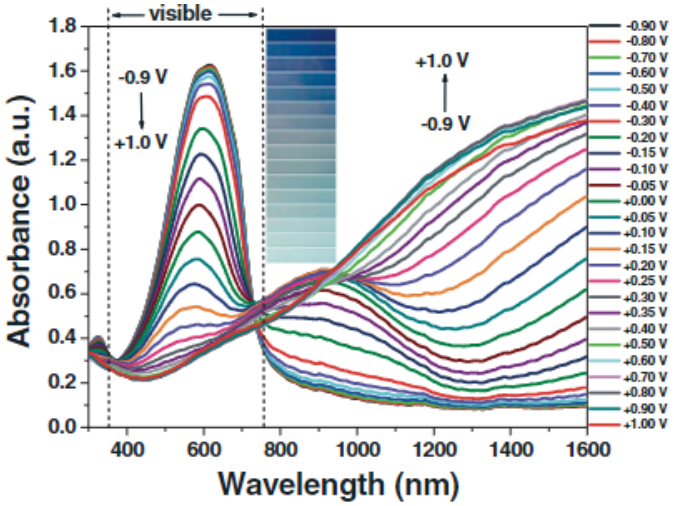

Figure 1.7: Spectroelectrochemistry of PEDOT. Reproduced with permission from ref. [44]. Copyright © 2004 WILEY-VCH Verlag GmbH & Co. KGaA, Weinheim.

Significant research in the field of ECPs has focused on synthesizing polymers that present different color transitions. Several tools can be employed to engineer the band gap, thereby tuning the color of ECPs. These include the incorporation of electron-poor and electron-rich moieties into the polymer backbone (donor-acceptor approach), limiting the conjugation length, controlling the backbone planarity, adjusting the bond length alternation, and creating copolymers with different monomer units [38], [45]. Using these approaches, researchers have synthesized electrochromic systems that span the visible color spectrum [46]. Figure 1.8 shows the chemical structure of several ECPs based on thiophene, EDOT, and poly(3,4-propylenedioxythiophene) (ProDOT) derivatives that have neutral states spanning across the visible region.

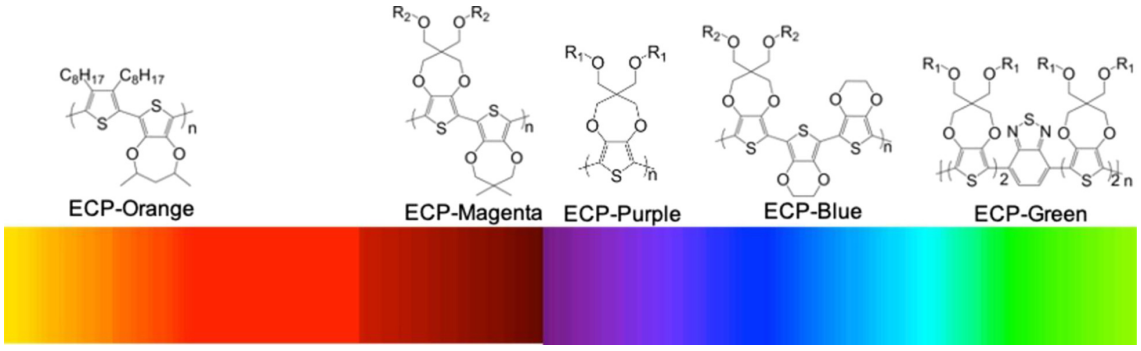

Figure 1.8: Structure of a series of ECPs with neutral state colors spanning the visible spectrum. Reproduced with permission from ref. [47]. Copyright © 2021 American Chemical Society.

1.3.4 Electropolymerization

While there are several synthetic routes to produce ECPs, electropolymerization, or anodic polymerization, is very attractive due to the high efficiency, speed, and simplicity of forming free-standing polymer films. In this route, a potential is simply applied to an electrochemical cell where the monomer species is solubilized. The earliest recorded electropolymerization dates back to 1882 with the electrodeposition of aniline by Letheby [48]. Since then, extensive studies have tested the effect of different monomers, solvents, salts, substrates, additives, and electrical protocols on the formation and properties of conjugated polymer films [49]–[59].

The precise mechanism for the electropolymerization reaction is still under debate, but the widely accepted theory is that the synthesis proceeds through the oxidation of the monomeric units to their radical cations, followed by subsequent cross-coupling steps that form radical cationic oligomers and polymers [60]. The overall reaction for the electropolymerization of EDOT is shown in Figure 1.9. For each monomer unit that cross-links, two electrons and two protons are removed to generate a final neutral polymer.

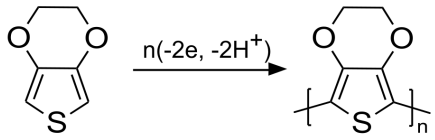

Figure 1.9: Overall reaction for electropolymerization of PEDOT.

Early investigations suggested that the mechanism followed a chain propagation reaction, whereby oligomer radicals continue to cross-couple with monomer radicals: i.e. monomer to dimer to trimer to tetramer, and so on [61]. However, more reccent studies have shown that it is more likely that the reaction proceeds with consecutive dimerization between oligomers of the same length [60], [62]: i.e. monomer to dimer to tetramer to octamer, and so on. This is due to the rapid decrease in the rate constants for the dimerization of the oligomeric species with growing chain length. While the rate constant for the dimerization of a thiophene radical cation monomer may be in the range of 10^9 M^{-1} s^{-1}, this decreases with increasing chain length, see Figure 1.10.

Models for the solid-state electrodeposition of conjugated polymer have been developed by monitoring the current response of the reaction. Generally the reaction proceeds by the successive oligomerization of monomer species in the diffusion layer at the vicinity of the electrode surface. The concentration of oligomers near the surface increases to create a high-denisty oligomeric region (HDOR). Further cross-linking leads to the deposition of insoluble polymer on the electrode surface via nucleation and growth processes. This is discussed in more detail in Chapter 2.

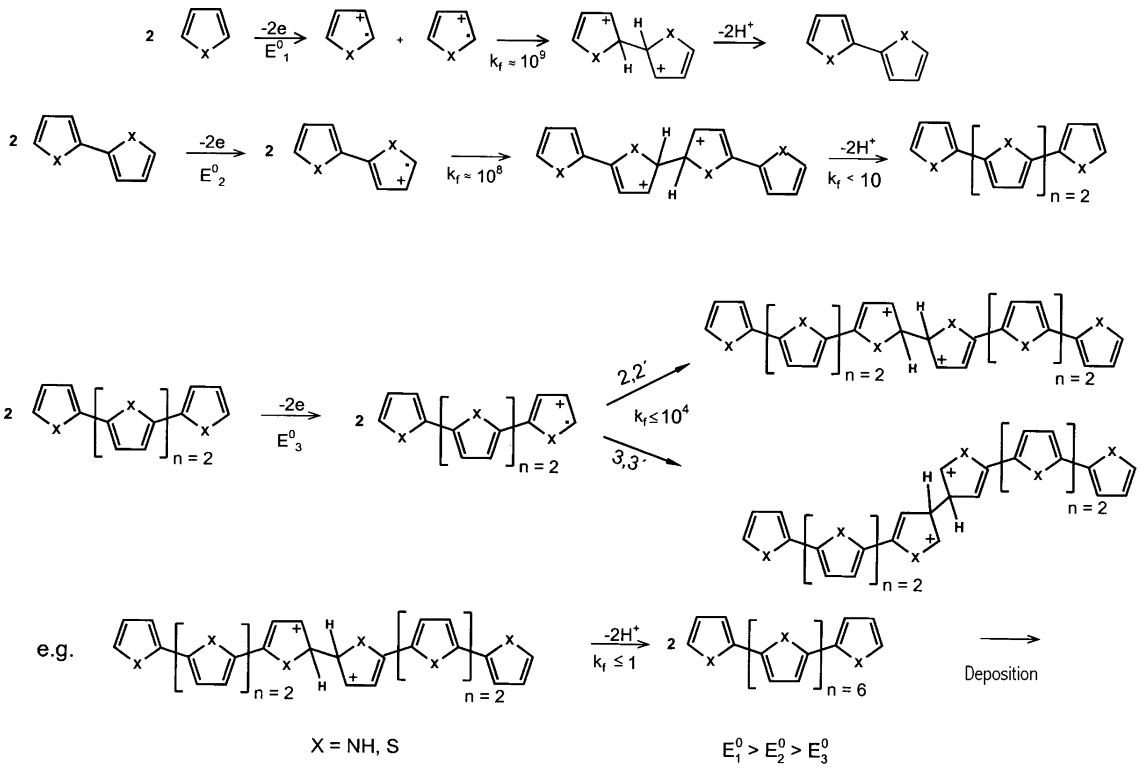

Figure 1.10: Inital steps of anodic electropolymerization of thiophene. Reproduced with permission from ref. [60]. Copyright © 2010 American Chemical Society.

1.4 Electrochromic Devices

1.4.1 Overview and Commercial Applications

When electrochromic materials are processed into devices they create structures that modulate light. There are several classes of electrochromic materials including metal oxides, viologens, conjugated polymers, metal coordination complexes, and metal hexacyanometallates [63]. ECDs generally fall into two categories: devices that operate in transmission mode, and devices that operate in reflection mode.

To date, the most successful commercial applications of ECDs have been as smart windows and mirrors for architectural and automobile sectors [64]. Responsive mirrors and windows can dynamically change their tint and have the potential to reduce energy usage, improve thermal control, create privacy screens, and generally allow for control of an indoor lighting environment [65]. Figure 1.11 shows commercial examples of electrochromic mirrors and windows. Gentex produces dimmable and self-dimmable windows and mirrors for automotive applications, and electronically dimmable windows for aerospace applications [66]. For example, Gentex electronically dimming mirrors were implemented in the Boeing 787 Dreamliner [67]. Other commercial developers of electrochromic glass include SageGlass, View, Inc., and Chromogenics [9], [68], [69].

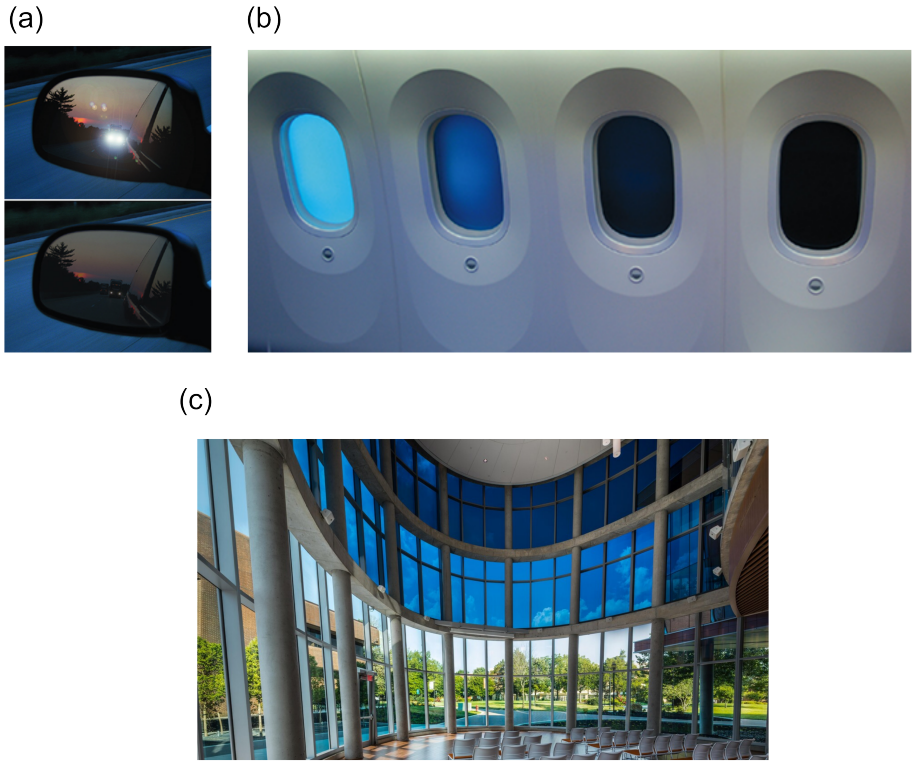

.

Figure 1.11: Commerical examples of ECDs in the form of an (a) electrochromic rear-view automobile windows from Gentex Corportation, (b) electrochromic dimming aircraft windows in a Boeing 787 Dreamliner by Gentex Corportation, and (c)window installations at Bowie University from SageGlass.

An emerging area for the application of ECDs is for displays. They are attractive due to their low power consumption, fast switching speeds, high angle-independent contrast, and ability to use flexible and thin materials [64]. Advancements in the field of printed electronics have made it possible to produce electrochromic displays using high-volume, commercial production techniques, such as screen printing [13], [24], [70], [71]. ECDs have the potential to address a broad variety of markets such as digital signage, advertising, wearables, mobile communicators, e-paper, and interfaces for smart label technologies and platforms [24], [47], [64], [70], [72], [73]. Figure 1.12 shows e-paper type reflective electrochromic devices for digital signage and smart label applications from Ynvisble and from RISE Research Institutes of Sweden [70], [74].

Figure 1.12: Commercial concepts of e-paper type ECDs in the form of (a) a logistics smart label from Ynvisible (b) a flexible pharmaceutical smart label from RISE Research Institutes of Sweden reproduced with permission from ref. [74], and (c) digital signage from Ynvisible.

1.4.2 Structure

There are several layers required to create a functional ECD stack. This includes substrates, conductive layers, an electrochromic layer, a charge storage layer, and an electrolyte layer. Figure 1.13 shows a schematic of the layers in an ECD. The final optical output of ECDs is also influenced by factors such as the polymer processing, device structure, electrolyte media, and encapsulation [75]–[77]. Electrochromic materials and conjugated polymers have already been introduced in Section 1.3 and in Section 1.4.1. The following section will focus on the other key layers and materials that make up an electrochromic device.

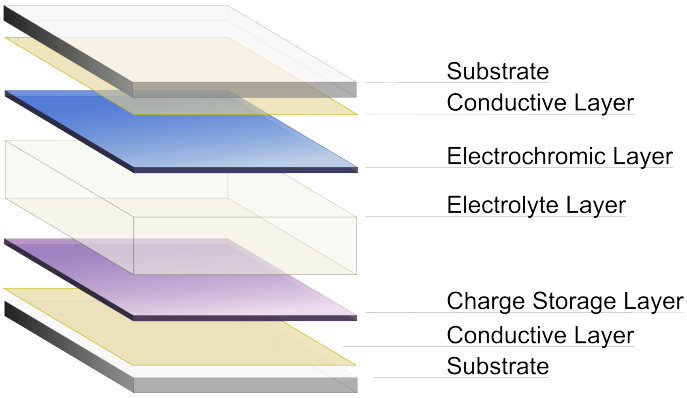

Figure 1.13: Schematic showing the structure and layers of an ECD.

1.4.3 Substrates

The substrates of ECDs can serve multiple functions. At a minimum, they are the base that the device is processed onto. But, they can also be critical to providing a barrier between the internal materials and the external environment during operation or giving the device its mechanical properties. Thus, the selection of an appropriate substrate depends heavily on the required durability, form factor, environmental stability, optical properties, and cost of the final ECD.

For transmissive ECDs both of the substrates on the device must be transparent. Glass and plastic films are the most popular choices at present. Glass has excellent optical transparency, durability, and availability. It also has a high barrier to both water and oxygen, protecting sensitive components within the stack. Many early commercial applications for ECDs such as windows and mirrors have utilized rigid glass substrates.

However, polymeric substrates have some key advantages, especially in terms of manufacturing. Their flexibility means that they can be used in high-volume roll-to-roll manufacturing lines. They are also lightweight, low-cost, and have reasonable transparency across the visible spectrum. The most common polymer substrates used in ECDs are poly(ethylene terephthalate) (PET), and poly(ethylene napthalate (PEN) [76]. Some key drawbacks for polymer substrates are degradation at high temperatures and high permeability to both oxygen and water. This limits the temperatures that can be used in the manufacturing, processing, and use of the ECDs. The barrier properties can be improved by the addition of commercial flexible barrier films, however, this has an associated cost [78]. For reflective devices, such as displays and mirrors, only one of the substrates needs to be transmissive. In this case, non-transparent substrates could be employed for one of the electrodes such as metal films, paper, and wood composites [24], [79].

1.4.4 Conductive Layers

A conductive layer is required in ECDs to provide electrical contact across the electrochromic film. Transparent conducting oxides (TCOs), typically wide-bandgap semiconductor oxides, have been employed in ECDs due to their high optical transparency and conductivity [80]. Several TCOs have been implemented for display applications including fluorine-doped tin oxide (FTO), ZnO, and aluminum-doped zinc oxide (AZO), however the most widely used is indium-doped tin oxide (ITO) due to its high optical transparency (> 80 %) and low sheet resistance ($< 10\ \Omega\ \mathrm{sq}^{-1}$) [47], [81]. However, the cost of ITO represents a significant proportion of the overall device cost, and there are risks in the supply chain due to the scarcity of indium [82], [83].

There are some alternatives to bypass the need for ITO and other TCOs in electrochromic devices. One method is by utilizing ECPs that have high intrinsic conductivities. There are several reports of using high-conductivity ECPs to serve as either the primary electrochromic film or as an underlying layer supporting a secondary electrochromic film

[84]–[89]. This has been mainly demonstrated with PEDOT derivatives, such as poly(3,4-ethylenedioxythiophene):polystyrene sulfonate (PEDOT:PSS), which have conductivities in the range of 10^3 S cm^{-1}. However, it has also been shown to work in small-area devices using ECPs with conductivities in the range of 0.1 - 1 S cm^{-1} [47]. The key drawback here is that the switching can be sluggish and non-uniform due to the voltage drop across the polymer film. As the ECP switches between its two states, a visual propagation front can be seen separating the high-conductivity and low-conductivity regions. This is sometimes referred to as a curtain effect and becomes more severe with increasing size of the working area. Other alternatives to TCOs are printed metal meshes, and carbon-based materials such as nanotubes and graphene [90]–[92].

1.4.5 Charge Storage Materials

As a redox reaction takes place to change the oxidation state of the electrochromic material on the working electrode, a simultaneous complementary redox reaction or capacitive charge storage mechanism must take place on the counter electrode. The material that undergoes this complimentary charge balancing reaction is the charge storage material. Several reports have shown the importance of a suitable charge storage material for long-term device stability [93]–[95]. The charge storage material should present long-term redox switching stability and should match the redox capacity of the electrochromic coloration reaction.

For transmissive devices, the charge storage material should either be transparent (such as minimally coloring changing polymers (MCCPs)) or have a complementary color transition (such as a cathodically coloring ECPs) to not compromise the overall optical output of the device. For reflective or non-transmissive devices the optical properties of the charge storage materials are not necessarily visible to the user so non-transmissive materials can be employed.

There are mixed reports on the use of ITO as a charge storage material for electrochromic devices. ITO does have some reversible redox capacity and several researchers have proposed and used it as a charge-balancing material in electrochromic devices [96]. However, prolonged cycling or exposure to low reductive potentials can lead to cathodic decomposition [95], [97], [98]. This is typically characterized by yellowing, browning, or the formation of a reflective coating in conjunction with an increase in sheet resistance and a decrease in redox capacity.

1.4.6 Electrolytes

The electrolytes used in electrochemical devices fulfill several purposes. Critically, they must provide ionic conductivity between the electrodes: neutralizing the local charge build-up at the electrode during redox processes. Electrolytes must be electrically insulating to avoid internal leakage between the electrodes. For some applications, electrolytes can also be used to provide spatial separation between the electrodes. The required chemical

and physical properties of the electrolyte depend on the specific application, nature of the electrochemical processes, electrode materials, and operating conditions. While electrolyte research has been heavily focused in the areas of battery and energy storage applications, many of the concepts and developments can be applied in the field of electrochromics. The following criteria are often used to evaluate the performance of an electrolyte: ionic conductivity, thermal stability, electrochemical stability, optical properties, mechanical properties, processability, cost, and toxicity.

Classical liquid electrolytes consist of dissociated ions (from salts, acids, or bases) in a solvent. Li^+ ions have been a very popular choice for electrochromic applications, but numerous other cations can be used, such as K^+, Na^+, and H^+ [99]. The best ion transport is achieved with solvents that have low viscosity, high dielectric constants, and are polar. The solvent should be able to complex at least one of the ions to achieve sufficient ionic transport. Figure 1.14 depicts the solvation of a Li^+ salt in an appropriately dissociating solvent.

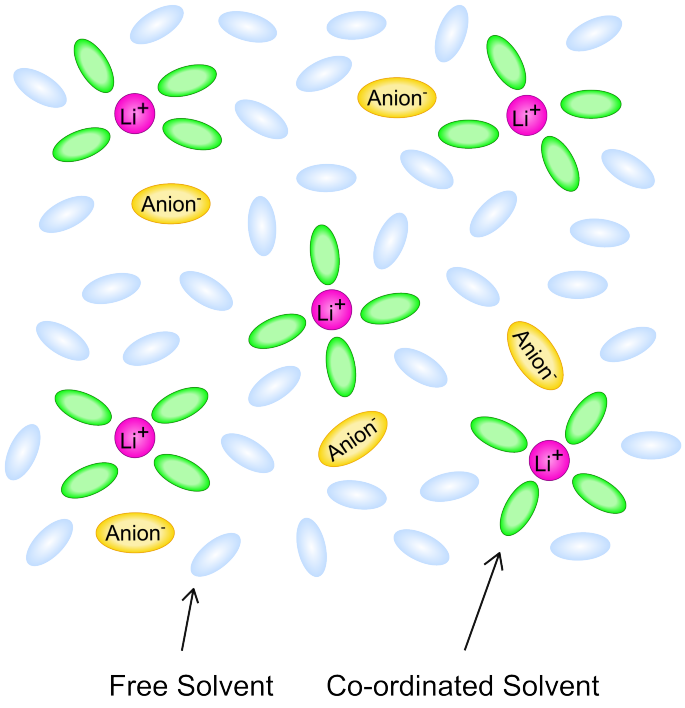

Figure 1.14: Schematic depicting the dissociation and co-ordination of a lithium salt in an electrolyte. Adapted from ref. [100].

Aqueous electrolytes present very high ionic conductivities (~0.8 S cm $^{-1}$ for aq. ~30 wt% Li_2SO_4 [101]). However, they are limited by their narrow voltage window. Therefore, high-dielectric aprotic organic solvents have been used to increase the stable voltage window of electrolytes. Cyclic organic carbonates such as ethylene carbonate (EC), and propylene carbonate (PC) have seen widespread use as they can easily dissolve lithium

salts and present good ionic conductivities (1.4 x 10^{-2} S cm $^{-1}$ for 1 M $LiClO_4$ in 1:1 EC/PC [102]). However, liquid electrolytes are often cited for safety concerns related to the flammability of organic solvents, limited mechanical support, and their inherent risk of leaking [103]. Thus, new classes of electrolytes such as solid polymer electrolytes, polymer gel electrolytes, ionic liquids, and composite electrolytes have been developed. Figure 1.15 gives a schematic representation of several classes of electrolytes.

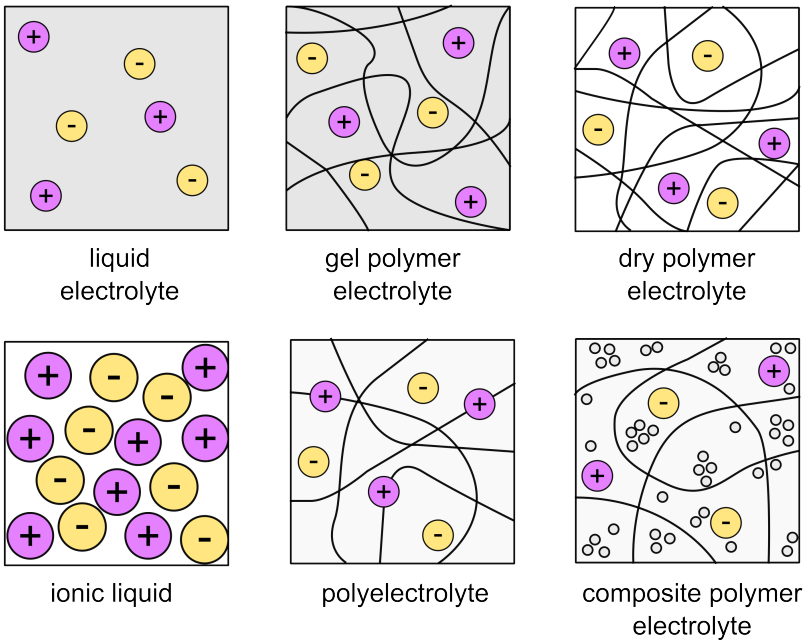

Figure 1.15: Types of electrolyte.

Solid polymer electrolytes (SPEs) replace the solvent used in liquid electrolyte with a solvating polymer. They present several advantages over liquid electrolytes such as reduced volatility, no possibility for leaks, and depending on the polymer they can be flexible, and have shock resistance. The solvating polymer should have sufficient donor power to complex the cations, enough flexibility to facilitate their movement, and an appropriate distance between the co-ordinating centers to allow hopping motion to take place [104]. Polyethylene-oxide (PEO) and its co-polymers have been widely studied in this regard. The ionic transport takes place primarily in the amorphous regions of the polymer, so strategies to improve the ionic conductivity have targeted reducing crystallinity and lowering the T_g [105]. However, the conductivities of SPEs are several orders of magnitude lower than liquid electrolytes (3.35 x 10^{-5} S cm $^{-1}$ for 15:85 $LiClO_4$ in PEO [106]).

GPEs are a three-phase system composed of a polymer network, inorganic salt, and low molecular weight solvent. They combine the properties of liquid electrolytes and dry polymer electrolytes. The polymer host imbues the material with mechanical stability and can limit the issue of leakage [107], [108]. Since the ions are transported primarily through the liquid phase they present higher ionic conductivities than dry polymer electrolytes. This also expands the number of polymers that can be used as a matrix since they do not

need to have the same electrical properties as those used in SPEs. In addition to PEO, other polymers such as polyvinylidene fluoride (PVdF), polypropylene-oxide (PPO), polyvinyl alcohol (PVA), polymethyl methacrylate (PMMA), and co-polymers have been used. The chemical structures of these polymers are shown in Figure 1.16.

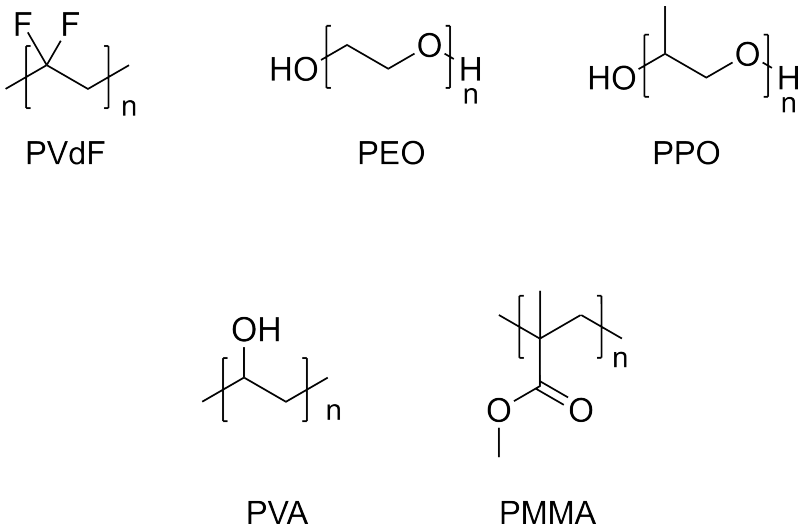

Figure 1.16: Some common polymers used for GPEs.

Cross-linked polymer networks can be generated by polymerizing chains with acrylates or vinyl monomers in addition to ultra violet (UV) photo-initiators. UV-cross linked polymer matrices are also interesting from a manufacturing perspective. The electrolyte can be coated or printed as a non-cured ink, and then gain mechanical stability after cross-linked under a UV lamp at a later stage in the manufacturing process.

Other interesting materials that have been developed and used for high-performance electrolytes are ionic liquids and polyelectrolytes. Ionic liquids are salts in the liquid phase at room temperature (T_m < 100 ^oC). They are attractive due to their non-flammability, chemical stability, and thermal stability [109], [110]. Polyelectrolytes, or single ion conductors, are polymer salts where one of the ionic species is chemically fixed to the polymer backbone. The charge-balancing ion is not chemically fixed to the polymer and free to move. Polyelectrolytes are particularly useful for applications where either the cationic or anionic species may have unwanted interactions with the electrodes [104], [111], [112].

Composite electrolytes refer to a class of electrolyte where inorganic filler materials have been added. This includes active fillers, which are themselves ion conductors, or passive materials in the form of inert oxides, such as TiO_2, SiO_2, and Al_2O_3 [113]–[115]. Their inclusion has the ability to improve room-temperature conductivity, mechanical stability, and electrolyte-electrode interface stability [115]. For electrochromic devices, ceramic fillers can also be used to change the optical properties of the layer, such as making it diffusely reflective and opaque. Although different classes of electrolytes have been addressed separately here, novel electrolytes can combine many of these materials as well as additives and rheology modifiers to tailor them for specific manufacturing

environments and applications.

1.4.7 Other Materials

In addition to the functional materials described above, additional structural layers and materials may be required for complex devices. This includes dielectrics, conductors, graphical layers, adhesives, and sealants.

1.5 Metrics for Evaluating Electrochromic Device Performance

1.5.1 Color

The perceived color of a material depends on the interplay between a light source, the object being viewed, and also the viewer. Light can interact with matter in a variety of ways, including absorption, reflection, scattering, and transmission, see Figure 1.17a. Depending on the nature of the material, these interactions contribute in different proportions. For an ECD the final color output will be the cumulative effect of how light is absorbed, reflected, scattered, and transmitted by each layer and interface in the stack.

Human vision can detect light in the range of approximately 380 - 780 nm. The longest wavelengths in this range are seen as red, and the shortest wavelengths in this range are seen as blue. The color of an ECP is the result of the absorption of light in the visible spectrum. If an ECP is illuminated with white light that spans the visible spectrum, then the observed color will be the complimentary color of what is absorbed, see Figure 1.17b. So, an ECP that absorbs blue light (435 nm - 480 nm) will appear yellow, and an ECP that absorbs orange light (595 nm - 650 nm) will appear blue.

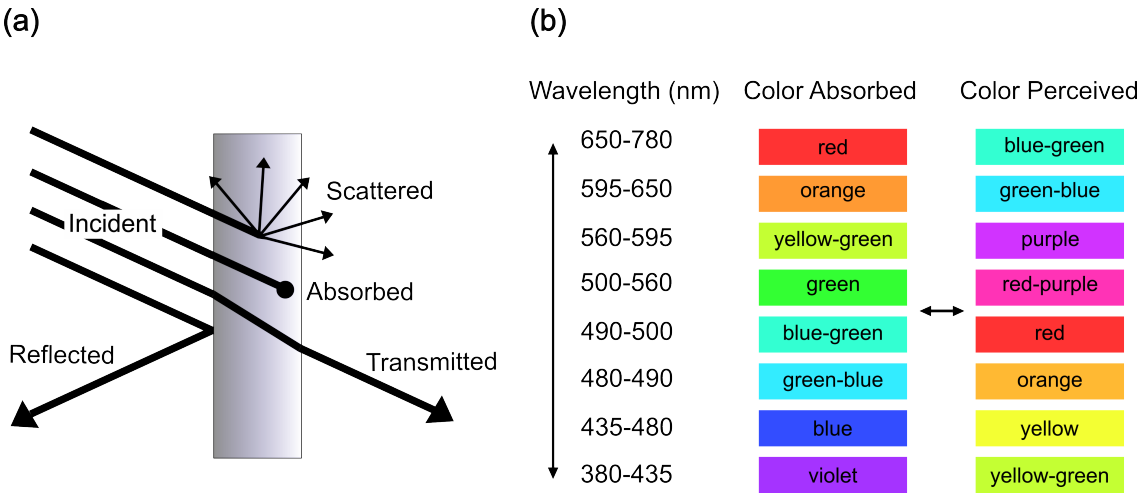

Figure 1.17: (a) Schematic showing the interactions of light with and object, and (b) depiction of the colors absorbed and the colors perceived for wavelengths of light in the visible spectrum.

Color systems allow us to quantify color perception systematically. The CIELAB 1976 L*a*b* color space is a widely adopted system in color sciences and in electrochromic research [116], [117]. It is represented in Figure 1.18. The L* value represents the lightness of the color. This ranges from black to white and is on a limited scale of 0 to 100. The a* and b* values both represent chromaticity, and there are no limits to their values. A positive a* value corresponds to red, a negative a* value corresponds to green, a positive b* value corresponds to yellow, and a negative b* value corresponds to blue.

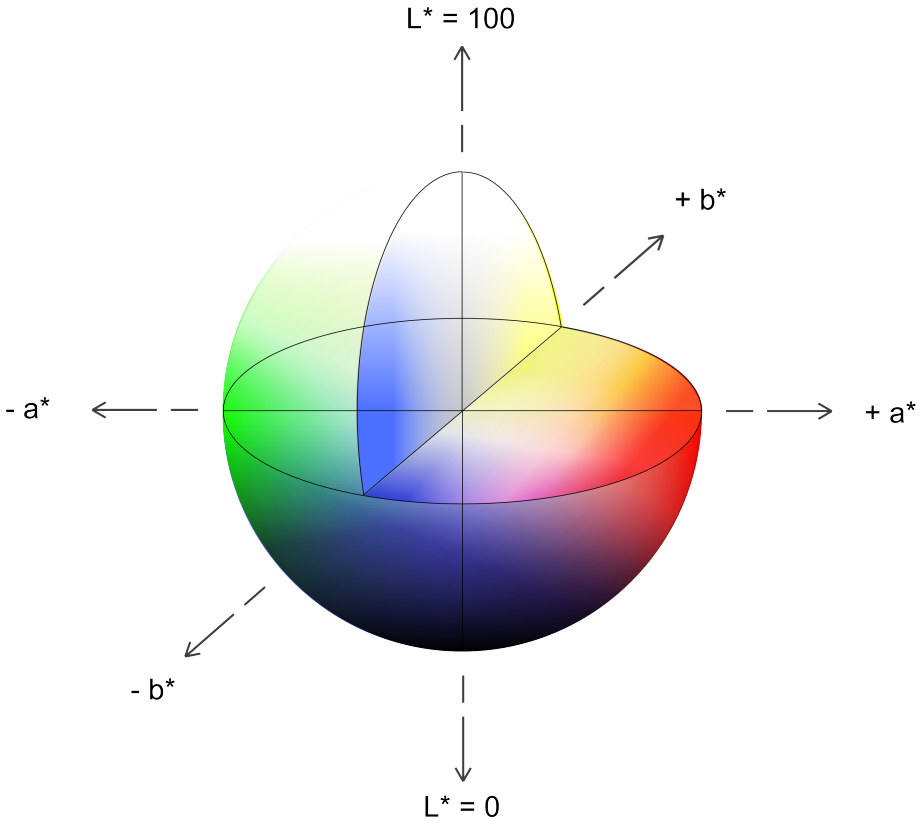

Figure 1.18: Representation of the CIELAB color space.

The terms commonly used to define the color states of transparent-colored ECP are bleached and colored. The bleached state is when the electrochromic material exhibits a low absorbance in the visible range, and the colored state is the state when the electrochromic material exhibits a high absorbance in the visible range.

1.5.1.1 Contrast

The contrast of an ECD defines the difference between its optical states. Several values can be used to describe the contrast of an ECD. Equation 1.1, Equation 1.2, and Equation 1.3 describe the contrast as the difference between the bleached and the colored states of and ECD for measurements in absorbance mode, transmittance mode, and reflectance

mode respectively. These are measured at a single wavelength, often the wavelength that corresponds to the maximum absorption of the colored state.

$$\Delta A_\lambda = A_{\text{colored}} - A_{\text{bleached}} \tag{1.1}$$

$$\Delta T_\lambda = T_{\text{bleached}} - T_{\text{colored}} \tag{1.2}$$

$$\Delta R_\lambda = R_{\text{bleached}} - R_{\text{colored}} \tag{1.3}$$

However, instead of reporting the contrast at only one wavelength, it is also possible to report the photopic contrast of and ECD. This value of contrast evaluates the contrast across a broader portion of the visible spectrum and also considers the sensitivity of the human eye at different wavelengths. This measure is useful for evaluating color states with broad absorption bands (such as black), rather than color states with narrow peaks. The photopic contrast in transmittance mode can be calculated as follows:

$$\Delta T_{\text{photopic}} = \frac{\int T(\lambda)S(\lambda)V(\lambda)d(\lambda)}{\int S(\lambda)V(\lambda)d(\lambda)} \tag{1.4}$$

where, $T(\lambda)$ is the transmittance spectrum of the device, $S(\lambda)$ is the normalized emmittance of the light source, and $V(\lambda)$ is the normalized spectral sensitivity of the human eye. The normalized photopic response of the eye, based on the CIE standard is shown in Figure 1.19 [118]. The peak of human photopic vision is around 555 nm.

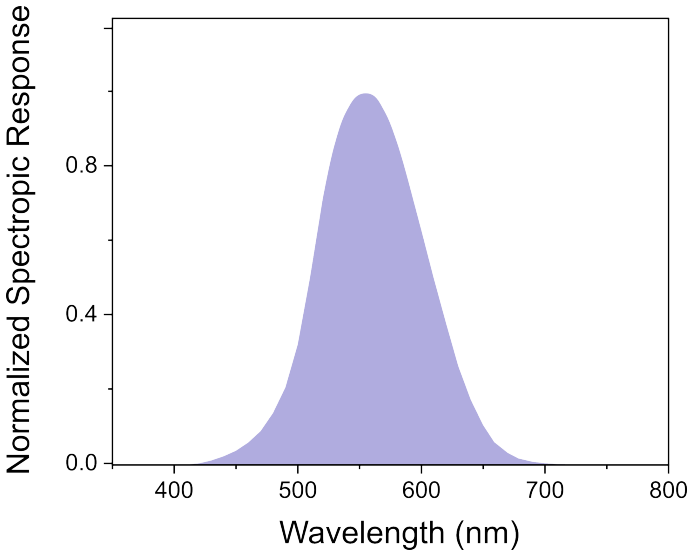

Figure 1.19: Normalized spectral response of the human eye according to the CIE V(λ) function.

The contrast of an ECD can also be defined in the CIELAB color space. The CIELAB color space is approximately uniform [119]. This means that the perceptual difference between two colors in CIELAB values should be represented by the Euclidean distance

between them. Thus, the contrast of an ECD can also be defined by the ΔE according to Equation 1.5. $(L_1^* - L_2^*)$ is the difference between the L values of the two optical states, $(a_1^* - a_2^*)$ is the difference between the a values of the two optical states, and $(b_1^* - b_2^*)$ is the difference between the b values of the two optical states.

$$\Delta E* = \sqrt{(L_1^* - L_2^*)^2 + (a_1^* - a_2^*)^2 + (b_1^* - b_2^*)^2} \tag{1.5}$$

1.5.2 Switching Speed

The switching speed of an electrochromic device describes how quickly it can change between its optical states. A common method to report the switching speed for an electrochromic device is to calculate the time that it takes to reach a defined percentage (commonly 60 %, 66 %, 80 %, 90 %, or 95 %) of the maximum contrast. However, the percentage that is reported is not standardized, making it challenging for researchers to compare the switching speeds in different reports.

To simplify this, Hassab *et al.* proposed a standardized method to calculate switching speeds for electrochromic devices [120]. This method consists of applying square-wave potential steps with variable periods, as shown in Figure 1.20a. From this, a contrast can be calculated for each pulse length, see Figure 1.20b. (Note that the timings presented in the figure are a modified version to those used by Hassab *et al.*).

The data from Figure 1.20c can be fitted with a standard exponential equation, see 1.6, where ΔT_{max} is the maximum contrast, and τ is a time constant. Given ΔT_{max} and τ, the switching speed can be calculated for any percentage of a switch.

$$\Delta T = \Delta T_{\max}(1 - e^{\frac{t}{\tau}}) \tag{1.6}$$

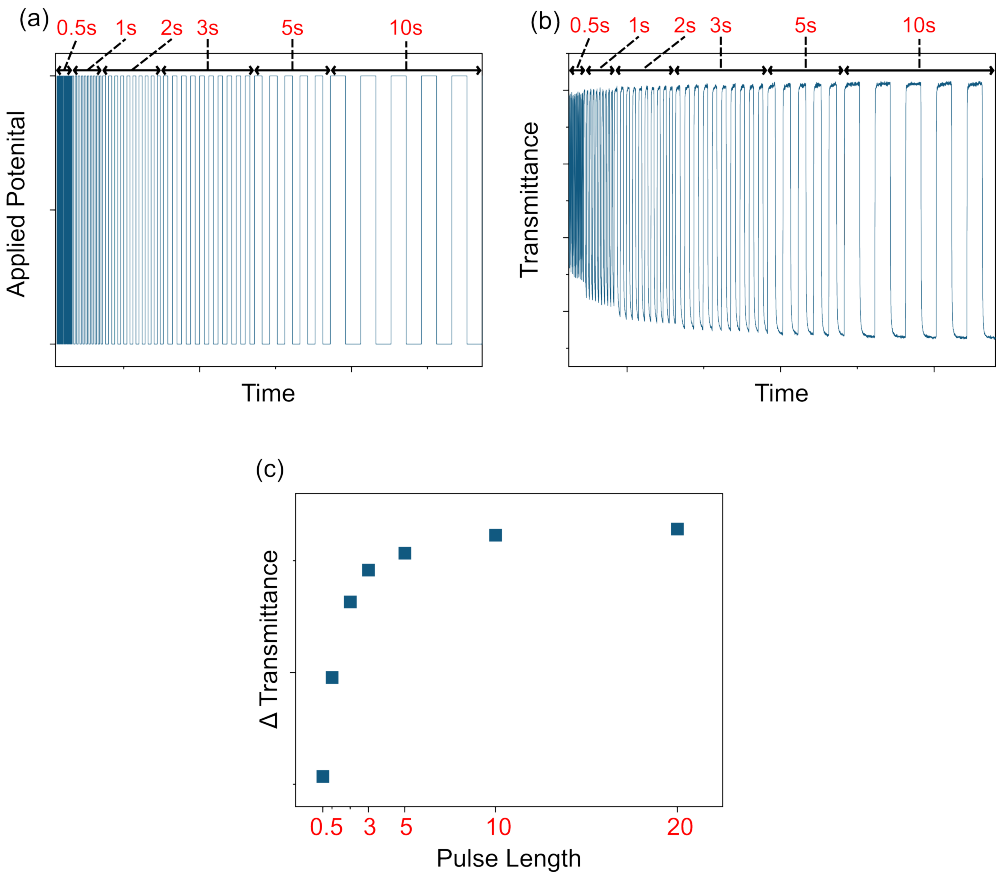

Figure 1.20: Method for calculating switching speed adapted from ref. [120], including (a) electrical driving protocol, (b) optical response to driving protocol, and (c) calculated contrast at each driving pulse length.

1.5.3 Coloration Efficiency

Coloration efficiency (CE) is a measure of the change in optical density (ΔOD) at a given wavelength per unit of charge (Q). It is calculated according to Equation 1.7, and ΔOD can be calculated according to Equation 1.8. CE is typically reported in the unit of $cm^2\ C^{-1}$. For ECDs, high coloration efficiencies reduce the energy requirements to switch between the two optical states.

$$CE(\lambda) = \frac{\Delta OD(\lambda)}{Q} \tag{1.7}$$

$$\Delta OD = log[\frac{T_{ox}}{T_{red}}] \tag{1.8}$$

1.5.4 Optical Memory

The optical memory is a measure of the persistence of the optical states of an ECD when the applied voltage is removed. This will determine how frequently a driving pulse will

have to be applied to the ECD to maintain the desired state. Thus, the CE and optical memory are key determinants for the overall energy efficiency of an ECD. The former determines how much energy is consumed per driving pulse, and the latter determines how often a driving pulse takes place to maintain the desired color state.

1.5.5 Cycling Lifetime

The cycling lifetime of an ECD is the number of times that the device can be switched between its optical states before it exhibits a defined drop in performance. The performance can be evaluated using any of the metrics outlined in this section (color, contrast, switching speed, coloration efficiency, optical memory, etc.).

1.6 *In Situ* Electropolymerization

1.6.1 Overview

In situ electropolymerization refers to the process of electrodepositing a film inside of an assembled electrochemical device. This is achieved by adding a monomer precursor to the electrolyte of a device and then applying a sufficient voltage to deposit a polymer film. Figure 1.21 shows the structure of a simple *in situ* polymerized device, where EDOT is used as a precursor to form PEDOT.

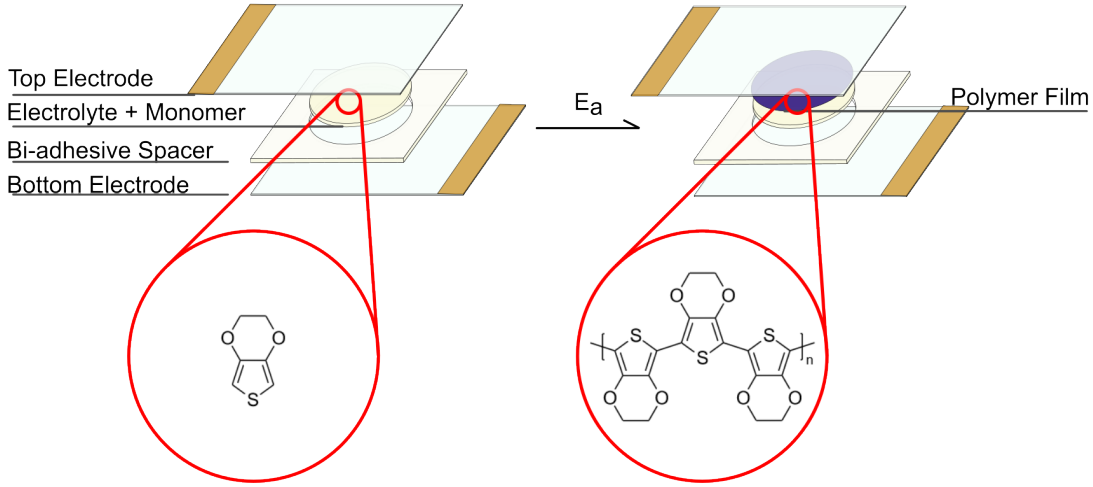

Figure 1.21: Schematic showing the construction and activation of a simple *in situ* electropolymerized device with EDOT as the precursor monomer.

The use of *in situ* electropolymerization to create irreversible visual indicators was first reported in a 2009 patent from Chromera Inc. [121]. The group of G. A. Sotzing has also produced a body of work exploring *in situ* electropolymerization as a simple and low-waste method to manufacture reversible electrochromic displays. In their work they

use a series of different monomer precursors to form electrochromic layers in both glass and PET-based devices [122]–[127]. They report a maximum photopic contrast of 53 % for glass-ITO devices with 2,2-Dimethyl-3,4-propylenedioxythiophene as the monomer precursor in a polymer gel with a mixture of propylene carbonate and diethylene carbonate as plasticizers [127]. Zhao *et al.* demonstrated *in situ* electropolymerization to produce reversible electrochromic devices with a copolymer of EDOT and anthracene [128].

1.6.2 Reversible vs. Irreversible Electrochromic Indicators

In principle, the *in situ* polymerized device can be used to create both reversible indicators and irreversible indicators. The key difference is in when the electropolymerization takes place. For the reversible form, *in situ* electropolymerization takes place during the manufacturing process of the indicator. The thickness of the ECP film is controlled by the voltage and the charge applied during the polymerization process. During use, the ECP film is switched with a driving voltage that is lower than the electropolymerization voltage to prevent further film formation. The color change during use comes from the oxidation and reduction process of the ECP film that was formed. See Figure 1.22a.

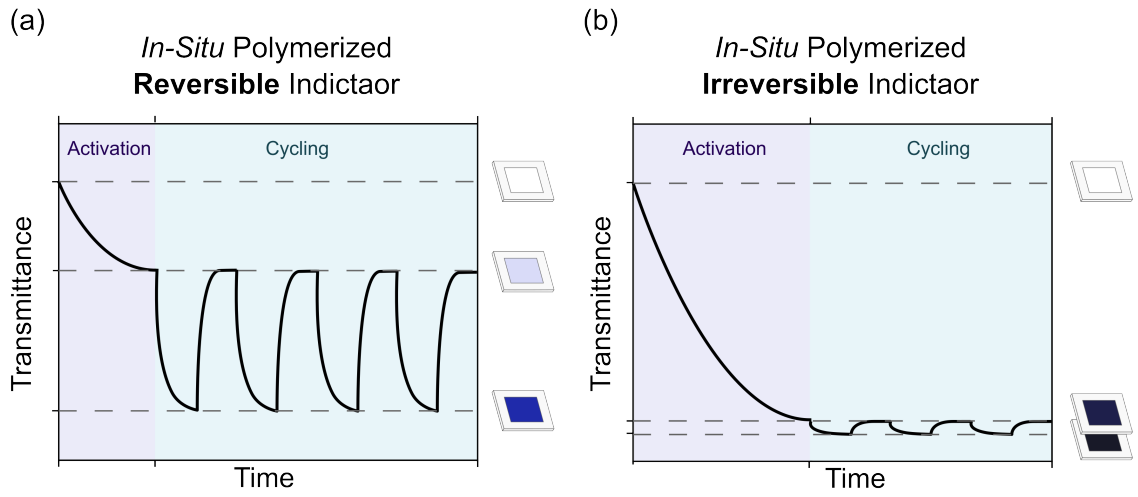

Figure 1.22: Comparison of activation and cycling performed for (a) reversible and (b) irreversible indicators. Both types of indicator use *in situ* electropolymerization.

For the irreversible form, the *in situ* polymerization takes place during the use of the indicator. The thickness of the ECP film in this case will be substantially thicker than in a reversible indicator. With increasing film thickness the contrast between the oxidized and reduced states decreases [129], [130]. The indicator is considered irreversible when the color states can not be differentiated by the human eye. The color change during use comes from the formation of the polymer film in the indicator. See Figure 1.22b. It is

important to note that the term 'irreversible' here refers to the perceived optical properties of the indicator, not to the electrochemical properties of the indicator.

For a reversible indicator the contrast between the oxidized and reduced states of the ECP film should be maximized, and the contrast between the indicator before activation and after activation is not important. For an irreversible indicator, the contrast between the oxidized and the reduced states of the ECP film should be minimized, and the contrast between the indicator before activation and after activation should be maximized.

1.6.3 Commercial Application for Irreversible Electrochemical Indicators

To understand the unique commercial potential for irreversible electrochromic indicators, it is necessary to consider what is currently available in the smart label market. A summary of commercial technologies for smart labels with sensing components is shown in Figure 1.23. A simple smart label consists of an indicator that has a direct change in color, intensity, or diffusion of color in response to a change in environmental conditions. Technologies have been developed to produce indicators that show response to temperature, impact, pH, humidity, light, and the presence of gases, chemicals, or biological species [5]–[7], [131]–[134]. Indicators have the advantage of being simple and low cost. Smart labels based on indicators are commercially available using both reversible and irreversible systems [135]–[141].

SMART Packaging/Labels with Sensing Components

	Indicators	Sensor with Visual Display/Indicator	Sensor with Non-Visual Output
Description	Indicator that changes color, intensity or diffusion of color in response to an environmental change.	Electronic sensor is integrated with a visual display or indicator, i.e. LCD, LED, EPD, or ECD.	Electronic sensor is integrated with a non-visual information output, i.e. RFID or NFC.
Commercial Examples	TimeStrip SpotSee (WarmMark®, TiltWatch®) 3BP (Damage-Indicating Packaging™) Evigence (SmartDot™, FMA™) Insignia (SafeTag, FreshTag)	Timestrip (Timestrip Complete, Timestrip Neo) tempmate.®-i1 Sensitech (TagAlert®) American Thermal Instruments (Logic360, Endicate™) Avery Dennison (TT Sensor Plus™)	Avery Dennison (Smartrac Temperature Logger NFC, TT Sensor Plus™ NFC Tag) RFID4U (Tagmatiks™) Molex (Smart Sensing Label)
Advantages	- Low-cost - Simple - No electronic components - Visual Output	- High Accuracy - Customizable thresholds - Data processing and storage potential - Visual Output	- High Accuracy - Customizable thresholds - Data processing and storage potential
Disadvantages	- Low Accuracy - Requires User to Interpret Color Changes	- Can require additional electronic components i.e. power source, microprocessor - High-cost	- Can require additional electronic components i.e. power source, microprocessor - No visual output

Figure 1.23: Summary of key advantages, and disadvantages of different form factors of smart labels and packaging. Examples of commercial products for indicators, sensors with visual displays/indicators, and sensors with non-visual outputs. Reproduced with permission from [142].

But, if more precise detection is required it can be advantageous to use an electronic sensor. This form of monitoring system has a higher cost but can offer greater functionality and customization to the user. In this case, the sensor is integrated with a power source, a micro-processor, and some form of data transmitter, such as RFID [143], [144], and NFC [144]. A more sophisticated variation of the smart label or packaging could additionally introduce a dynamic visual indicator or display that would directly convey critical information to the user without the need for a data reader.

Examples of dynamic visual interfaces that have been employed in smart labels include light emitting diodes (LEDs) [145]–[148], electrophoretic displays (EPDs) [9], ECDs [47], or liquid crystal displays (LCDs) [149]. All of these forms of visual indication pose unique properties, in particular in terms of their bi-stability. LEDs for example, require a constant current to maintain their emitting state. ECDs are sometimes commercially referred to as 'semi bi-stable' [47], [70], [150]. They do not require constant power to maintain a color state, only periodic pulses, making them relatively low-power. EPDs and some LCDs are fully bi-stable [151], [152]. This makes them highly power-efficient when the visual output does not need to be changed frequently.

However, for all of the aforementioned technologies, the visual output is electrically reversible. For some applications, such as anti-counterfeiting, authenticity labeling, or tamper-proof packaging, a visual output with a truly permanent color change can be a key selling point. Thus, it is of interest to develop an irreversible electrochromic indicator to use as a visual interface for smart labels and packaging. Figure 1.24 shows an example of an impact-detecting smart label where irreversible functionality would be a unique selling point.

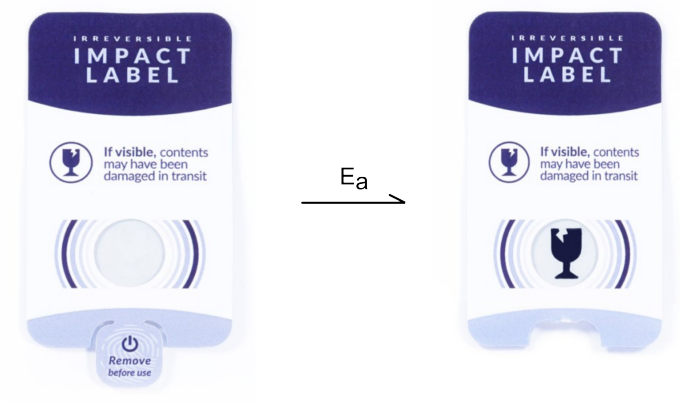

Figure 1.24: Demonstrator of an irreversible electrochromic indicator as an impact label to be used for logistics and transportation applications.

1.7 Framework and Layout of the Dissertation

The work presented in this thesis is primarily the result of CHARISMA: a European Union Horizons 2020 ITN with reference number 814299 [153]. This program supported nine early stage researchers (ESRs) located at the University of Vienna in Austria, Tampere University of Technology in Finland, NOVA University of Lisbon in Portugal, Ynvisible GmbH in Germany, and LCR Hallcrest Ltd in the UK. The overarching goal of the project is to develop chromogenic displays and labels with irreversible color change for smart label applications. The work was split into the following industrial research objectives (IROs):

IRO1 Molecular design and preparation of materials showing irreversible chromogenic changes for engineering irreversible chromogenic displays.

IRO2 Design and preparation of molecular materials that change their conductive capabilities when their physical state changes (e.g. melting) following an external stimulus (e.g., temperature).

IRO3 Development of the power unit and circuitry.

IRO4 Prototyping of the final smart label and development of a business study.

The work of this dissertation contributes to IRO1, and IRO4. In particular the development and engineering of irreversible electrochromic indicators. Electrochromism is the phenomenon where the color of a material can be changed by the application of a voltage. Conventionally, the coloration and discoloration processes should be reversible. However, the work in the CHARISMA project targets electrochromism with only one singular color transition.

Chapters 2 through 5 of this thesis focus on the development of irreversible electrochromic indicators via *in situ* electropolymerization. Chapter 2 explores the influence of a GPE on the *in situ* electropolymerization of EDOT. This is critical since GPEs are typically employed in electrochromic devices due to their improved stability and safety compared to liquid electrolytes. This chapter also characterizes EDOT based irreversible indicators and analyzes the contribution of different chemical processes to the overall device coloration.

Chapters 3 and 4 focus on characterizing and improving the performance of irreversible elecrochromic indicators for commercial applications. In Chapter 3 the electrical and optical properties are tuned by exploring a range of different monomer precursors. In Chapter 4 the operating conditions and thermal stability of the irreversible indicators are addressed.

The culmination of the work in the previous chapters in demonstrated in Chapter 5. This chapter reports on the integration work that was performed in collaboration with the other ESRs in the CHARISMA project. This includes characterizing the activation of

different variations of the irreversible indicators with printed supercapacitors, and then producing a flexible smart label with printed supercapacitors, and a chemical thermal sensor.

Chapter 6 moves beyond the scope of the CHARISMA project and describes the development of reversible *in situ* polymerized indicators. More than the previous chapters, this work focuses on the methods of manufacturing and demonstrates *in situ* electropolymerization in a fully printed electrochromic stack. The electropolymerization process is further tuned to optimize the cycling lifetime and contrast of the indicators.

2

Influence of a Polymeric Gel on the *In Situ* Electropolymerization of 3,4-ethylenedioxythiophene

This chapter has been adapted from the published open-access paper "Howard, E. L. *et al.*, Influence of a polymeric gel on the in situ electropolymerization of 3,4-ethylenedioxythiophene and application in irreversible electrochemical indicators, *J Appl Electrochem*, Sep. 2023, doi:10.1007/s10800-023-01991-z".

2.1 Background and Motivation

In contrast to conventional ECDs which produce a reversible color change in response to an applied voltage, irreversible electrochromic indicators generate a single permanent color change in response to an applied voltage. This format of irreversible electrochromic indicator is envisioned for use in a broad range of applications including healthcare, food packaging, logistics, and authenticity labeling. One approach to developing irreversible electrochemical indicators is via *in situ* electropolymerization. These indicators are produced by solubilizing monomers in the electrolyte of a vertical device structure. The indicator is activated by applying a sufficient potential to electropolymerize the species *in situ*. If the monomers absorb in the ultraviolet region and the polymer absorbs in the visible region, the result is a transparent to colored optical transformation. With increasing electrochromic film thickness the contrast between the oxidized and reduced states decreases [129], [130]. The indicator is considered irreversible when the color states cannot be differentiated by the human eye. The use of *in situ* electropolymerization to create irreversible visual indicators was first reported in a 2009 patent from Chromera Inc. [121].

The properties of electropolymerized films are dependent on a range of environmental factors, including the nature and concentration of the monomer, solvent, and salt, as well as the substrate and the electrical perturbation (i.e., potentiostatic, potentiodynamic, galvanostatic) [49]–[59]. Generally, the deposition proceeds via oxidation of monomers at the electrode surface and subsequent oligomerizations, building up a high-density oligomeric region. Once the high-density oligomeric region is established in front of the electrode surface, film formation proceeds via nucleation and growth processes [60].

One of the key differences between conventional electropolymerization and *in situ* electropolymerization, is that *in situ* electropolymerization is likely to be performed in a GPE rather than in a liquid electrolyte. This is because GPEs have improved stability and safety compared to liquid electrolyte, and are thus more suitable for use in commercial devices. However, there are a limited number of studies exploring how a GPE influences the electropedosition process. Sotzing *et al.* found that the *in situ* electropolymerization of poly(2,2-dimethyl-3,4-propylenedioxythiophene) (PProDOT-Me_2) the photopic contrast could be optimized by modifying the composition of binary plasticizer mixtures, and both the photopic contrast and polymerization charge density could be modified by tuning the cross-linking density of a poly(ethylene glycol) dimethacrylate gel network [125], [127]. Interestingly in another report of *in situ* electropolymerization, Zhao *et al.* produced a copolymer with EDOT and an anthracene derivative in a device using a poly(ethyleneglycol) (PEG) gel electrolyte and found that they could form a polymer *in situ* that they could not form in a solution of just the plasticizer, proposing that the *in situ* format may assist the film deposition process [154].

Thus, the goal of this chapter is to further investigate how a polymer gel matrix influences the polymer electrodeposition process and to characterize this effect for *in*

situ polymerized irreversible electrochemical indicators. This is initially studied in a 3-electrode electrochemical cell set-up using a platinum disk working electrode and then tested in flexible indicators with ITO coated PET substrates. EDOT was selected as the monomer precursor for this study. It is colourless in solution, broadly commercially available and has a low oxidation potential arising the electron donating nature of its alkoxy substituents [155]. This, along with its solubility in the binary EC and PC mixture used in our electrolyte, make it a promising candidate for irreversible electrochemical indicators [156]. Further, the polymer PEDOT presents good stability in air and at higher temperatures, which is key to develop indicators that can be used in a broad range of environmental conditions [157], [158]. UV cross-linkable EO-PO-AGE terpolymer Zeospan 8030, the structure shown in Figure 2.1, was selected for the gel electrolyte as it has been used industrially for the production of electrochromic devices [159]. The terpolymer composition is 91% ethylene oxide, 6% allyl glycol ether and has T_g of −57 °C, density of 1.16 g cm $^{-3}$, and T_m of 40 °C [160], [161]. The abbreviation 'PC:EC:$LiClO_4$ + 10 % ZEO' is used for the gel electrolyte, and the abbreviation 'PC:EC:$LiClO_4$' is used for the liquid electrolyte.

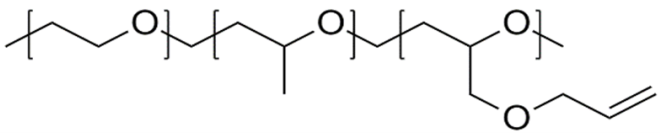

Figure 2.1: Chemical structure of EO-PO-AGE Zeospan 8030 polymer.

2.2 Results and Discussion

2.2.1 3-Electrode Cell

We used both potentiodynamic and potentiostatic techniques to investigate the electrodeposition of PEDOT in the liquid and gel electrolytes. Cyclic voltammetry (CV) is a potentiodynamic method where the potential of the working electrode is ramped linearly over time. The current response in a CV can be used to determine the oxidation potential of the monomer, the formation of a polymer film, and the electrochemical behavior of the deposited film.

The first scan of the CV response of electropolymerization of 25 mM EDOT in liquid and gel electrolyte are shown in Figure 2.2a. A rapid increase in the current density, ascribed to the initial oxidation and cross-coupling reactions of the monomer, occurs at a lower potential (0.7 V vs. Ag/Ag^+) in the gel electrolyte than in the liquid electrolyte (0.8 V vs. Ag/Ag^+). The same CV protocol was conducted in monomer free electrolytes to investigate the electrochemical response of the electrolyte, the first scan is shown in Figure 2.2b. For the gel electrolyte, a 0.14 mA cm^{-2} peak is observed at 0.62 V vs. Ag/Ag^+.

The same peak is observed in the gel electrolyte with monomer and is attributed to the polarization of the gel matrix.

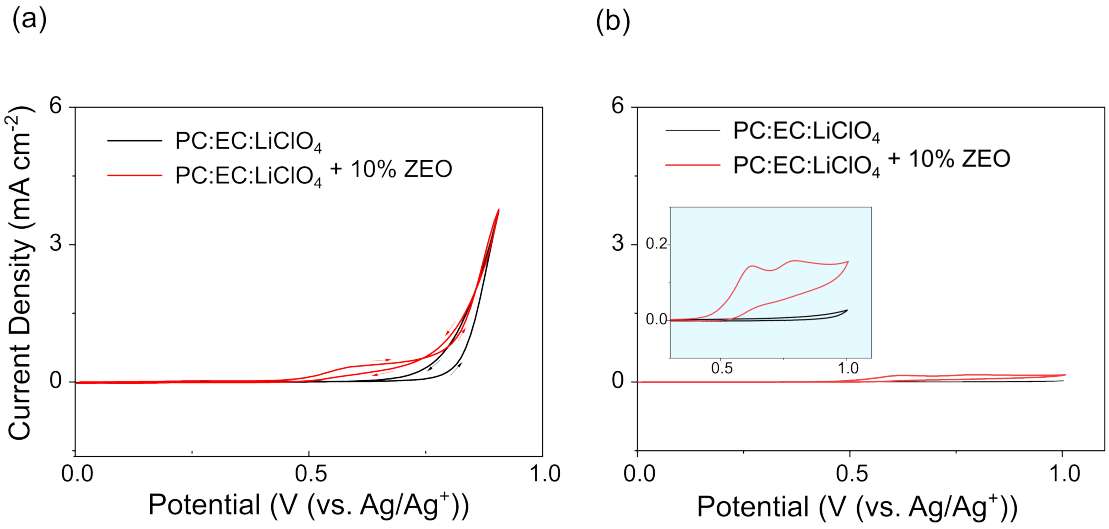

Figure 2.2: First scan on of a CV in liquid and gel electrolytes (a) with 25 mM EDOT monomer, and (b) without EDOT monomer. Scan rate is 0.05 V s^{-1}.

Scans 1-10 of the same CV experiment are shown for electropolymerization in liquid and gel electrolyte are shown in Figure 2.3a and Figure 2.3b. The appearance of broad oxidation and reduction peaks below the oxidation potential of the monomer indicates that a polymer film is deposited from both samples. In the liquid electrolyte, the increase in current density for the polymer's cathodic redox peak (~0.090 mA cm^{-2}) is greater than in the gel electrolyte (~0.054 mA cm^{-2}) for consecutive scans. The increase in cathodic redox charge density for each cycle is a measure of the increase in the number of rechargeable redox sites, suggesting that more polymer film is formed from the liquid electrolyte after 10 cycles than from the gel electrolyte.

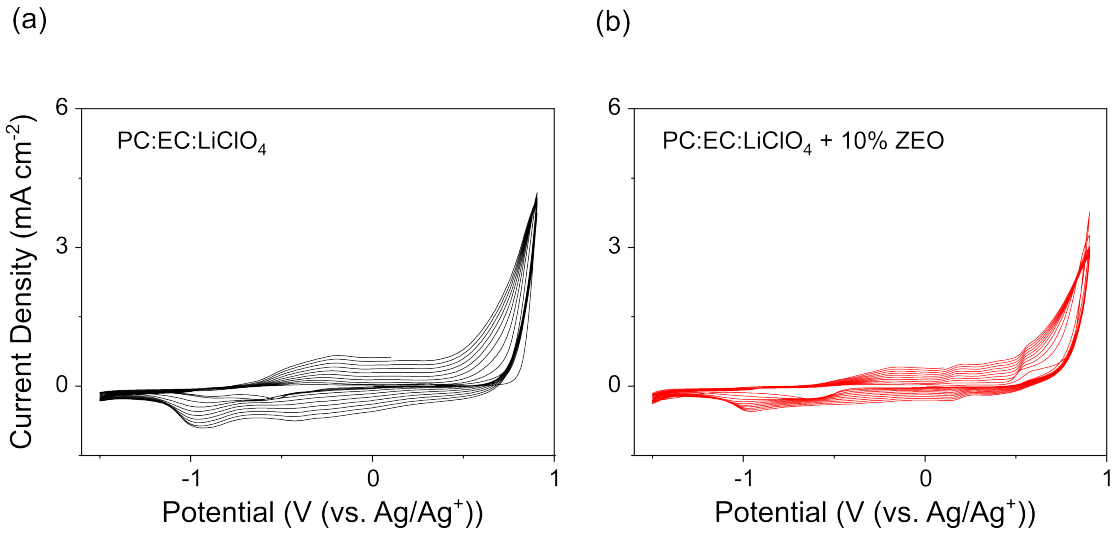

Figure 2.3: Scans 1-10 of CV in (a) liquid and (b) gel electrolyte with 25 mM EDOT. Scan rate is 0.05 V s^{-1}.

Potentiostatic techniques can be used to investigate the nature of the deposition process during electropolymerization. The electrical protocol and an experimental current-time transient for the deposition of EDOT using the potential step method is shown in Figure 2.4. The following regions are observed:

A-B: The pre-conditioning potential is applied (less than the oxidation potential of the monomer). A sharp peak is observed due to the charging of the double layer capacitance.

B-C: The film forming potential is applied. Oxidation of monomers begins at the electrode surface. Generation of soluble oligomers occurs, forming a high density oligomeric region in front of the electrode surface. This region is characterized by a diffusion controlled j ~$t^{-1/2}$ relationship. The time at the current minimum is referred to as the induction time (τ).

C-D: After the induction time, nucleation and growth on the electrode surface produce an increase in the current density. A maximum ($t(j_{max})$, j_{max}), and decrease in the current density is indicative of nuclei overlap, reducing the effective surface area, and/or the transition to a diffusion-controlled process [58], [59].

D: Subsequent current density steps or peaks suggest a multi-step or layer-by-layer electrodeposition process [162].

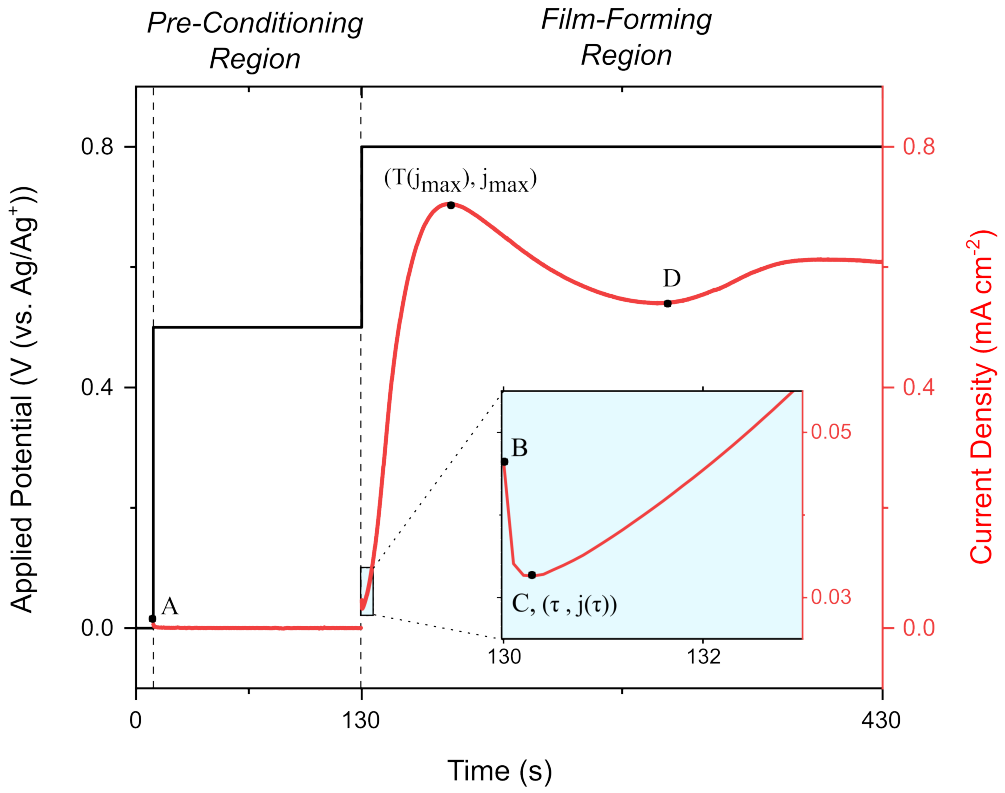

Figure 2.4: Electrical protocol for potential step method, and current-time transient of 25 mM EDOT in liquid electrolyte at 800 mV applied potential.

Figure 2.5a and Figure 2.5b show the current time transients during the film forming region for films formed over a range of potentials in the liquid and gel electrolyte. The general features of the deposition of EDOT in liquid electrolyte in this study are consistent with those previously reported in the literature [59], [162]. After 300 s in the gel electrolyte, a visible polymer film is deposited on the electrode at potentials above 640 mV, whereas in liquid electrolyte a visible polymer film is only deposited at potentials above 720 mV. This amounts to a 80 mV reduction in the potential required for film formation. In the liquid electrolyte, above 790 mV the transients show a second peak in the current density, suggesting a multi-step deposition process. However, in the gel electrolyte, even at high potentials, the process remains single step and the current density gradually decreases to a low current density plateau.

Figure 2.6a shows the total charge consumed by the samples over the 300 s interval. There is a clear cross-over point where at potentials less than 770 mV more charge is consumed in the samples with the gel electrolyte, whereas at potential greater than 770 mV more charge is consumed in the samples with the liquid electrolyte. Although we can not exclude that other side reactions may contribute to this charge, it suggests that more polymer is formed from the gel electrolyte at lower potentials. The crossover point in the

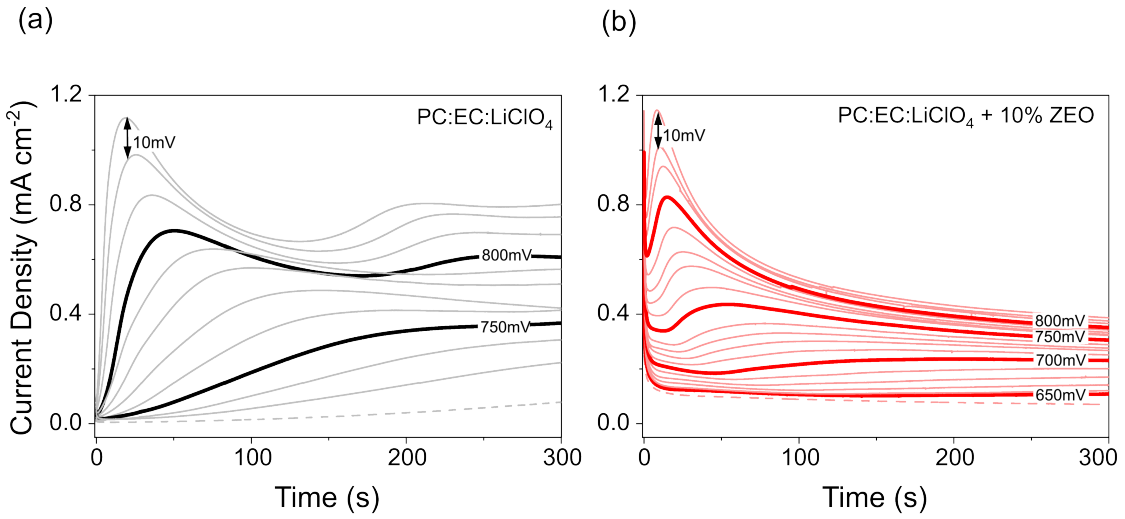

Figure 2.5: Current-time transients for electropolymerization of 25 mM EDOT in (a) liquid, and (b) gel electrolyte over a range of potentials. The interval between transients is 10 mV. Dashed line indicators that no visible polymer is formed on the electrode surface.

charge consumption shifts to higher potentials for shorter time periods, see Appendix A.2. Additionally, at the same potentials, a rapid increase in current density to the plateau ($t(j_{max})$, j_{max}) occurs faster in the gel electrolyte than in the liquid electrolyte, see Figure 2.6b. This could indicate that initial polymer deposition and transfer to diffusion-controlled processes occurs faster in the gel electrolyte compared with the liquid electrolyte. Overall, the results from the 3- electrode cell suggest that the gel matrix produces faster polymerization rate at lower potentials and short time periods compared to the liquid electrolyte.

A hypothesis for the observations concerns the nature of monomer and oligomer diffusion. In a liquid phase, species are free to migrate in all directions, whereas in a gel phase the migration of species is limited by a 3-dimensional polymer matrix. As the relative ratio between the size of the migrating species to the pore size of the gel increases, movement is limited by steric hinderance and may require uncoiling or reptation [163]. This phenomenon is commonly exploited in gel electrophoresis.

In the context of the current study, the mobility of monomers and oligomers through the gel matrix is expected to decrease with growing chain length. Compared to monomeric species which may diffuse to and from the electrode surface, oligomers formed near the electrode surface would encounter more steric hinderance limiting diffusion back to the bulk. This potential trapping effect of oligomers near the electrode surface may facilitate the formation of the high-density oligomeric region, which is critical for the early stages of the deposition.

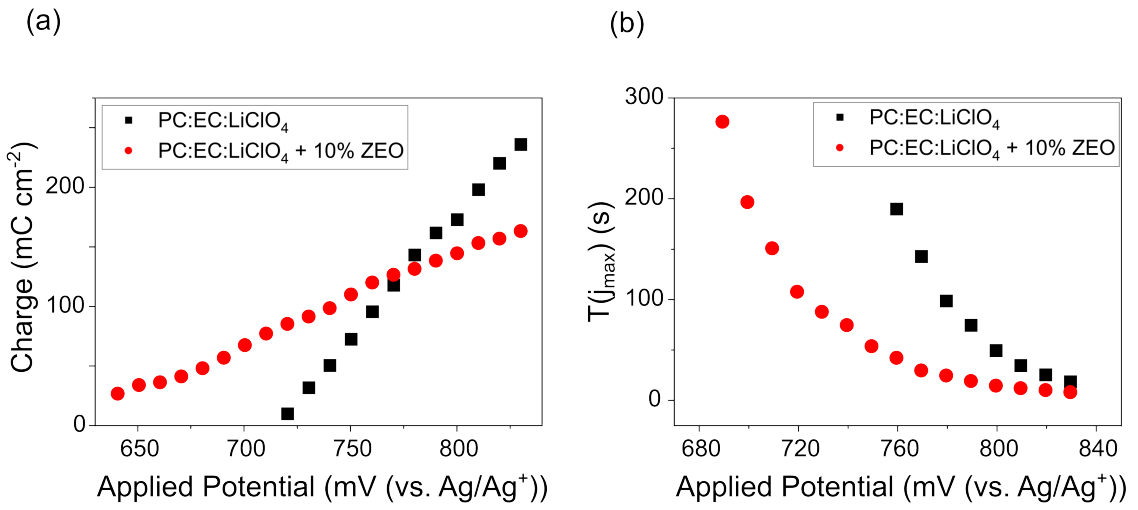

Figure 2.6: (a) Charge consumption at 300 s for electropolymerization of 25 mM EDOT in liquid and gel electrolytes, and (b) T(jmax) vs. applied potential at 300 s for electropolymerization of 25 mM EDOT in liquid and gel electrolytes.

2.2.2 Irreversible Electrochemical Indicator

PET-ITO based irreversible electrochemical indicators were constructed to determine whether the trends identified in the three-electrode cell were also observed in a device format. Triplicates of liquid and gel electrolyte indicators were activated over the range of potentials from 2.3 – 3.2 V. The indicators were activated by applying a sufficient potential to electropolymerize the monomers *in situ*. The transmittance of the indicators was measured at 555 nm, the peak of human photopic vision, over the duration of the activation. Figure 2.7 shows the results of this experiment for selected periods. After 300 s of activation at the specified potential, 0 V is applied for 5 s to short-circuit the device. The decrease in the transmittance when the indicator is short-circuited is attributed to the electrochemical reduction of the PEDOT film on the working electrode. The transmittance of the indicator when it is short-circuited is important to consider since the indicators will drift to this color state when the activation potential is removed.

For all potentials measured, the gel electrolyte indicators measure a higher change in transmittance after 300 s of activation. The difference in transmittance is greater at lower potentials. At 2.3 V, the gel electrolyte indicators have a change in transmittance of 40.1% after 300 s, compared 10.9% in the liquid electrolyte indicators, see Figure 2.8a. The standard deviation between the triplicates was higher in the liquid electrolyte indicators than in the gel electrolyte indicators. Figure 2.8b shows the coloration efficiency of the irreversible electrochemical indicators as a function of potential. The coloration efficiency is higher for the gel electrolyte indicators than the liquid electrolyte indicators at all of the potentials tested.

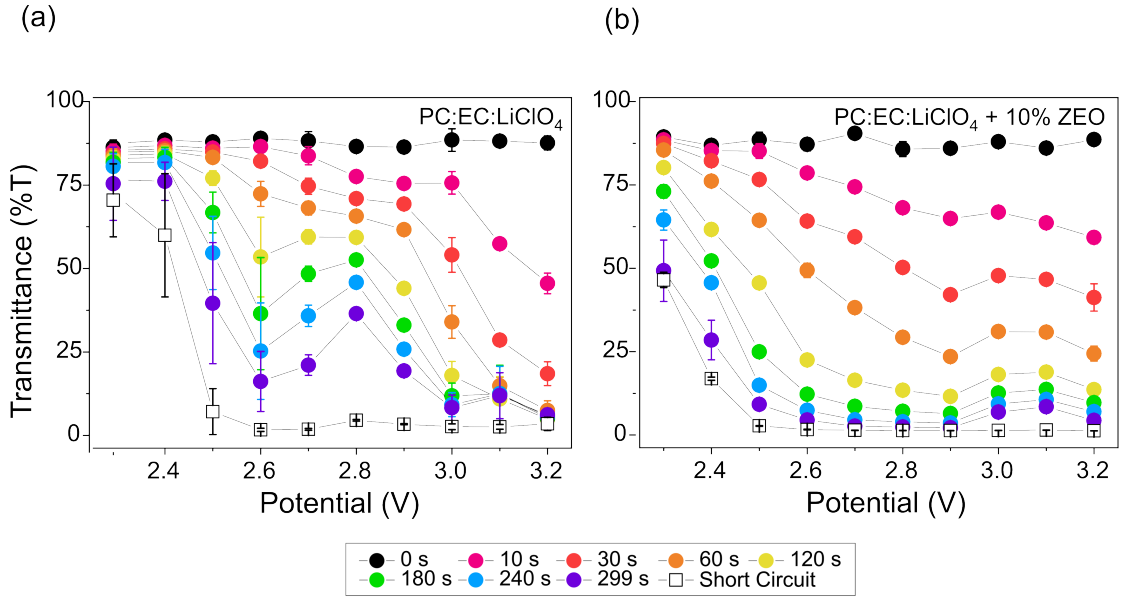

Figure 2.7: Optical transmittance at 555 nm of PET-ITO indicators with *in situ* electropolymerization of 25 mM EDOT in (a) liquid, and (b) gel electrolyte over a range of potentials. Short-circuit is the transmittance of the indicators after 0 V for 5 seconds following the 300 s activation.

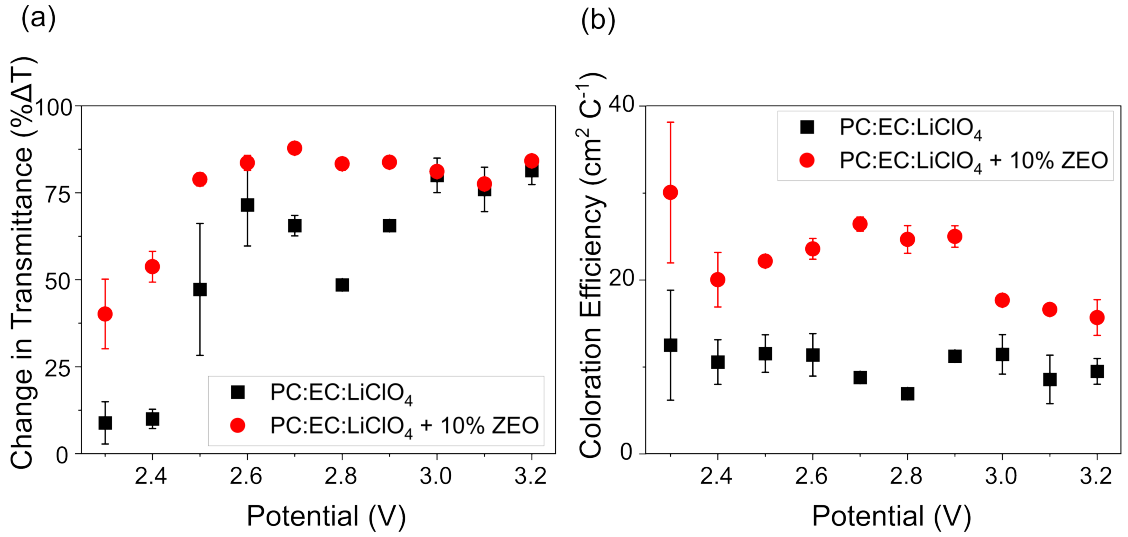

Figure 2.8: (a) Change in transmittance and (b) coloration efficiency of PET-ITO indicators with *in situ* electropolymerization of 25 mM EDOT in liquid and gel electrolyte over a range of potentials. Coloration efficiency and change in transmittance are measured at 555 nm for 300 s of activation.

Digital images of liquid and gel electrolyte indicators activated at 2.3, 2.5 and 3.0 V are shown in Figure 2.9. In addition to faster activation, the indicators with gel electrolyte show greater visual homogeneity. At 2.3 and 2.5 V, the liquid electrolyte indicators have color change primarily in the center of the working area, as opposed to the gel electrolyte indicators which have visually uniform color change across the full working area.

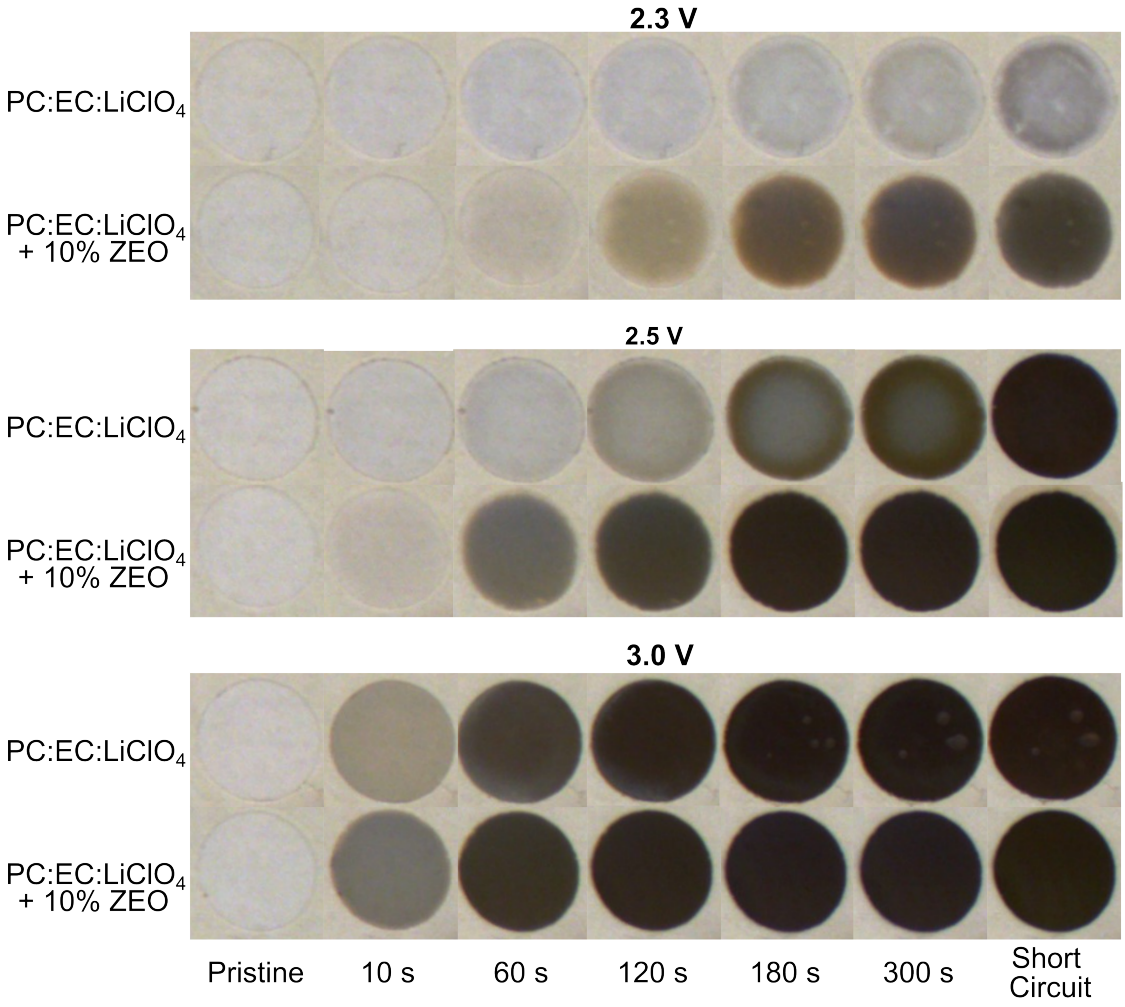

Figure 2.9: Color-corrected digital images of PET-ITO indicators with *in situ* electropolymerization of 25 mM EDOT activated at 2.3, 2.5 and 3.0 V. Images are taken of the pristine indicator before activation, during activation at 10, 60, 120, 180, and 300 s time points, and when the indicator is short-circuited after 300 s of activation.

2.2.3 Analysis of Electrodes Post-Activation

After activation, the indicators were delaminated and the working electrodes and counter electrodes were analyzed separately. The photopic contrast of the working electrode, counter electrode, and full device for the indicators is shown in Figure 2.10. The overall color change in the indicators is a combination of the color change on the working and

counter electrode. In this case, the color change on the counter electrode is attributed to reduction of the ITO coating on the PET-ITO substrate. While this reaction is considered to be parasitic in traditional electrochemical devices [97], [164], [165], it improves the change in transmittance and opacity for these irreversible indicators.

The anomalous increase in the transmittance for the liquid electrolyte indicators in the range of 2.6-3.0 V and for the gel electrolyte indicators in the range of 2.9-3.2 V is primarily derived from trends in the transmittance of the ITO reduction on the counter electrode, see Figure 2.10.

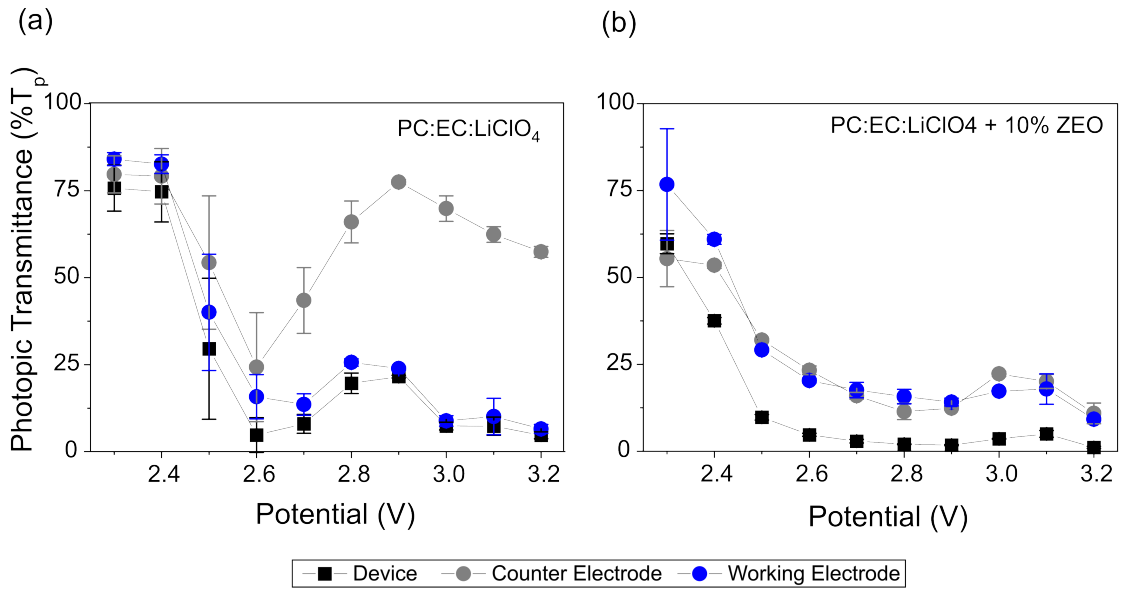

Figure 2.10: Photopic transmittance of full device, counter electrode, and working electrode from (a) liquid electrolyte and (b) gel electrolyte devices versus activation potential. Indicators activated for 300 s, but measurements taken after 1 week at OCP. Measurements of the working electrode of gel devices include the electrolyte layer, while measurements of working electrode of liquid indicators do not include the electrolyte layer.

2.3 Conclusion

In this work, we studied the influence of a polymer gel electrolyte on the electropolymerization of EDOT and demonstrated the use of *in situ* polymerization for irreversible electrochemical indicators. We found that the addition of UV cross-linkable EO-PO-AGE terpolymer as a gel matrix lowers the overpotential, increases the change in transmittance, and improves the coloration efficiency for film formation for irreversible electrochemical indicators. These initial observations indicate the need for further studies investigating the effect of gels on the electropolymerization process and highlight the potential to optimize electrolytes specifically for this form of irreversible electrochemical indicator.

2.4 Materials and Experimental Methods

Electrolyte Composition: EC (99%) and PC (99.5%) were obtained from Sigma Aldrich, lithium perchlorate (98%) was obtained from Alfa Aesar, photo initiator Phenylbis(2,4,6-trimethylbenzoyl)phosphine oxide was obtained from TCI Chemicals, and Zeospan 8030 was obtained from ZEON Chemicals. All chemicals were used as received. A PC:EC:$LiClO_4$ ratio of 1:0.47:0.098 was maintained. Liquid electrolytes were mixed in vials using a roll bar mixer. Gel electrolytes were formulated by incorporation of 9.95 wt% Zeospan 8030 and 0.5 wt% photo initiator to the pre-mixed liquid electrolytes using a stainless steel blade mixer.

3-Electrode Cell: The working electrode was a Platinum disk electrode (1.8 mm diameter), which was polished to a mirror-like surface with 0.05 µm alumina slurry and rinsed in ethanol prior to each experiment. The counter electrode was a platinum mesh flag (1x1 cm^2), and the reference electrode was non-aqueous Ag/Ag^+ in 0.01 M $AgNO_3$ and 0.1 M TBAP/ACN filling solution ($E_{1/2}$ for Fc/Fc^+: 0.05 V). For experiments with liquid electrolyte, the working electrode was immersed directly in the monomer electrolyte solution. For experiments with gel electrolyte, a 0.1 cm^3 cylinder of the gel electrolyte with monomer was cured directly onto the tip of the working electrode with a LOCTITE 500 W mercury vapor bulb for 120 s, and then immersed into a liquid electrolyte solution with the same monomer concentration, see Figure 2.11.

Indicator Construction: Flexible indicators were fabricated using a vertical device architecture composed of two 80 $\Omega\square^{-1}$ PET-ITO electrodes (Eastman, FLEXVUE) and a 220 µm adhesive spacer material (Nitto Denko, D9605). The working area is a 1 cm^2 area circle. The electrolytes were drop cast and the indicators were manually sealed. For the gel electrolyte, curing was performed with a LOCTITE 500 W mercury vapor bulb for 120 s. Copper tape was added to improve the electrical contact to the power source.

Electrical and Optical Characterization: Electrochemical experiments were carried out on an AUTOLAB PGSTAT100N potentiostat. Optical spectroscopy was performed on a Agilent Cary 300 UV-Vis Spectrophotometer. Digital images were captured with a IDS Imaging UI-3590CP-C-HQ Camera and color corrected using an x-rite colorchecker included in frame for each photo. Analysis of individual electrodes after activation was performed by gently peeling apart the two electrodes, see Figure 2.13. The GPE consistently delaminated onto the electrode with the PEDOT film.

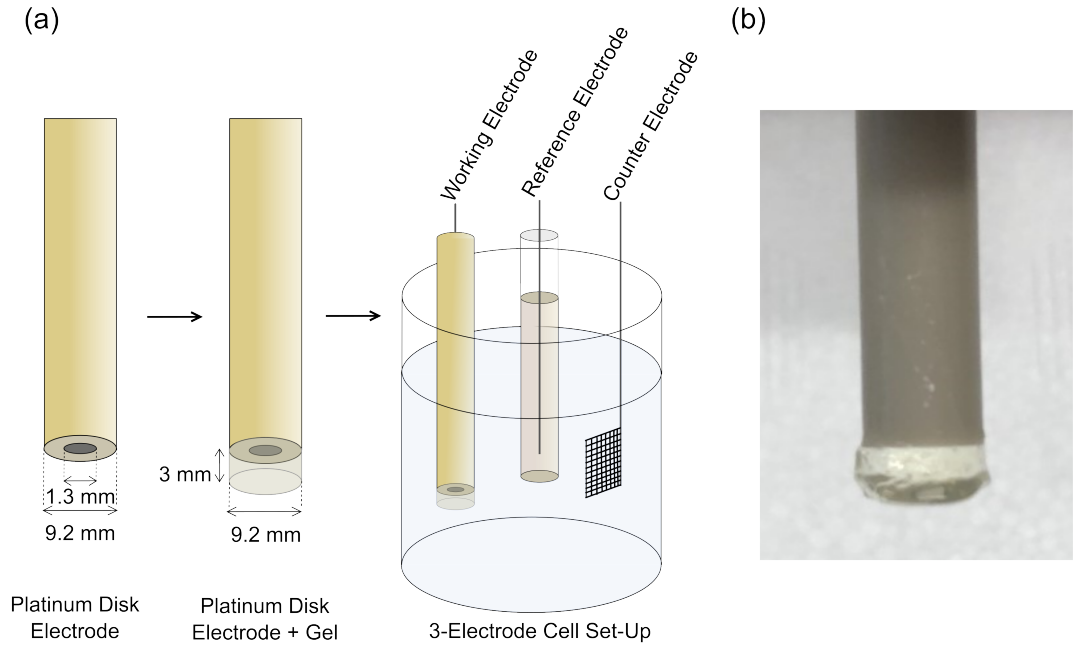

Figure 2.11: (a) Schematic of 3-electrode cell construction and set-up with gel electrolyte sample, and (b) a digital image of the working electrode with a cylinder of cured gel electrolyte.

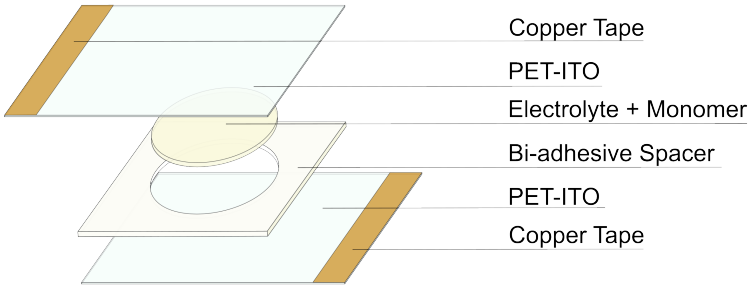

Figure 2.12: Schematic of showing the construction of the indicators.

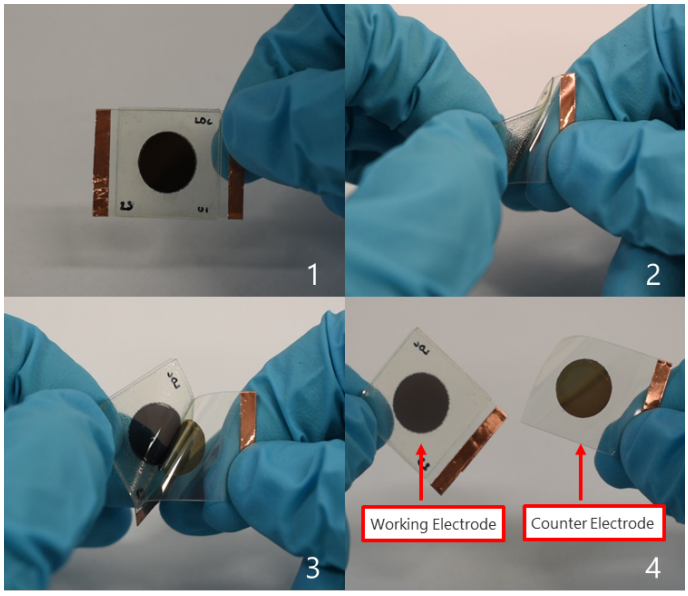

Figure 2.13: Digital images of PET-ITO device separation after *in situ* electropolymerization of 25 mM EDOT. Working electrode with PEDOT film and counter electrode with reduced ITO are identified.

3

Exploration of Indicator Functionality and Color via Monomer Selection and Tuning

The author was the main responsible for the planning, execution, interpretation, and discussion of the work presented in this chapter. Portions of Section 3.2.1 in this chapter were published in the conference paper "Howard, E. L., Pourkheirollah, H. *et al.* Integration of Supercapacitors to Trigger in situ Electropolymerization for Irreversible Visual Indicators. in *2023 IEEE International Conference on Flexible and Printable Sensors and Systems (FLEPS)* 1–4 (2023). doi:10.1109/FLEPS57599.2023.10220370". Section 3.2.2 is original to this dissertation.

3.1 Background and Motivation

To successfully commercialize irreversible electrochromic indicators, it is useful to be able to tune their electrical and optical properties. From an electrical perspective, lowering the activation potential (E_a) and increasing the CE will make it possible to activate the irreversible electrochemical indicators with low-voltage, low-current density power sources. This is critical for smart label applications where the power sources must be small, thin, compact, and light-weight. From an optical perspective, being able to produce irreversible electrochemical indicators that form different colors expands the design opportunities and allows the customer to tailor the color for the specific application.

The E_a of an irreversible electrochemical indicator is primarily determined by the oxidation potential of the monomer system. The CE is primarily determined by the number of electrons transferred in each cross-linking step (typically in the range of 2.07-2.60 F mol^{-1} per monomer reacting [60]), as well as the length and absorptivity of the polymer formed. One avenue to improve both of these parameters is by employing longer oligomers as the precursor monomers of the indicators.

The trends of oligomer series have been studied both experimentally and computationally for many conjugated systems [39], [166]–[173]. In Section 1.3.1 the evolution of the band-gap with increasing number of thiophene rings was highlighted, but trends with conjugation length are observed for other physical and chemical properties of conjugated systems. Figure 3.1 shows the oxidation potential (E_{ox}), and the maximum absorption wavelength (λ_{max}) for oligomers with an increasing number of thiophene units.

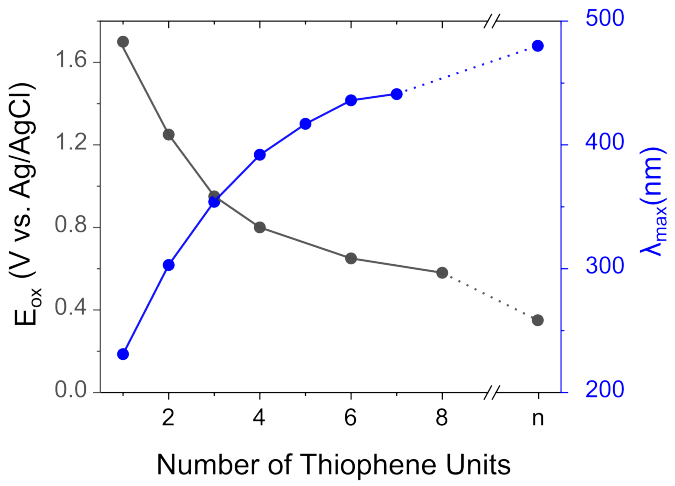

Figure 3.1: Oxidation potential (E_{ox}) and maximum absorption wavelength (λ_{max}) for thiophene oligomers with increasing number of rings. The E_{ox} data is from ref [171] for oxidation in CH_2Cl_2/$TBAPF_6$ vs. Ag/AgCl. The λ_{max} data for thiophene oligomers is from ref. [172], and λ_{max} data for polythiophene is from ref. [174].

Thus, starting with longer chain-length oligomers would directly reduce the activation

potential of the indicators. However, there is a limitation on the length of precursor that can be used. With increasing oligomer length, there is also a decrease in the reactivity of the radical species, a decrease in their stability, a decrease in their solubility, and the absorption spectrum of the precursor will move into the visible range. These properties must be carefully balanced to create an indicator with optimal overall performance.

One route to modify the band-gap of conjugated polymers is the formation of copolymers [175], [176]. The electrical and optical properties of the copolymer can present a mixture of the properties of the corresponding homopolymers and can be tuned by modifying the ratio for the monomers from each component. Copolymerization via electropolymerization is carried out by adding two monomers to the electropolymerization media. The ratio of the monomers in the resultant polymer can be controlled by varying the feed ratio [175].

EDOT has been a popular choice of co-monomer due to the low oxidation potential, environmental stability, and conductivity of PEDOT [155], [157], [158]. Successful copolymerizations have been reported with edot and several other monomer units, such carbazole [177], pyrrole [178], napthalene [179], anthracene [128], and pyrene [180]. Many of the resultant co-polymers exhibit multi-chromism, where the conjugated polymer switches between multiple color states [181]. The formation of multichromic films in *in situ* polymerized devices would be a simple and economical avenue to expand the color-gamut that is available for smart label indicators.

This chapter broadly explores how the selection of precursor monomers can be used to modify the properties of *in situ* polymerized indicators. Section 3.2.1 explores how the electrical properties can be tuned by starting with oligomers as the precursor material instead of a monomer. Section 3.2.2 explores how forming co-polymers with mixtures of two monomer precursors can be used to finely tune the color of the *in situ* polymerized indicators.

3.2 Results and Discussion

3.2.1 Oligomer Approach to Tune Electrical Properties

The monomers EDOT, 2,2′-bis(3,4-ethylenedioxythiophene) (biEDOT), 2,2-bithiophene (bithiophene), and 2,2:5,2-Terthiophene (terthiophene) were evaluated. BiEDOT is the dimer of EDOT and bithiophene and terthiophene are the dimer and trimer respectively of thiophene. The chemical structures of these molecules are shown in Figure 3.2.

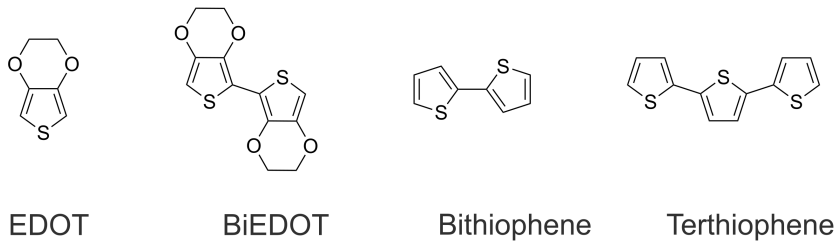

Figure 3.2: Chemical structure of EDOT, biEDOT, bithiophene and terthiophene.

The first scan of CV measurements of the EDOT, biEDOT, bithiophene, and terthiophene indicators are shown in Figure 3.3a. The E_a of the irreversible electrochemical indicator can be identified in the CV by the rapid increase in the current density from monomer oxidation and subsequent cross-linking steps. The E_a of EDOT, biEDOT, bithiophene, and terthiophene are approximately 2.5 V, 2.0 V, 2.6 V, and 2.3 V respectively. Compared to EDOT, using biEDOT results in a 500 mV decrease in the E_a of the indicator, and compared to bithiophene, using terthiophene results in a 300 mV decrease in the E_a of the indicator.

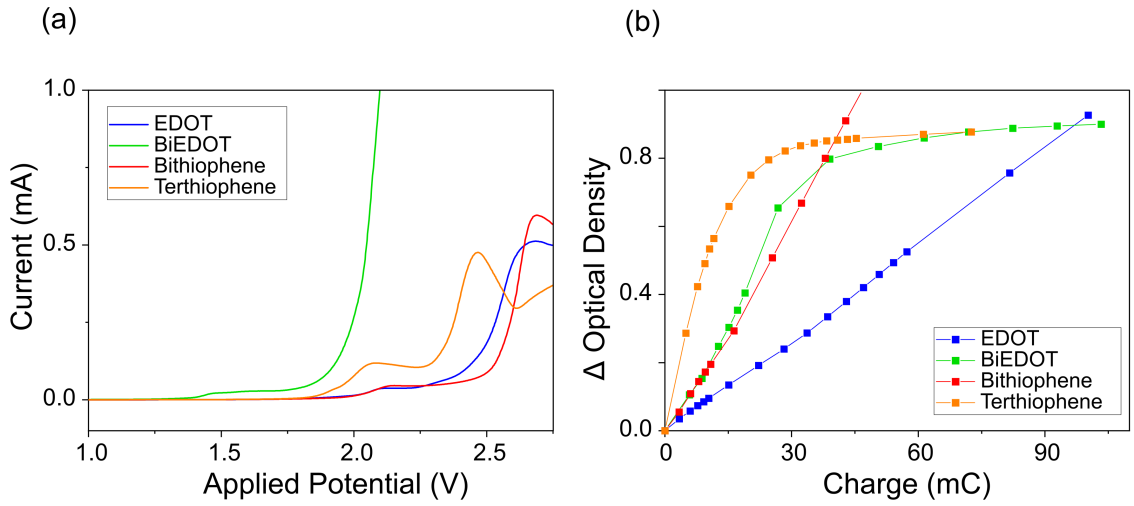

Figure 3.3: (a) First forward scan of a CV of indicators at 10 mV s^{-1}, and (b) change in optical density at 555 nm as a function of current when activated potentiostatically at 3 V.

The change in optical density as a function of charge during potentiostatic activation is shown in Figure 3.3b. For a change in optical density of 0.5, the CE of EDOT, biEDOT, bithiophene, and terthiophene are 9 cm^2 C^{-1}, 24 cm^2 C^{-1}, 21 cm^2 C^{-1} and 49 cm^2 C^{-1} respectively. The coloration efficiency for the indicator with the biEDOT precursor is more

than double the coloration efficiency for the indicator with the EDOT precursor, and the coloration efficiency of the indicator with the terthiophene precursor is around 2.5 times the CE of the indicator with the bithiophene precursor. Starting with an oligomer instead of a monomer means fewer cross-linking steps are required to produce a polymer with the same number of repeat units. Thus, increasing the overall coloration efficiency of the process.

Figure 3.4 shows the absorption spectra of indicators with all four monomers before activation, and after activation. As the conjugation length of the starting species increases, the absorption spectrum will shift out of the UV region and into the visible region. For some applications, it could be beneficial to have the starting species absorbing in the UV region since a transparent to colored visual change may be more visually appealing. The EDOT, and bithiophene indicators have no absorption in the visible spectrum, and the inactivated indicators are visually transparent. The terthiophene indicator has some absorbance in the visible. The biEDOT indicator has a strong absorbance in the visible range and the inactivated indicator is visibly yellow in color.

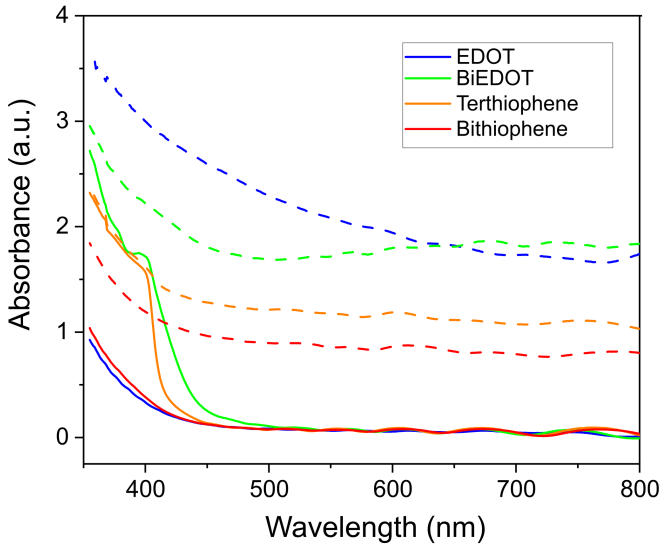

Figure 3.4: Visible absorption spectrum for inactivated (solid line) and activated (dashed line) indicators with 10 mg ml^{-1} EDOT, BIEDOT, bithiophene, and terthiophene as precursor.

Figure 3.5 shows digital images of indicators with all four monomers before activation, after activation, and after activation when the indicators no longer have an applied potential and have drifted back to open circuit potential (OCP). The poly(terthiophene) indicators are orange at OCP, while the poly(bithiophene) indicators are red at OCP. This difference in the color states between the poly(bithiophene) and poly(terthiophene) indicators is likely the result of differing distributions of conjugation lengths in the deposited films. There are conflicting reports on the effect of starting oligomer chain length on the conjugation length of the polymer film that is formed from electropolymeration. A decrease in the

overall conjugation length for films formed with longer oligomers has been reported for oligothiophenes [60], [182], [183], and $\beta - \beta$-disubstituted oligothiophenes [62]. However, other studies have reported an increase in conjugation length or no effect on the conjugation length with increasing starting chain length. [184], [185]. The results seen here suggest that the terthiophene indicator likely reaches a lower degree of polymerization than the bithiophene indicator.

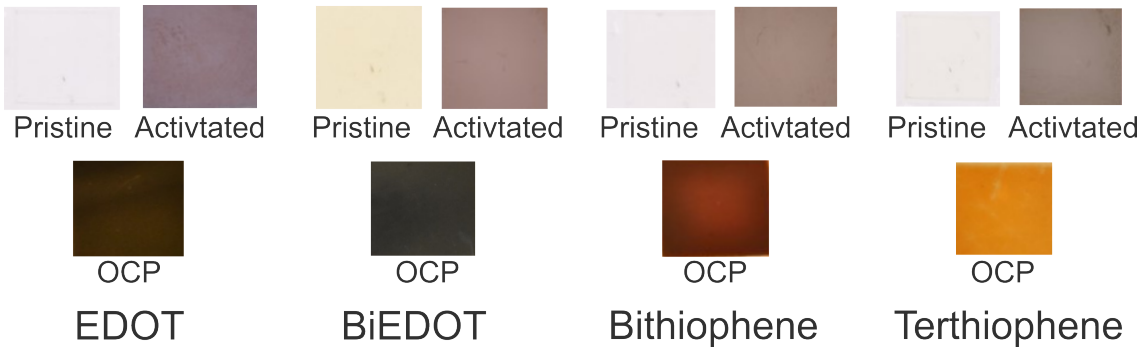

Figure 3.5: Digital images of pristine indicators, activated indicators at activation potential and activated indicators at OCP for 10 mg ml^{-1} EDOT, BIEDOT, bithiophene, and terthiophene as precursor.

3.2.2 Co-Polymer Approach to Tune Optical Properties

3.2.2.1 *In Situ* Electropolymerization of EDOT and Anthracene

There are several reports of the electropolymerization of EDOT-anthracence copolymers and their analogs. These are summarized in Table. 3.1. The broad color palette achieved in these studies, as well as the low-cost and broad commercial availability of anthracene, make it a promising candidate for creating colorful *in situ* polymerized indicators.

Table 3.1: Previous reports of EDOT-anthracene copolymers and analogs.

Monomers	λ_{max}	Supporting Electrolyte	Colors	Ref.
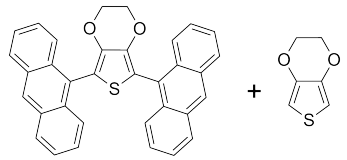	484 nm	BFEE	Violet, Light Yellow, Green, Blue	[154]
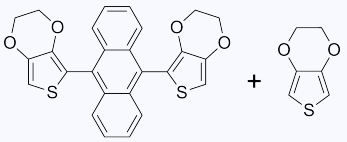	505 nm 519 nm 544 nm 588 nm	0.1 M $LiClO_4$ in ACN	Yellow, Blue, Red, Claret-Red, Gray	[186]
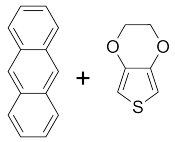	470 nm 503 nm 507 nm	BFEE	Red, Brown, Yellow-Green, Blue-Green, Light-Blue, Dark-Blue	[187]

However, the direct copolymerization of EDOT and anthracene is challenging due to anthracene's high oxidation potential and the low solubility of the monomer and its oligomers [187]. Thus, reports of EDOT-anthracene copolymers have either started with functionalized anthracene derivatives or, utilized BFEE, a strong lewis acid, in the electropolymerization media to lower the oxidation potential of anthracene [60], [179], [188]. But, from a commercial perspective having to undertake costly synthesis steps to functionalize the anthracene is not desirable, and the flammability and acute toxicity of BFEE should prohibit its use in such a consumer electronic application.

A report from Tao *et al.*, explored the copolymerization of 2,5-bis(anthrancen-9-yl)-3,4-ethyldioxythiophene with various thiophene and selenophene derivatives. When they attempt to electropolymerize 2,5-bis(anthrancen-9-yl)-3,4-ethyldioxythiophene in various electrolytic solutions, including BFEE, ACN, and PC, either no polymer film is deposited, or the polymer film is not stable on the electrode, excluding the ability utilize the electrochromic properties of the film. However, when they perform the same electropolymerization in a solid state device with a PMMA based GPE they can deposit a polymer film and operate the device [154]. In Chapter 2 the influence of the Zeospan 8030 GPE on the electropolymerization of EDOT was explored. In this case, we found that the gel lowered the potential required to form a film in an indicator format, and increased the efficiency of the reaction. Based on these results, it is interesting to explore whether the

electropolymerization of EDOT and anthracene in an *in situ* electropolymerized device with the Zeospan 8030 GPE could yield multichromic films.

PET-ITO devices with EDOT:anthracene in 10:0, 9:1, 8:2, and 6:4 ratios were assembled. The total concentration of monomer in the electrolyte was maintained at 25 mM. The first forward scan of a CVs with a scan rate of 50 mV s^{-1} is shown in Figure 3.6a for all of the devices. As the proportion of anthracene in the devices increases, the onset of the anodic current shifts to higher potentials. Three scans of CV were performed in the range of 0 - 3.5 V at a scan rate 50 mV s^{-1}. The third scan of the same CV for the devices is shown in Figure 3.9b. Broad oxidation and reduction peaks are observed in all of the devices and are indicative of polymer film formation.

To study their spectroelectrochemical behavior, glass-ITO indicators were constructed with EDOT:anthracene in 10:0, 9:1, 8:2, and 6:4 ratios. The devices were activated potentiostatically with 3.2 V until 20 mC of charge was consumed. The absorbance spectrum of the devices before activation, and the spectroelectrochemistry of the devices after activation are shown in Figure 3.7. For the inactivated devices, the addition of anthracene leads to increased absorption near the UV range, with a peaks appearing around 358 nm and 378 nm. All of the devices have a change in their absorption spectrum during activation, and the activated devices present electrochromic behavior, where the absorption can then be modulated by changing the voltage applied.

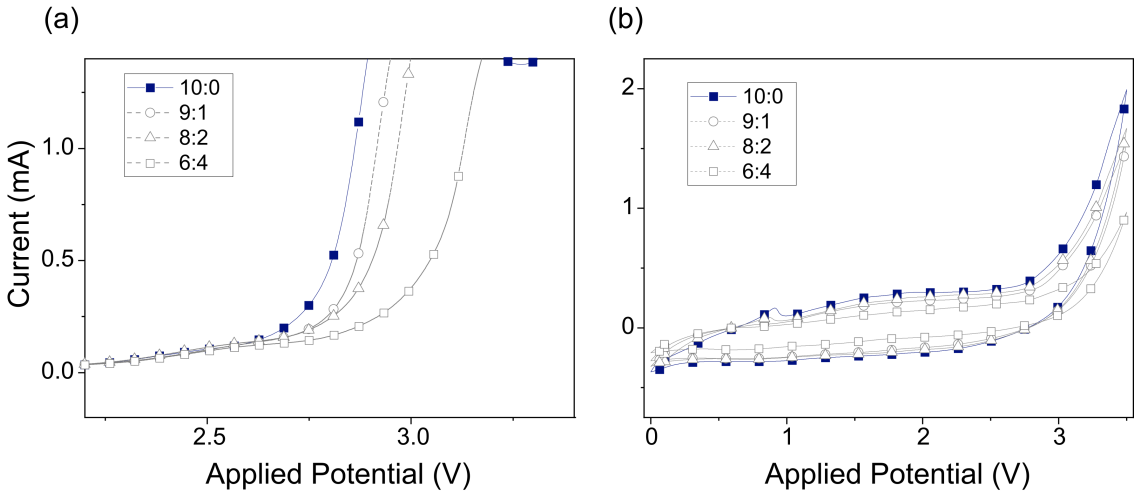

Figure 3.6: (a) First forward scan, and (b) third scan of a CV during *in situ* electropolymerization of devices of EDOT:Anthracene with PET-ITO substrates. Scan rate is 50 mV s^{-1}, and voltage window is from 0 - 3.5 V.

The devices with 10:0, 9:1, and 8:2 exhibit a similar peak around 600 nm. However, an increasing proportion of anthracene leads to a reduction in the absorption of this peak at 600 nm and a relative increase in the absorption in the 400 - 500 nm range. Digital images of the glass-ITO devices are shown at varying potentials in Figure 3.8. For the 10:0, 9:1,

and 8:2 devices, the color change is primarily between two hues.

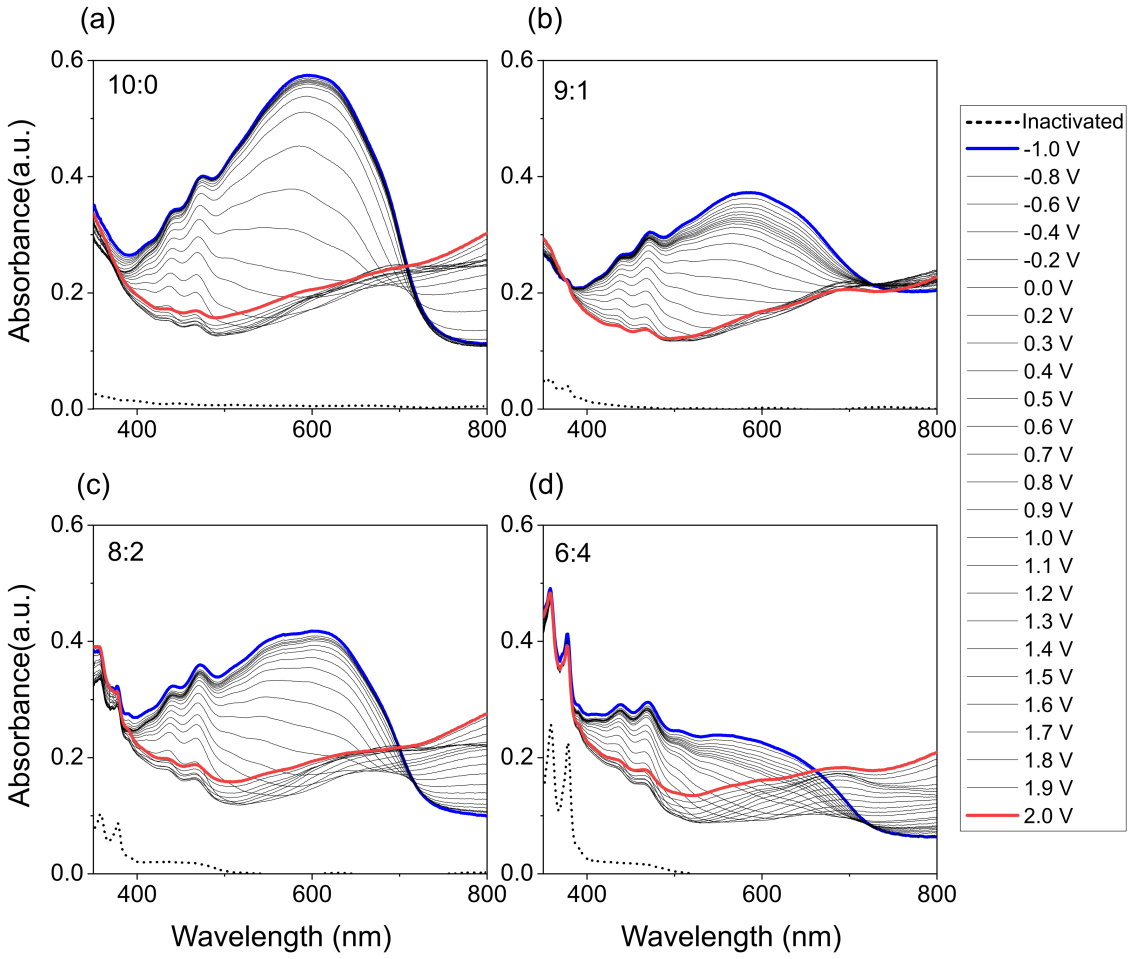

Figure 3.7: Spectro electrochemistry of devices of EDOT:Anthracene with Glass-ITO substrate. Devices have EDOT:Anthracene ratio of (a) 10:0, (b) 9:1, (c) 8:2, and (d) 6:4 and are activated at 3.2 V until total charge of 20 mC is consumed.

In contrast, the device with a 6:4 feed ratio exhibits clear multichromic behavior, with the peaks shifting to different wavelengths at different applied potentials and exhibiting different hues. At lower potentials (-1.0 V), the absorption is broad but with a decrease in the 700 - 800 nm range, yielding a garnet-red color. With increasing potential this shifts to dark-orange, amber, light-green, and then turquoise.

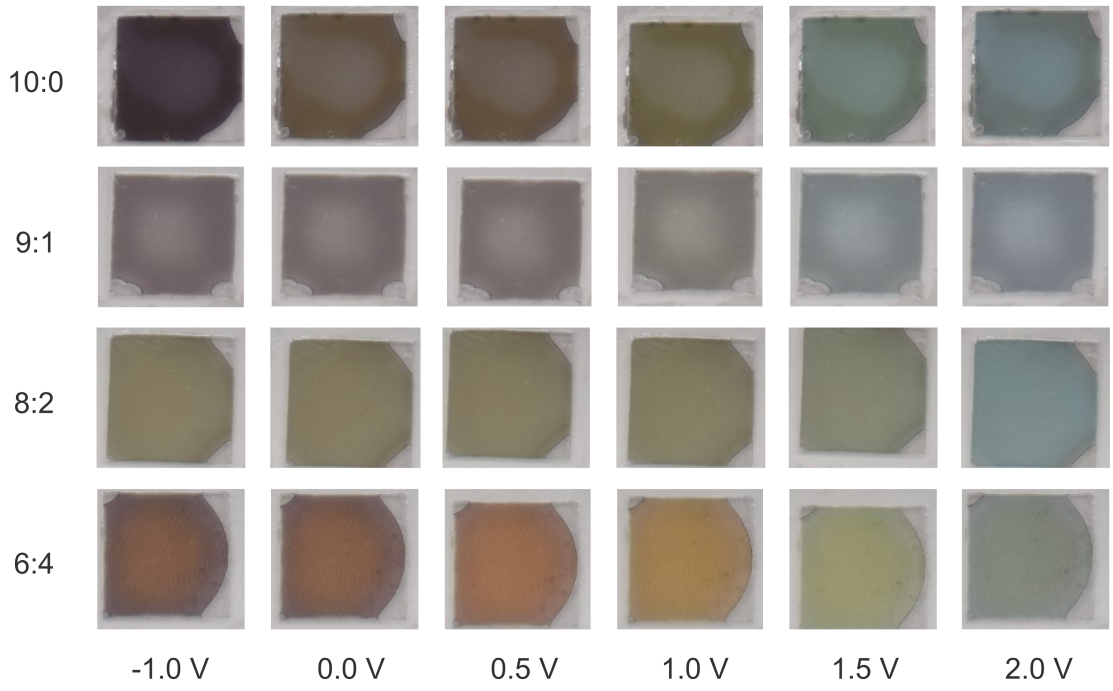

Figure 3.8: Digital Images of devices of EDOT:Anthracene with Glass-ITO Substrate. Devices activated at 3.2 V until total charge of 20 mC is consumed.

3.2.2.2 *In Situ* Electropolymerization of EDOT and Pyrene

Pyrene is another promising candidate for co-polymerization with EDOT. Several prior reports have successfully reported multichromic copolymers based on EDOT, pyrene, and their analogs. These are summarized in Table 3.2. Unlike anthracene, the successful copolymerization of pyrene with EDOT has been demonstrated in standard electropolymerization media such as ACN and dichloromethane (DCM). Thus, the goal here is simply to explore whether the electropolymerization of EDOT and pyrene can also be used in an *in situ* electropolymerized device to form multichromic indicators.

Table 3.2: Previous reports of EDOT-pyrene copolymers and analogs.

Monomers	λ_{max}	Supporting Electrolyte	Colors	Ref.
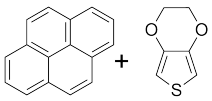	384 nm 409 nm 427 nm	0.1 M TBAP in ACN	Gray-Green, Green, Dark Steel-Blue, Light Steel-Blue, Yellow, Olive, Orange, Light-Brown	[180]
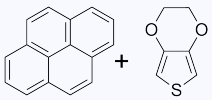	436 nm	$LiClO_4$ in ACN	Not Specified	[189]
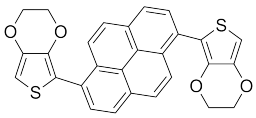	464 nm	0.2 M $NaClO_4$ in 1:1 ACN and DCM	Brown, Grayish-Green, Grayish-Blue, Steel Blue	[190]

The first forward scan of a CVs a scan rate 50 mV s^{-1} for PET-ITO devices with EDOT:pyrene in 10:0, 9:1, 8:2, 6:4, and 0:10 ratios are shown in Figure 3.9a. The total monomer concentration was maintained at 25 mM. The devices with the mixtures of EDOT and pyrene monomer exhibit a lower onset of anodic current than the devices with only EDOT and pyrene. This agrees with the observations made by Zhang *et al.* for EDOT and pyrene copolymers formed in ACN with TBAP as a supporting electrolyte [180]. In their study, they suggest that the lowering of the onset of anodic current indicates that there is an interaction between the two monomers.

The third scan of the same CV for the devices is shown in Figure 3.9b. For the device with only pyrene, two separate peaks are present around 2.9 V, and 0.5 V. Prior studies in ACN and 1,2-dichloromethane show that the electroxidation of pyrene does not yield a polymer, rather only oligomers reaching the maximum of a tetramer [191]. Broad oxidation and reduction peaks are observed in the device with EDOT and the devices with mixtures of EDOT and pyrene. This is indicative of polymer film formation.

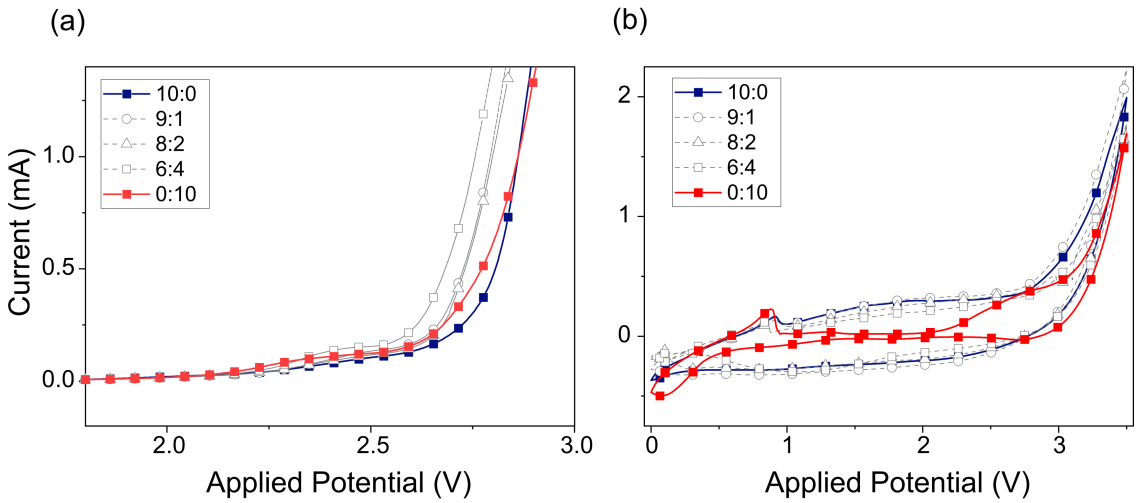

Figure 3.9: (a) First forward scan, and (b) third scan of a CV during *in situ* electropolymerization of devices of EDOT:Pyrene with PET-ITO substrates. Scan rate is 50 mV s^{-1}, and voltage window is from 0 - 3.5 V.

Glass-ITO indicators were constructed with EDOT:pyrene in 10:0, 9:1, 8:2, 6:4, 4:6 and 0:10 ratios. The devices were activated potentiostatically with 3.0 V until 20 mC was consumed. The absorbance spectrum of the devices before activation, and the spectroelectrochemistry of the devices after activation are shown in Figure 3.10. For the inactivated devices, the addition of pyrene leads to increased absorption near the UV range, with a peak appearing around 375 nm. All of the devices have a change in their absorption spectrum during activation. For devices with EDOT and mixtures of EDOT and pyrene the devices present electrochromic behavior, where the absorption can then be modulated by changing the voltage applied, see Figure 3.10 a-e.

The device with EDOT as the starting monomer has a peak with maximum absorption at 595 nm at -1.0 V. This is characteristic of PEDOT films. As pyrene is added to the devices, there is a red-shift of the absorption peak at -1.0 V. The maximum absorption shifts from 595 nm, to 588 nm, to 582 nm, to 567 nm, and then 422 nm for ratios of 10:0, 9:1, 8:2, 6:4, and 4:6 respectively. This observed red-shift suggests that the optical properties of the device arise from the formation of a co-polymer rather than a blend of PEDOT and oligomers of pyrene [180]. The pyrene device, Figure 3.10 e, does not exhibit electrochromism after activation. While the electrochromic behavior of pyrene oligomers and polypyrene has been previously reported, they are prone to over-oxidation at anodic potentials [180], [191].

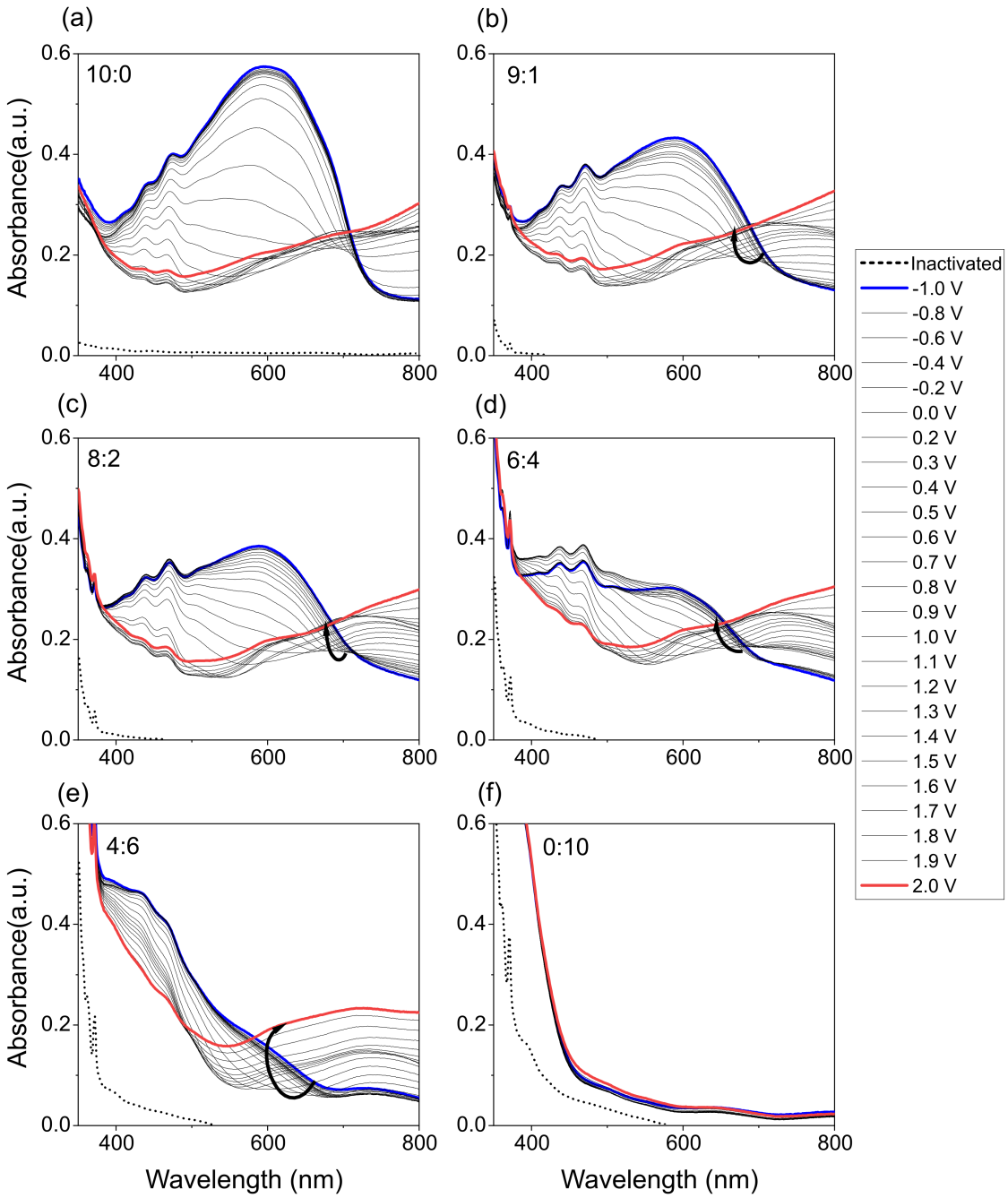

Figure 3.10: Spectroelectrochemistry of devices of EDOT:Pyrene with Glass-ITO substrate. Devices have EDOT:Pyrene ratio of (a) 10:0, (b) 9:1, (c) 8:2, (d) 6:4, (e) 4:6, and (f) 0:10 and are activated at 3 V until total charge of 20 mC is consumed.

Digital images of the glass-ITO devices with 9:1, 8:2, 6:4, and 4:6 ratio of EDOT:pyrene at different voltages are shown in Figure 3.11. The visual colors observed in the devices with mixtures of EDOT and pyrene present a broad range of colors. The device with 4:6 ratio presents clear multichromism with a shift from orange, to amber, to yellow to light-green.

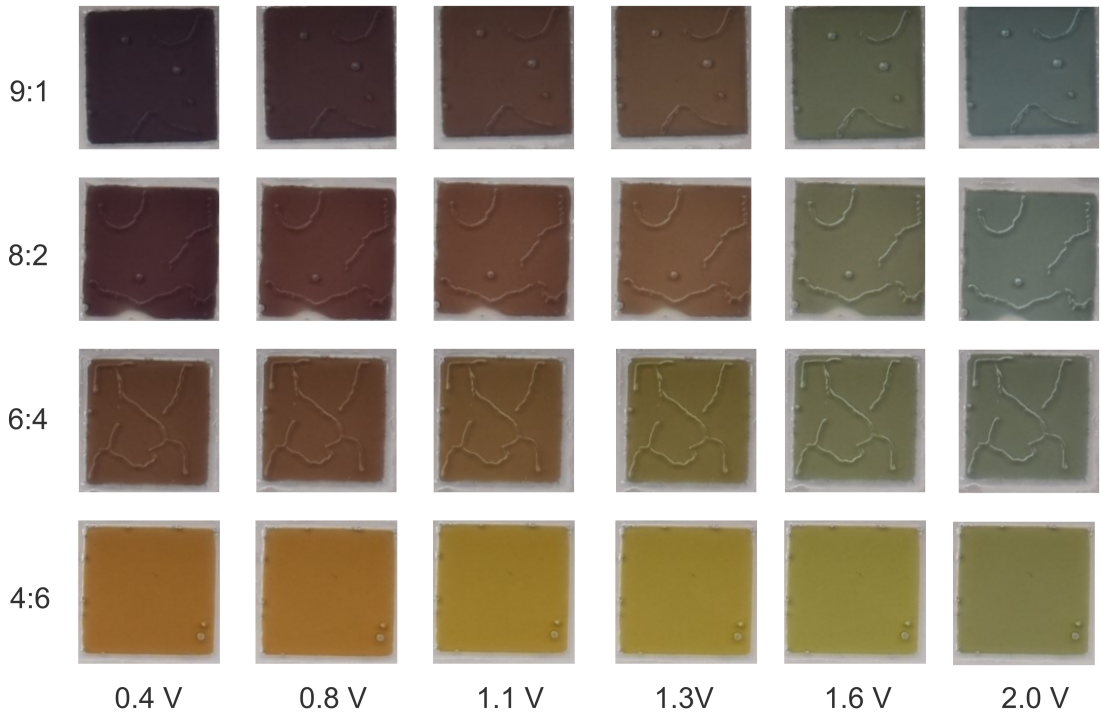

Figure 3.11: Digital Images of devices of EDOT:Pyrene with Glass-ITO Substrate. Devices activated at 3.2 V until total charge of 20 mC is consumed.

3.3 Conclusion

Overall, the results described here show that the electrical and optical properties of irreversible electrochemical indicators can be tuned by the selection of the monomer species. Using mixtures of monomers as precursors for *in situ* polymerized devices is a viable route to create multichromic indicators. The devices with a 6:4 ratio of EDOT:anthracene, and with a 4:6 ratio of EDOT:pyrene both produced films that exhibited color spanning several hues in the visible spectrum.

Utilizing oligomers in place of monomers is a simple and straightforward method to reduce to the activation potential and increase the CE of the indicators. The lowest E_a was observed with biEDOT indicators, requiring only 2.0 V for the electrodeposition. The highest CE was observed with terthiophene at 49 cm^2 C^{-1}. However, longer chain length oligomers present lower stability than their monomeric counterparts. Thus, a critical step to determining the validity of using oligomers would be to evaluate this impact on the overall stability of the indicator. This topic is explored in depth in Chapter 4.

3.4 Materials and Experimental Methods

Oligomer Approach to Tune Electrical Properties

Electrolyte Composition: Electrolyte was produced as outlined in 2.4. 10 mg ml^{-1} of monomer precursor was mixed into the EC:PC:$LiClO_4$ solution before adding the Zeospan 8030 polymer.

Indicator Construction: Flexible devices were fabricated using a vertical device architecture composed of two 80 $\Omega\square^{-1}$ PET-ITO electrodes (Eastman, FLEXVUE) and a 220 µm adhesive spacer material (Nitto Denko, D9605). The working area is a 1 cm^2 square. The electrolyte is cured using a LOCTITE 500 W mercury vapor bulb for 120 s. Copper tape was added to improve the electrical contact to the power source.

Characterization: CVs of the indicators were performed with an AUTOLAB PGSTAT100N potentiostat at a scan rate of 10 mV s^{-1}. Potentiostatic activation of the indicators was performed using the same potentiostat in a Varian Cary 300 UV-Vis Spectrophotometer. The indicators were activated by applying 3.0 V for 300 s. The optical response was monitored by measuring the absorbance of the indicator at 555 nm. The baseline for the optical measurements was air.

Co-Polymer Approach to Tune Optical Properties

Electrolyte Composition: Electrolyte was produced as outlined in 2.4. The monomer precursor was mixed into the EC:PC:$LiClO_4$ solution before adding the Zeospan 8030 polymer. The total concentration of monomer was maintained at 25 mM.

Indicator Construction: Flexible devices were fabricated using a vertical device architecture composed of two 80 $\Omega\square^{-1}$ PET-ITO electrodes (Eastman, FLEXVUE) and a 220 µm adhesive spacer material (Nitto Denko, D9605). The working area is a 1 cm^2 square. The electrolyte is cured using a LOCTITE 500 W mercury vapor bulb for 120 s. Copper tape was added to improve the electrical contact to the power source. Glass-ITO devices were fabricated in the same manner, but using 20 $\Omega\square^{-1}$ (Techinstro, TIXY001) ITO coated glass slides.

Characterization: CVs were performed on the PET-ITO indicators using an AUTOLAB PGSTAT100N potentiostat. The glass-ITO devices were activated by applying a fixed potential on an AUTOLAB PGSTAT100N potentiostat The activation protocol is cut off when the charge delivered to the system reaches 20 mC. Spectroelectrochemistry was performed on glass-ITO indicators in a Varian Cary 300 UV-Vis Spectrophotometer in conjunction with an AUTOLAB PGSTAT100N potentiostat. Spectra were measured from -1.0 V to + 2.0 V in intervals of 0.1 V. The spectra were measured at each potential after

the current response had stabilized. A glass-ITO device with a monomer-free electrolyte was used as a baseline for the measurements.

4

Operating Conditions and Environmental Stability of Irreversible Indicators

The author was the main person responsible for the planning, execution, interpretation, and discussion of the work presented in this chapter. The data collection for sections 4.2.2 and 4.2.3 was performed together with another collaborator. The work reported in this chapter is original to this dissertation.

4.1 Background and Motivation

Considering that one of the key target markets for irreversible electrochemical indicators is logistics monitoring, it is essential that they can function in the diverse environments of the global supply chain. Cargo ships and containers can experience extreme temperature conditions depending on various factors such as the season, time of day, transport route, and weather. A technical report from Xerox Corporation in 2006, measured a maximum temperature of 57 ^{o}C on a container on the route from Japan to Memphis, and a minimum of -29 ^{o}C on the same route [192]. On their website, the Transport Information Service of Germany reports that even in 25 ^{o}C weather, the interior of containers can reach up to 50 ^{o}C [193].

The operating temperature for an electronic component refers to the range of temperature where a device can operate effectively. What is classified as an effective operation may vary depending on the use cases and specific application of the component. In the case of irreversible electrochromic indicators, the two key criteria that will be used to evaluate the performance are the contrast of the activation and the speed of the activation. The rate of coloration at different temperatures is expected to be primarily influenced by the rate of the electropolymerization reaction at different temperatures.

There are several reports on the influence of temperature on electropolymerization. For an electrochemical quartz micro-balance study on the electrodeposition of oligio-p-phenylene, Kvarnstrom *et al.* found that an increase in temperature led to an decrease in the efficiency of the deposition [194]. This is attributed to the solubility of the oligomers decreasing with decreasing temperature, leading to earlier precipitation on the electrode. Sabouraud *et al.* found that at higher temperatures during the electropolymerization of pyrrole, more side reactions occurred with the solvent, and the polymer was more prone to nucleophilic attacks leading to overall more structural defects in the film [195]. Luo *et al.*, and Seki *et al.* both report an increase in the current density for the electrodeposition of EDOT [196], [197].

Another key specification for electronic components is their shelf life or the time that a component can be stored and remain usable. Environmental factors such as temperature, moisture, chemicals, mechanical stress, radiation, biological species, or combinations of these can induce degradation [29]. The overall stability of the irreversible indicators will be determined by the stability of the individual components (substrate, electrolyte, precursor monomer, adhesive) as well as their interactions. In previous reports, limitations in environmental stability of ECDs have been attributed to adverse reactions with atmospheric oxygen and moisture [76], [78], [198]. It can be challenging to perform shelf-life testing in real-time at room temperature, as the experiment may last years. Performing environmental stability tests at higher temperatures can provide key insights into the degradation processes in shorter periods. This is referred to as accelerated aging.

This chapter aims to measure the operational temperature range and the long-term

stability of irreversible electrochemical indicators. Their operational temperature is determined for EDOT based indicators by activating them over a broad range of temperatures and measuring their performance. The shelf-life of the indicators is determined by storing indicators at a 60 °C accelerated aging condition for 147 days, and then measuring their performance at set time points. This was evaluated for EDOT, biEDOT, bithiophene, and terthiophene based indicators to determine the influence of the monomer precursors on the stability. Then the same experiment was performed for EDOT indicators with the addition of different classes of commercial antioxidants and stabilizers in an attempt to improve the stability of the irreversible indicators.

4.2 Results and Discussion

4.2.1 Temperature Dependence on Kinetics of EDOT Indicator Activation

In this section, the performance of EDOT based irreversible indicators is evaluated as a function of temperature. The activation kinetics for EDOT indicators activated between -20 °C and 60 °C are shown in Figure 4.1a, and their current response during the first 100 s of this activation is shown in Figure 4.1b. Three indicators were tested for each temperature and exhibited good reproducibility. Overall, the variation in the final transmittance was less than 5% between the replicas at all temperatures tested.

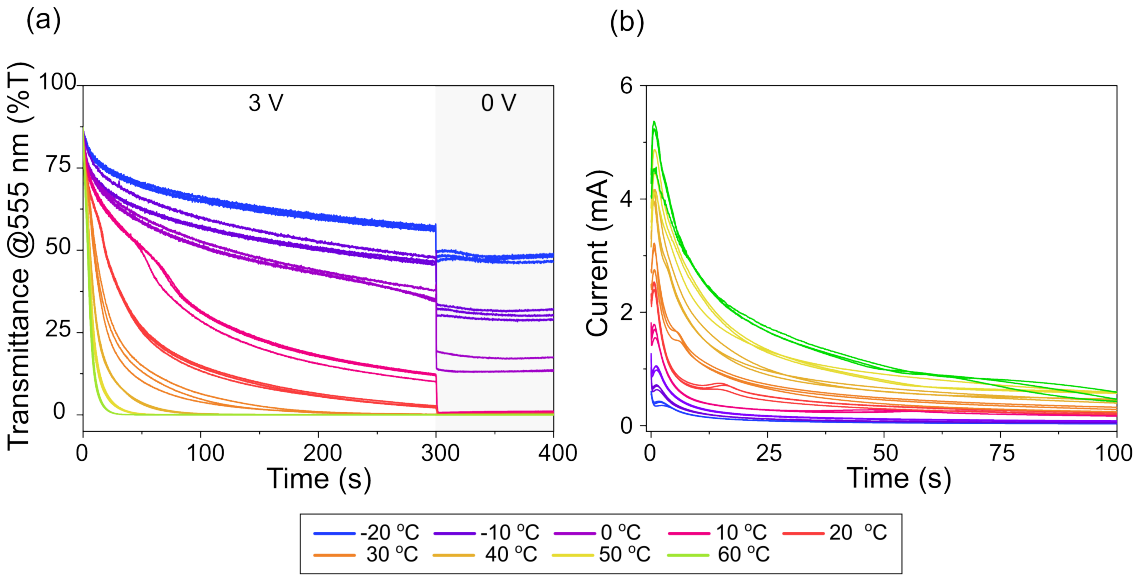

Figure 4.1: (a) Change in transmittance at 555 nm, and (b) current during the activation of 25 mM EDOT indicators over a range of temperatures. Activation was performed by applying 3 V for 300 s and then applying 0 V for 120 s. Three indicators were measured at each temperature from -20 °C to 60 °C in increments of 10 °C.

The EDOT indicators have faster activation with increasing temperature. At 60 °C the indicators drop below 10% transmittance in less than 12 s. At 50 °C this takes 16 s, at 40 °C is takes 30 s, at 30 °C this takes around 60 s, and at 20 °C this takes around 130 s. The indicators activated at 10 °C, 0 °C, -10 °C, and -20 °C do not drop below 10% transmittance during the 300 s activation period.

Digital images of the same indicators are shown in Figure 4.2. For all of the temperatures, there is no clear difference between the triplicates, again indicating good reproducibility between devices. All of the indicators activated at 0 °C and higher show an excellent contrast and appear visually uniform and black. However, the indicators activated below 0 °C show a poor contrast. At -10 °C the activated indicators are a light brown color, and at -20 °C the activated indicators are a yellow color.

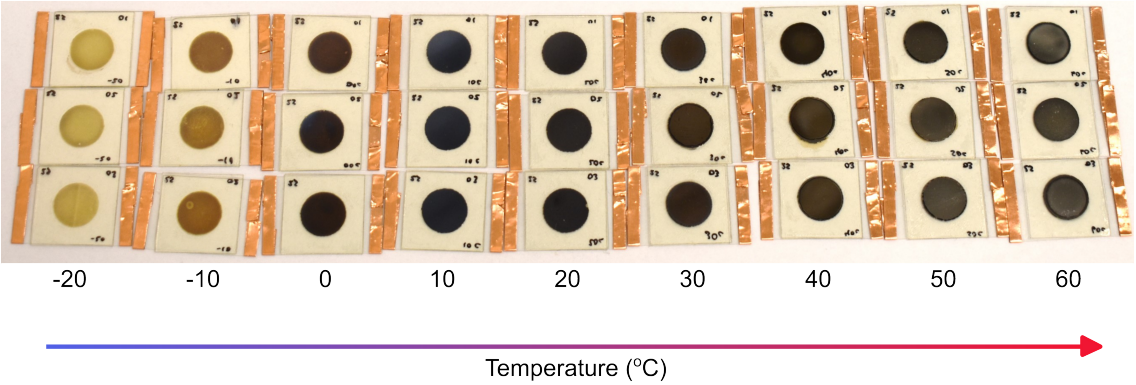

Figure 4.2: Digital images of indicators with 25 mM of EDOT activated over a range of temperatures. Activation was performed by applying 3 V for 300 s, and then applying 0 V for 120 s. Three indicators were measured at each temperature from -20 °C to 60 °C in increments of 10 °C.

After activation, the absorption spectra of each indicator were measured. Then the indicators were delaminated and the absorption spectrum of the working electrode (PEDOT film), and the counter electrode (ITO) were also recorded. The photopic transmittance of the full device, the working electrode, and the counter electrode is shown in Figure 4.3 at each temperature.

The indicators activated at 10 °C and higher all reach a final average photopic transmittance of less than 1%. As previously reported in Chapter 2, the overall coloration of the indicator is a combination of the electropolymerization reaction occurring on the working electrode, and a reduction reaction occurring on the PET-ITO counter electrode. There is a decrease in the photopic transmittance of the working electrode as the temperature during activation increases from -20 °C to 10 °C. This indicates that a thicker PEDOT film is deposited with increasing temperature. But, above 10 °C this trend plateaus. The photopic transmittance of the counter electrode decreases for the indicators activated

at higher temperatures. Images of the counter electrode after activation are shown in Appendix B.1. At lower temperatures, the electrode presents a light brown discoloration, and at higher temperatures, the discoloration is opaque and reflective.

The change in optical density in relation to the charge consumed for the activation of the indicators over the same range of temperatures is shown in Figure 4.4. The relationship between these two metrics defines the CE of the process. For the first 15 mC of charge consumed (Figure 4.4b), the indicators activated at lower temperatures have a slightly higher CE. However, at higher values of charge consumed (Figure 4.4a) this relationship inverts and the CE is greater for indicators activated at higher temperatures.

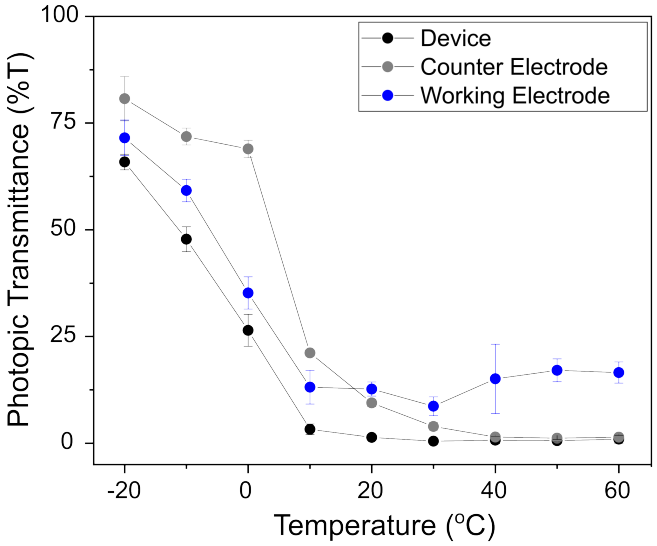

Figure 4.3: Photopic contrast of full device, working electrode, and counter electrode of 25 mM EDOT indicators activated over a range of temperatures. Activation was performed by applying 3 V for 300 s, and then applying 0 V for 120 s. Three indicators were measured at each temperature from -20 °C to 60 °C in increments of 10 °C.

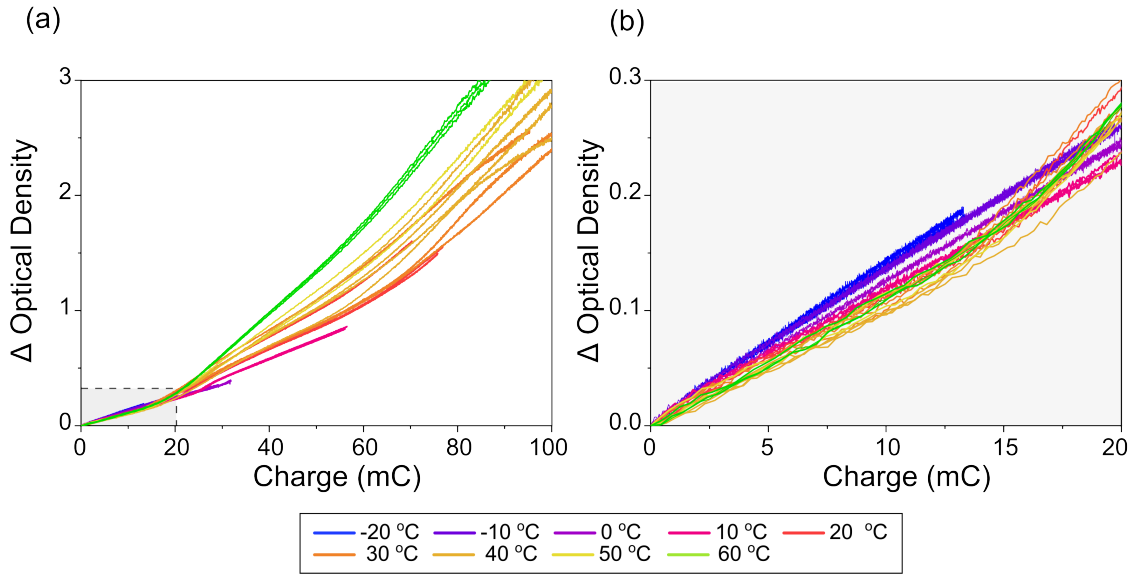

Figure 4.4: Change in optical density vs. charge for 25 mM EDOT indicators activated over a range of temperatures. Activation was performed by applying 3 V for 300 s, and then applying 0 V for 120 s. Three indicators were measured at each temperature from -20 °C to 60 °C in increments of 10 °C.

4.2.2 Influence of Monomer Species on Shelf-Life of Indicators

The environmental stability of irreversible indicators was evaluated by measuring their performance after prolonged exposure to 60 °C. Four variations of the indicator were assembled using the precursor monomers explored in Chapter 3, i.e. EDOT, biEDOT, bithiophene, and terthiophene. Generally, the degradation of the indicators over time was characterized by discoloration in both the active and inactive areas, as well as a reduction in the contrast of the indicator during activation.

Figure 4.5 shows digital images of the indicators before and after activation at 0, 14, 28, 62, and 147 days of exposure to the 60 °C. Over this period, all of the indicators show distinct changes in their visual appearance. Outside of the working area, where there is only the PET-ITO substrate and the adhesive spacer material, there is a gradual yellowing that occurs over time.

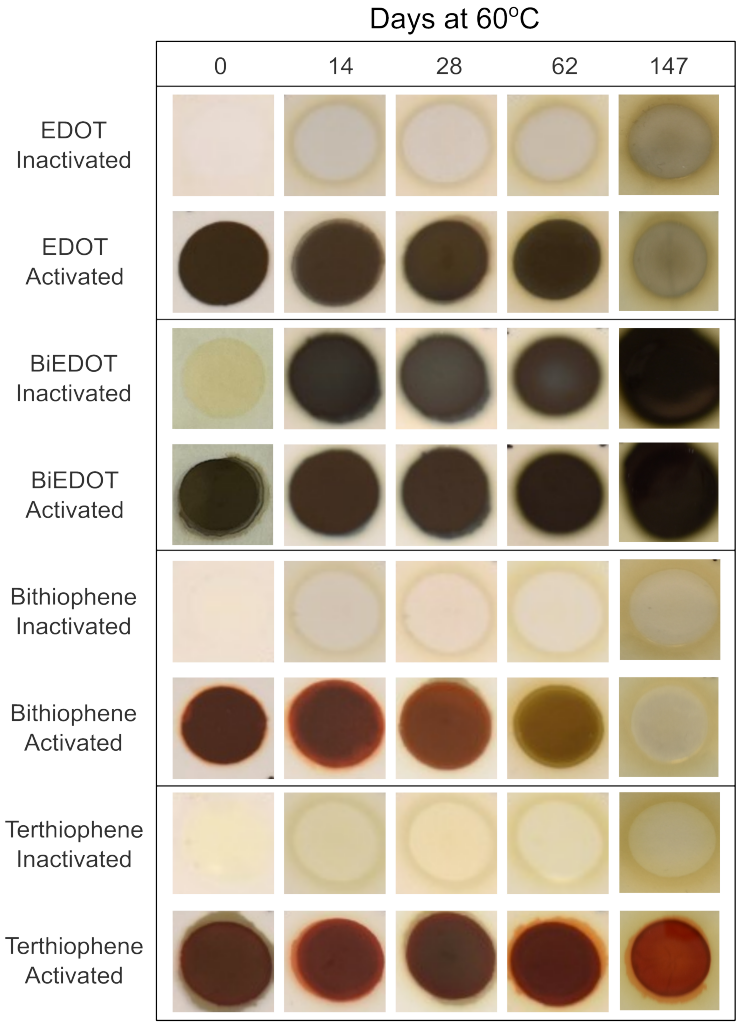

Figure 4.5: Digital images of inactivated and activated indicators with EDOT, biEDOT, bithiophene, and terthiophene after exposure in the oven at 60 °C. The activation protocol was 3 V for 300 s, followed by 0 V for 120 s.

The discoloration in the active area of the inactivated indicators is monitored by measuring their transmittance. This is shown in Figure 4.6a, for 0, 14, 28, 62, 104, and 147 days of exposure. The bithiophene and the terthiophene indicators show the least discoloration over time. The bithiophene indicators drop from an average inactivated transmittance of 86.8 % to 79.8 %, and the terthiophene indicators drop from an average inactivated transmittance of 86.2 % to 78.4 %. The majority of the loss in inactivated transmittance for the bithiophene and terthiophene indicators occurs within the first 14 days (4.6% and 5.8% respectively). From day 14 to day 147 they only present an additional drop in transmittance of 1.8% and 2.0% respectively.

The inactivated transmittance of the EDOT indicators drops from 88.1% to 60.1%. This 28% decrease occurs gradually over the 147-day testing period. The biEDOT indicators

present the strongest discoloration over time. Already at day 14, the inactivated transmittance drops to 34.3%, and by day 62, this reaches 10 %. In prior studies of EDOT oligomers, their instability has been identified and attributed to the high reactivity of the terminal α-positions on the molecules [199]–[201].

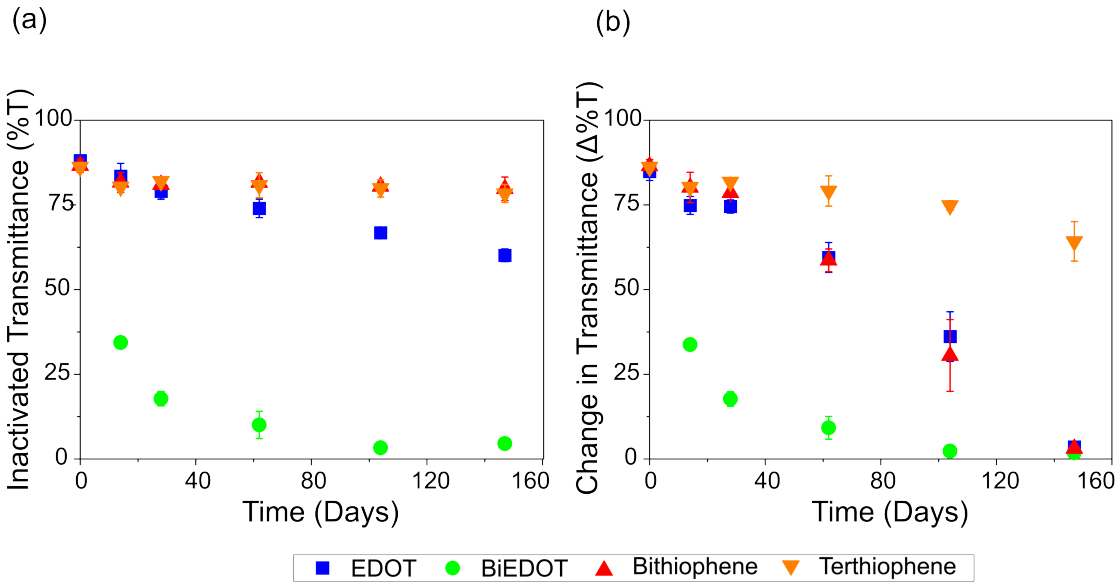

Figure 4.6: Inactivated transmittance (a) and change in transmission during activation (b) for indicators with EDOT, biEDOT, bithiophene, and terthiophene after exposure in the oven at 60 °C. The activation protocol was 3 V for 300 s, followed by 0 V for 120 s. Transmittance is measured at 555 nm.

The change in transmittance during activation for the indicators at 0, 14, 28, 62, 104, and 147 days of exposure is shown in Figure 4.6b. All of the indicators show a decrease in the contrast they can achieve during activation after exposure to 60 °C. The biEDOT indicators show the least contrast during activation at all time points tested. The decrease in the contrast is a result of the discoloration of the inactivated state of the indicator. The EDOT and bithiophene indicators also show a significant decrease in the contrast they can achieve over time, and after 147 days the contrast for both of these indicators reaches zero. In the digital images of Figure 4.5, we can see that the final color state of the bithiophene indicators shifts from a red color on day 0 to a yellow color by day 62 of exposure. The terthiophene indicators present the best performance over time. Before exposure to 60 °C they have an activation contrast of 86.2%, and after 147 days of exposure, have an activation contrast of 64.2%.

4.2.3 Influence of Stabilizers on Shelf-Life of Indicators

One approach to improving the stability of organic and polymeric materials is the addition of antioxidants and stabilizers. Antioxidants are used to inhibit the auto-oxidation and thermal-oxidative that take place in the presence of oxygen [202]–[204]. There are several classes of commercial stabilizers. Primary antioxidants interrupt oxidation by reacting with peroxy, alkoxy, hydroxyl, and alkyl radicals [202]. These are often used in conjunction with secondary antioxidants which react with the hydroperoxides formed by reactions with primary antioxidants [202]. Another class of stabilizer is hindered amine light stabilizer (HALS). While they are conventionally classed as light stabilizers, they have also shown good performance as long-term thermal stabilizers [202], [205].

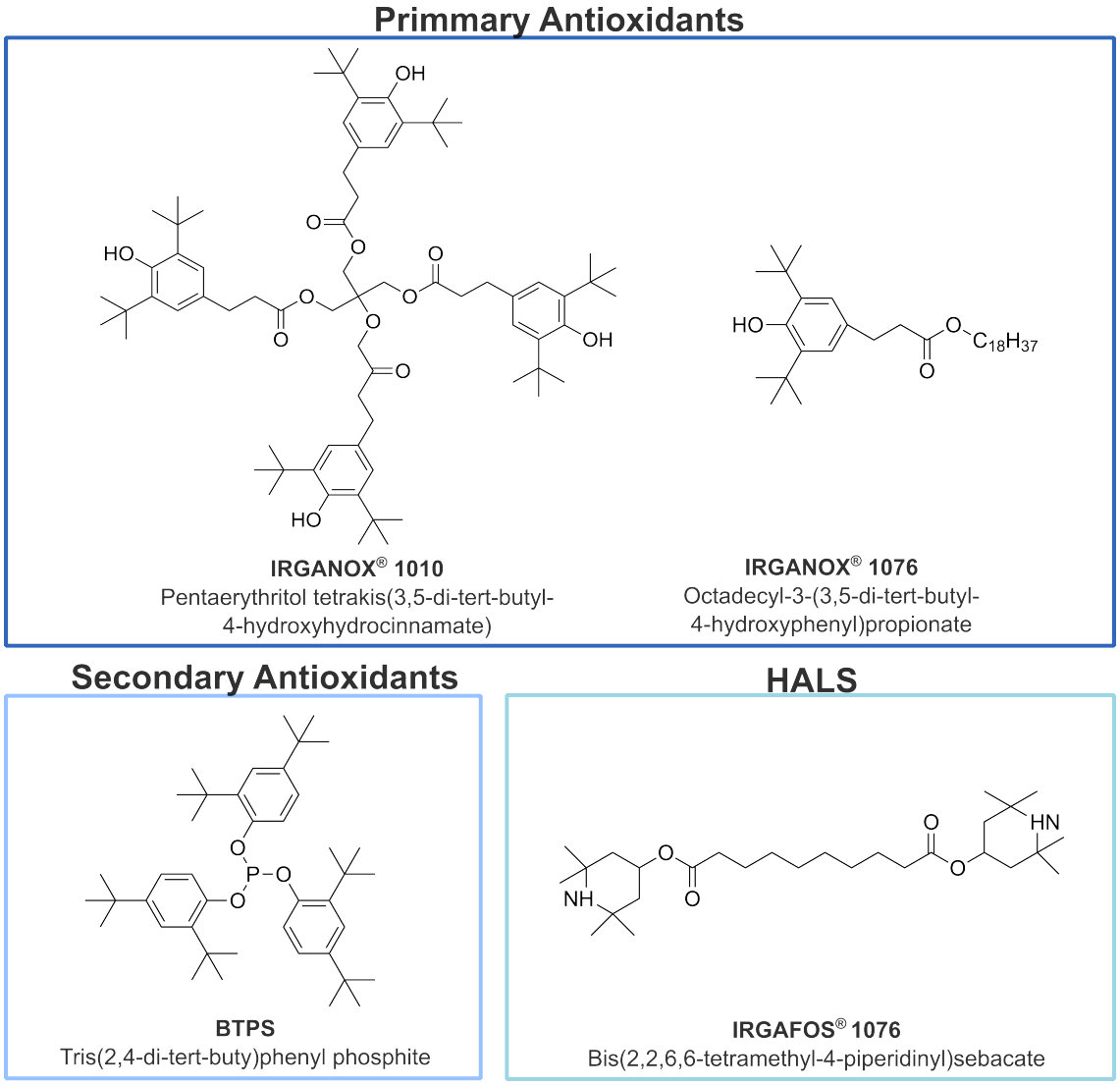

Figure 4.7: Chemical structures of the stabilizers used for the long-term stability studies.

Three stabilizer systems were employed for this study. The first system (referred to as stabilizer 1) consists of bis(2,2,6,6-tetramethyl-4-piperidinyl)sebacate (BTPS), a HALS

stabilizer. The second system (referred to as stabilizer 2) consists of pentaerythritol tetrakis(3,5-di-tert-butyl- 4-hydroxyhydrocinnamate) (IRGANOX 1010) as a primary antioxidant in conjunction with tris(2,4-di-tert-buty)phenyl phosphite (IRGAFOS 168) as a secondary antioxidant. The third system (referred to as stabilizer 3) consists of octadecyl-3-(3,5-di-tert-butyl- 4-hydroxyphenyl)propionate (IRGANOX 1076) as a primary antioxidant in conjunction with tris(2,4-di-tert-buty)phenyl phosphite (IRGAFOS 168) as a secondary antioxidant. The chemical structures of all of these stabilizers are shown in Figure 4.7.

The influence of the stabilizer systems on the stability of the indicators was measured in the same manner as for the monomers is Section 4.2.2. Figure 4.5 shows digital images of the indicators before and after activation at 0, 14, 28, 62, and 147 days of exposure to the 60 °C. Again, all of the indicators show a clear yellowing of the PET-ITO substrate and the adhesive spacer outside of the working area.

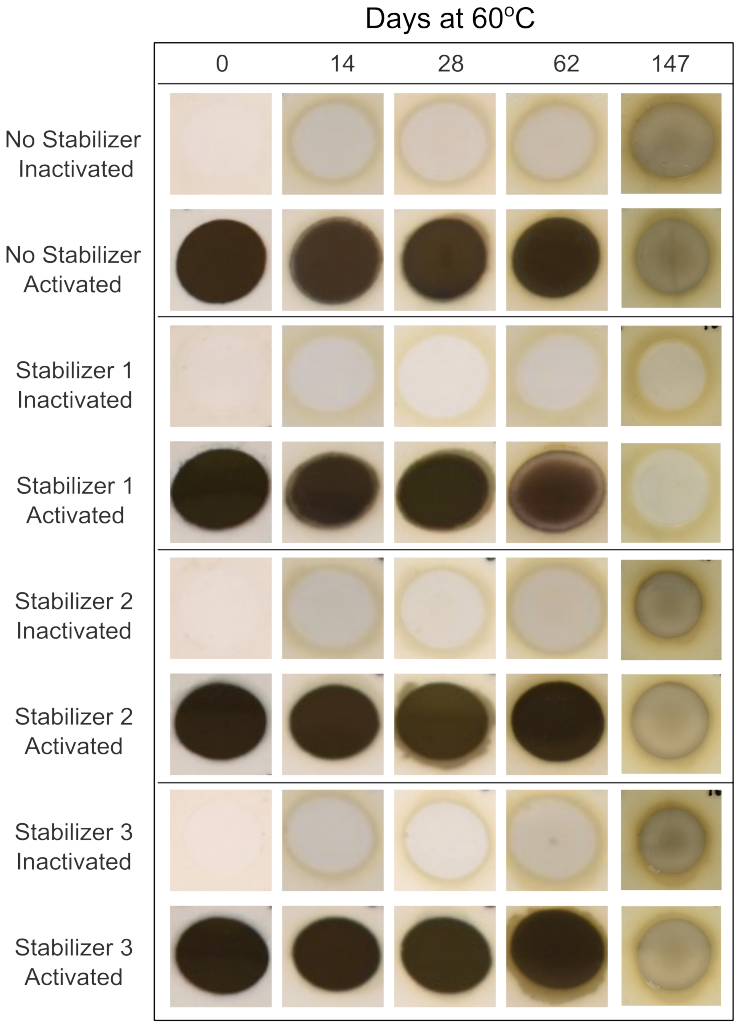

Figure 4.8: Digitial images of inactivated and activated indictaors with stabilizer systems 1, 2 and 3 after exposure in the oven at 60 °C. The activation protocol was 3 V for 300 s, followed by 0 V for 120 s.

The discoloration in the active area of the inactivated indicators was monitored by measuring their transmittance. This is shown in Figure 4.9a, for 0, 14, 28, 62, 104, and 147 days of exposure. The addition of the primary and secondary antioxidant systems (stabilizer 2 and stabilizer 3) has no significant impact on the discoloration of the inactivated indicators. They show degradation very similar to the EDOT indicators without added stabilizer. However, the indicators with the HALS (stabilizer 1) show almost no discoloration in the active area over the 147-day testing period.

The change in transmittance during activation for the indicators at 0, 14, 28, 62, 104, and 147 days of exposure is shown in Figure 4.6b. In this case, the addition of the various stabilizer systems to the EDOT indicators yields no significant improvement in the performance. The indicators with and without stabilizers degrade at a comparable rate in this regard.

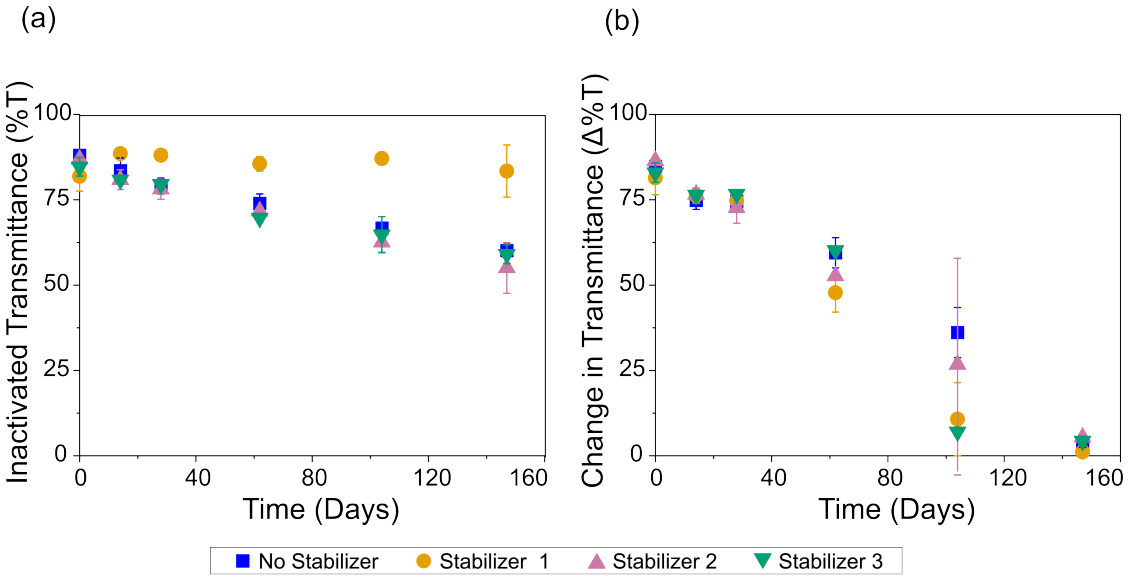

Figure 4.9: Inactivated transmittance (a) and change in transmission during activation (b) for 25 mM EDOT with stabilizer systems 1, 2 and 3 after exposure in the oven at 60 °C. The activation protocol was 3 V for 300 s, followed by 0 V for 120 s. Transmittance is measured at 555 nm.

4.3 Conclusion

This chapter explored the operational temperature range and environmental stability of irreversible indicators. For EDOT based indicators, activation was observed in the full temperature range from -20 °C to 60 °C. However, the coloration becomes sluggish with decreasing temperature, and below 0 °C the indicators did not achieve an opaque final color state. This introduces some limitations to the environments which this indicator could be used, for example, it may not be appropriate for smart labels that need to operate in sub-zero supply chains.

Furthermore, the shelf-life studies indicate that the long-term stability of the indicators is heavily influenced by the stability of the monomer precursor. The greatest stability was seen in the terthiophene indicators, which exhibited minimal loss in performance after 147 days at 60 ^{o}C, while the biEDOT indicators showed strong discoloration within the first 14 days at the same condition. The addition of commercial antioxidants and stabilizers showed limited capacity to improve the shelf-life stability of EDOT indicators. The indicators with the HALS stabilizer maintained the best performance over the 147 days, with almost no discoloration to the inactivated indicator over time. However, after 147 days there was no visible coloration during activation. The primary and secondary antioxidants exhibited almost no change in performance compared to the stabilizer-free indicators. If the primary degradation pathway of the system is due to reaction with atmospheric oxygen and water, a better avenue to improving the stability could be by utilizing substrates and sealants with improved barrier properties [76], [198], [206], [207].

4.4 Materials and Experimental Methods

Temperature Dependence on Kinetics of EDOT Indicator Activation

Electrolyte Composition: Electrolyte was produced as outlined in 2.4. 25 mM of EDOT precursor was mixed into the EC:PC:$LiClO_4$ solution prior to adding the zeospan 8030 polymer.

Indicator Construction: Flexible devices were fabricated using a vertical device architecture composed of two 80 $\Omega\square^{-1}$ PET-ITO electrodes (Eastman, FLEXVUE) and a 220 µm adhesive spacer material (Nitto Denko, D9605). The working area is a 1 cm^2. The electrolyte is cured using a LOCTITE 500 W mercury vapor bulb for 120 s. Copper tape was added to improve the electrical contact to the power source.

Characterization: All measurements were performed in a Binder MKF056-230V Alternating Climate Chamber. Samples were acclimated in the oven for 10 minutes before each measurement. Optical spectroscopy was performed on an Agilent Cary 300 UV-Vis Spectrophotometer. Optical fibers were inserted through the ports on the sides of the chamber and fixed to a probe holder designed for measuring films. The activation of the indicators was measured by following the transmittance at 555 nm, the peak of human photopic vision. Potentiostatic device activation of 3 V for 300 s was performed with an AUTOLAB PGSTAT100N potentiostat. The cables of the potentiostat were contacted via a port on the side of the chamber. The set-up for this measurement in shown in

Influence of Stabilizers and Monomers of Shelf-Life of Indicators

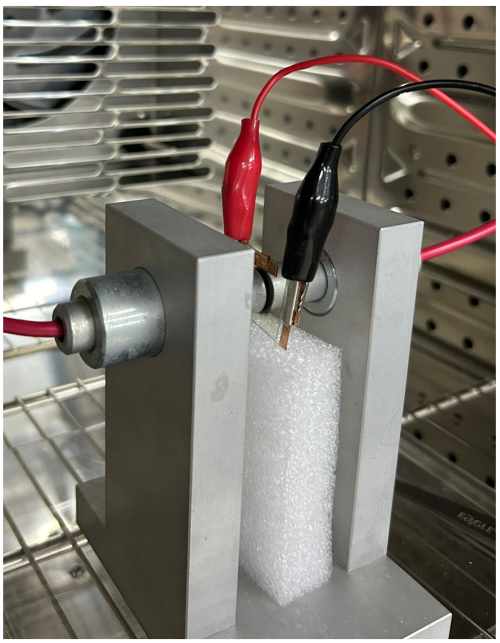

Figure 4.10: Experimental set-up for measuring indicator activation kinetics at different temperatures inside a climate chamber. The optical fibers are connected to a spectrophotometer.

Electrolyte Composition: Electrolyte was produced as outlined in Section 2.4. 10 mg ml^{-1} monomer precursor was mixed into the PC:EC:$LiClO_4$ solution prior to adding the zeospan 8030 polymer.The three stabilizer systems were 0.5 wt% Bis(2,2,6,6-tetramethyl-4-piperidinyl)sebacate (BTPS) (referred to as stabilizer 1), 0.1 wt% Pentaerythritol tetrakis(3,5-di-tert-butyl-4-hydroxyhydrocinnamate) (IRGANOX 1010) + 0.02 wt% Tris(2,4-di-tert-butyl)phenyl phosphite (IRGAFOS 168) (referred to as stabilizer system 2), and 0.1 wt% Octadecyl-3-(3,5-di-tert-butyl-4-hydroxyphenyl)propionate) (IRGANOX 1076) + 0.02 wt% Tris(2,4-di-tert-butyl)phenyl phosphite (IRGAFOS 168) (referred to as stabilizer system 3). The stabilizers were mixed by adding them to vials of electrolyte and leaving them on the roll mixer overnight.

Indicator Construction: Flexible devices were fabricated using a vertical device architecture composed of two 80 $\Omega\square^{-1}$ PET-ITO electrodes (Eastman, FLEXVUE) and a 220 µm adhesive spacer material (Nitto Denko, D9605). The working area is a 1 cm^2. The electrolyte is cured using a LOCTITE 500 W mercury vapor bulb for 120 s. Copper tape was added to improve the electrical contact to the power source.

Accelerated Aging: All of the samples were stored in a Binder DIN 12800 oven over a four-month time period. The samples were held in specialized 3D printed plastic holders,

see Figure 4.11, to maintain even spacing between the indicators in the oven. The temperature and humidity of the oven were monitored by an Amprobe TR200-A data logger. The average temperature in the oven over the first 28 days of the experiment was 59.9 °C with a standard deviation of 1.0 °C. The average humidity in the oven over the first 28 days of the experiment was 13.6 % relative humidity (RH) with a standard deviation of 9.4 % RH. A plot of the temperature and humidity in the oven over the first 28 days with 10-minute sampling periods is in Appendix B.2.

Characterization: Optical spectroscopy was performed on an Agilent Cary 300 UV-Vis Spectrophotometer. The activation of the indicators was measured by following the transmittance at 555 nm, the peak of human photopic vision. Potentiostatic measurements were performed with an AUTOLAB PGSTAT100N potentiostat. Digital images of the indicators were taken before and after the indicators were activated.

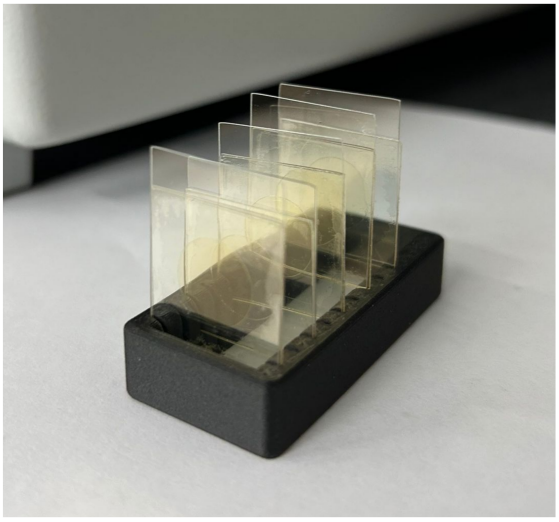

Figure 4.11: Indicators in a 3D printed sample holder for environmental stability testing.

5

Integration of Irreversible Indicators into a Flexible Smart Label

This chapter is based on a manuscript that is in preparation. The work in this chapter is a collaboration with the Institute of Organic Chemistry at the University of Vienna, the Faculty of Information Technology and Communication Sciences at Tampere University, the Faculdade de Ciencias e Tecnologia at the Universidade NOVA de Lisboa, LCR Hallcrest, and Ynvisible in the context of the CHARISMA European Project.

The author was jointly responsible for the planning, and execution of the experimental work. The supercapacitors were independently developed and produced by collaborators at Tampere University. The thermal sensor was independently developed by collaborators at Universidade NOVA de Lisboa, and LCR Hallcrest. The substrates were provided by Ynvisible Production.

Portions of Section 5.2 integrating the irreversible electrochemical indicators with supercapacitors were published in the conference paper "Howard, E. L., Pourkheirollah, H. *et al.* Integration of Supercapacitors to Trigger In-Situ Electropolymerization for Irreversible Visual Indicators. in *2023 IEEE International Conference on Flexible and Printable Sensors and Systems (FLEPS)* 1–4 (2023). doi:10.1109/FLEPS57599.2023.10220370".

5.1 Background and Motivation

The cold chain refers to the channel that moves temperature-sensitive products from production to the end-user. Careful uninterrupted cold-chain management is crucial for transporting a broad range of goods that are either heat-sensitive, cold-sensitive, or both. Examples of goods that may be transported under cold chain management include chemicals, pharmaceuticals, vaccines, biological samples, horticultural products, food, and beverages. For food products, improper storage can not only lead to a drop in quality but also increase risks for contamination and food safety [208], [209]. Improper storage of vaccine products can lead to a decrease in effectiveness, putting human health at risk [210].

Thus, temperature tracking is a central component of managing cold-chain products. IoT and intelligent sensing platforms, such as smart labels and packaging, are well-positioned to address this. There has been a focus by researchers to develop smart elements, such as sensors, power sources, RFID tags, and displays, that can be manufactured onto common substrates in a low-cost, high-volume manner [209]. Several research reports have demonstrated printed smart labels with RFID and NFC carriers [211]–[213]. One example of a printed smart label was demonstrated by Thin Film Electronics ASA for temperature detection which also includes a visual display element [214].

Irreversible electrochromic indicators have unique market potential in this area of smart labels for cold chain applications. Having a visual interface means that users can assess the quality of the product directly on the item. Further, the permanence of the activated color state removes any reliance on the electronics after the temperature has been breached. To produce a working prototype of a flexible smart label utilizing the irreversible indicator, it needs to be integrated with a power source and a temperature sensor on a flexible substrate. These elements need to be able to provide sufficient voltage and power at the correct temperature threshold to trigger the *in situ* electropolymerization reaction.

The incorporation of an energy storage module into a smart label allows them to function over a prolonged period without reliance on external power grids. Over the past decade, researchers have become increasingly interested in SCs, an alternative to batteries for electrical energy storage [215]. The benefits of SCs over conventional rechargeable batteries include high power density, lightweight, long cycle life, low internal resistance, short charge/discharge times, wide temperature range of operation, recyclability, and a low environmental impact [215]–[222]. While previous studies [223] have demonstrated reversible switching of electrochromic displays using SCs, electropolymerization requires a significantly greater voltage and charge than reversible redox switching of the corresponding polymer.

One method to develop sensors that produce a change in electrical conductivity in response to temperature is by using first-order liquid-solid phase transitions in percolated composite materials [224]. For example, Zheng *et al.* demonstrated two orders of magnitude

change in electrical conductivity at 18 °C for suspensions of graphene in hexadecane [225]. In this case, the increase in conductivity when the temperature drops below 18 °C is the result of the agglomeration of the graphene sheets along the grain boundaries during the phase change. Other reports of composite materials with solid-liquid phase conductivity transitions have been reported with other nanoparticles including copper nanowires, carbon nanotubes, graphite nanofibers, and carbon black [226]–[230]. In this study, we employ a thermal sensor developed by Behera *et al.* composed of carboxylic acid functionalized multi-wall carbon nanotubes in a mixture of hexadecane and 1-hexadecanol [231]. They report an electrical conductivity switching ratio of $\sim 10^3$ upon a decreasing temperature ramp in the range of 11 °C to 15 °C.

This chapter explores the integration of the irreversible electrochromic indicators with the other flexible electronic components developed by partners in the European Union Horizons 2020 ITN CHARISMA (reference number 814299) project. In Section 5.2.1 the activation of indicators with printed SCs is characterized. This is performed for EDOT, biEDOT, bithiophene, and terthiophene indicators. Then, in Section 5.2.2 a flexible smart label is demonstrated with a chemical thermal sensor, printed supercapacitors, and the indicators on a PET substrate with a screen-printed silver circuit. Smart labels are assembled and characterized using both EDOT and terthiophene irreversible indicators.

5.2 Results and Discussion

5.2.1 Activation of Irreversible Indicators with Printed Supercapacitors

The electrical properties of EDOT, biEDOT, bithiophene, and terthiophene indicators, calculated in Section 3.2.1, are summarized in Table. 5.1.

Table 5.1: Key electrical properties of irreversible electrochemical indicators based on different monomer systems.

Monomer System	Activation Potential (V)	Coloration Efficiency ($cm^2\ C^{-1}$)
EDOT	2.5	9
biEDOT	2.0	24
bithiophene	2.6	21
terthiophene	2.3	49

The electrical properties of the printed aqueous SCs are summarized in Table. 5.2. The initial voltage is the potential measured across the SCs after they have been fully charged, and the capacitance is the ratio between the charge transferred between the electrodes to the potential between them. The equivalent series resistance is the resistive component of the system. In an ideal capacitor, this should be zero. As the number of SCs in series increases, the initial voltage increases, and the overall capacitance decreases.

Table 5.2: Key electrical properties of printed supercapacitors connected in series.

Number of SCs	Initial Voltage (V)	Overall Capacitance (mF)	Equivalent Series Resistance (Ω)
1	1.2	170	7.5
2	2.4	85	15
3	3.55	60	22

All four indicator systems were activated using both two and three SCs connected in series. The transmittance across the indicators and the voltage across the SCs were recorded simultaneously. The results are shown in Figure 5.1. When the SCs are connected in series with the indicators, if the initial voltage of the SC is greater than the E_a of the indicators then the *in situ*-polymerization will begin. The film forming process will proceed as the SC module discharges until the voltage of the module drops below the E_a of the indicator. At this point, the potential is too low to oxidize further monomers within the indicator and feed the electropolymerization reaction.

While both two and three SCs in series have a high enough initial voltage to begin the activation with the EDOT, since the CE of EDOT is so low, 9 cm^2 C^{-1}, three SCs in series are required to fully activate the indicator with Δ T>80 %. When only two SCs are used, a ΔT of only 55 % is achieved. Bithiophene likewise shows full activation with three SCs, but only a Δ T of 33 % when two SCs are used. Both biEDOT and terthiophene can be fully activated with both two and three SCs in series.

For all the monomer systems tested, faster activation is observed with three SCs than with two SCs, as the speed is dependent on the voltage. The transmittance data for activation with a 3 V coin-cell battery is also shown in Figure 5.1, as this would be an alternative to SCs in a label.

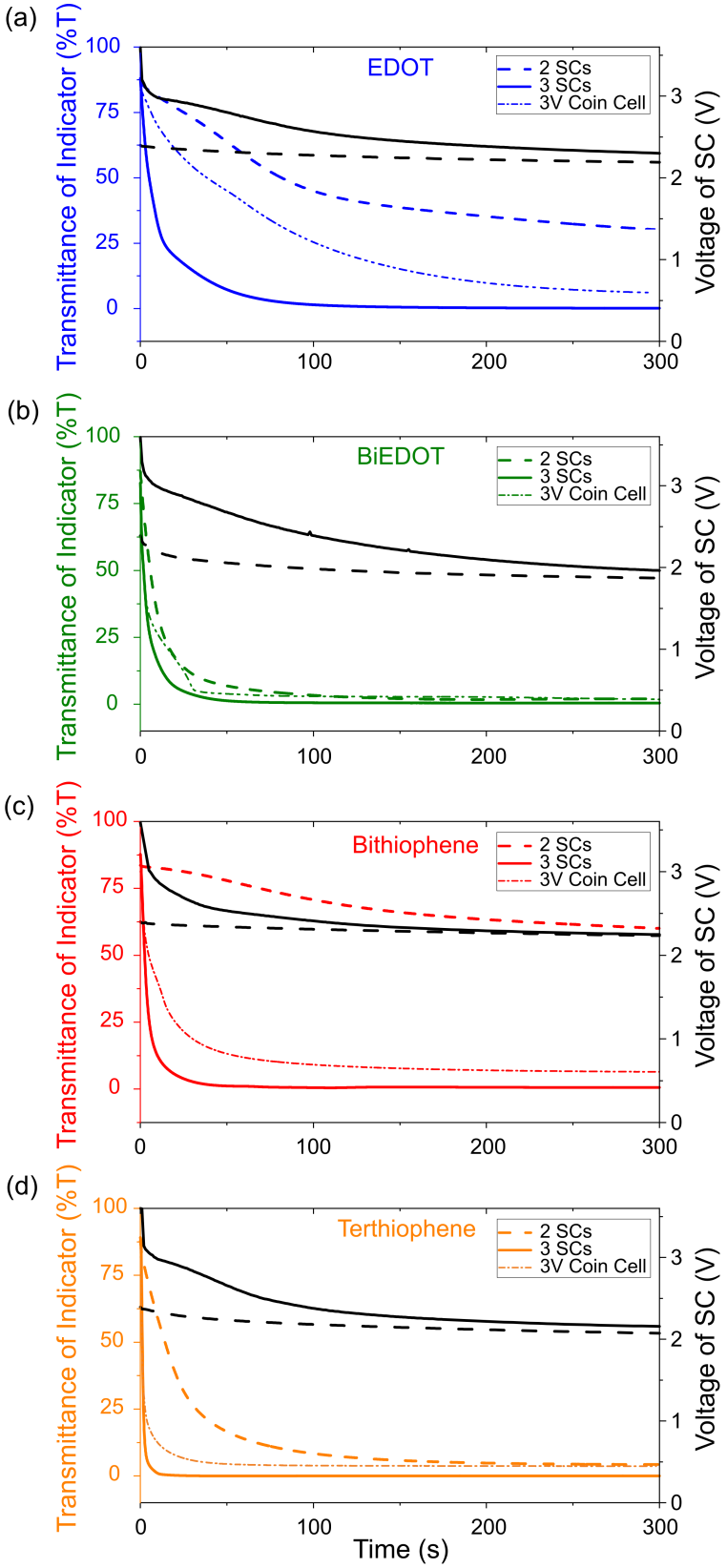

Figure 5.1: Transmittance of indicators during activation with 2 SCs, 3 SCs and a 3 V coin-cell battery for (a) EDOT, (b) biEDOT, (c) bithiophene, and (d) terthiophene. Right y-axis shows the voltage of the SCs during activation.

5.2.2 Integration of Irreversible Indicators into a SMART Label with Chemical Thermal Sensor and Supercapacitors on Flexible Substrate

The smart label was produced by connecting the indicator, SCs and the thermal sensor on a PET substrate with a printed silver circuit. The design of the silver circuit is shown in Figure 5.2a and the layout of the components on the substrate is shown in Figure 5.2b. Both the sensor and the SCs consist of offset conductive substrates and have their electrical contacts in opposing planes. Two segments of the silver circuit were printed on the front side of the substrate, and one segment of the silver substrate was printed on the back side of the substrate with cuts located around the pads. Thus, both the sensor and the SCs were connected with one electrode on the front side, and one electrode on the back side of the substrate.

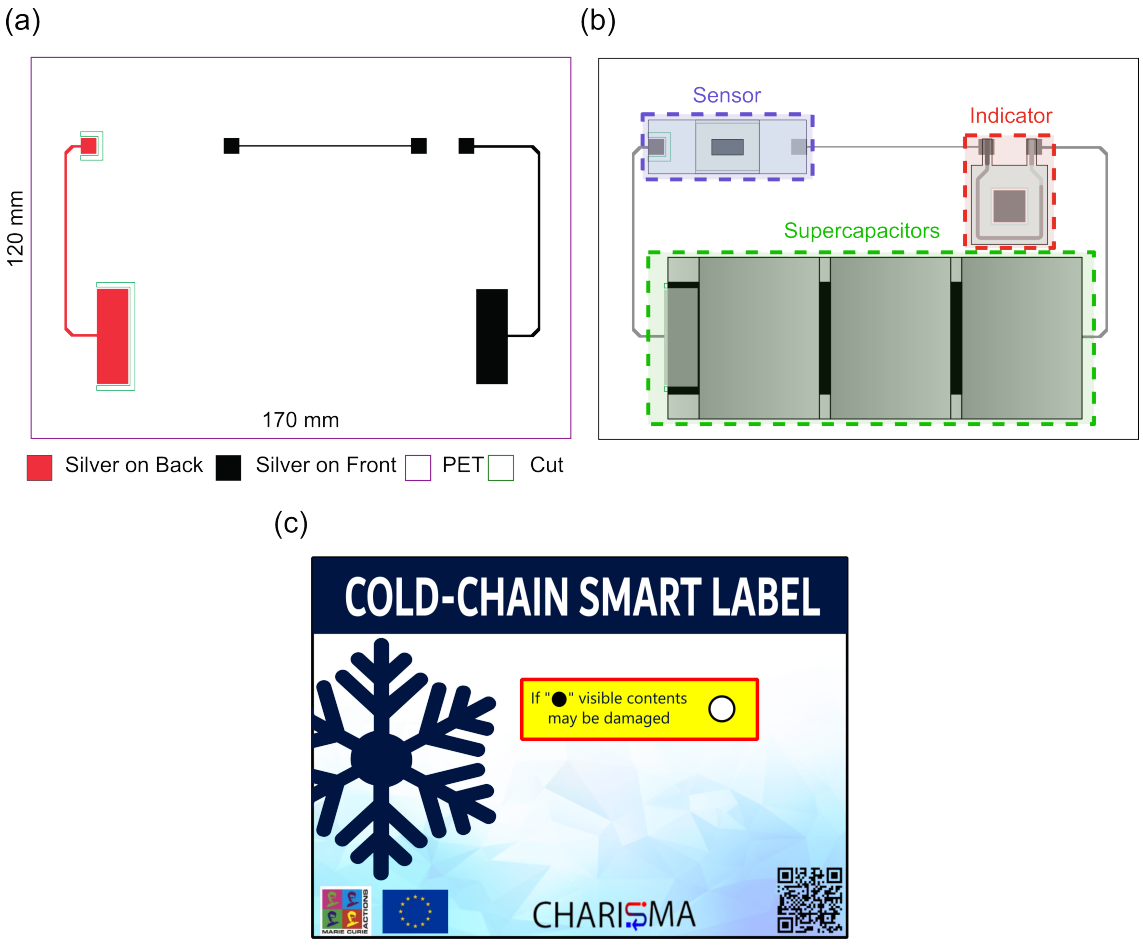

Figure 5.2: (a) Layout of the printed silver circuit and cust on the substrate, (b) layout of the components on the smart labels, and (c) design for the graphical vinyl overlay on the smart label.

The circuit was assembled with three SCs, and all of the elements are connected in series. A graphical design, see Figure 5.2c, was inkjet printed onto a vinyl sticker and then laminated on the front side of the label with a circle cut out in the location of the indicator.

A white piece of paper was mounted behind the label so the inactive indicator appears visually white. The full label was loaded into a climate chamber and then exposed to a decreasing temperature ramp from 30 °C to 0 °C. For a smart label assembled with an EDOT indicator, the voltage across the sensor, SCs, and the indicator during the temperature ramp are shown in Figure 5.3a. The reflectance of the EDOT indicator during the same ramp is shown in Figure 5.3b.

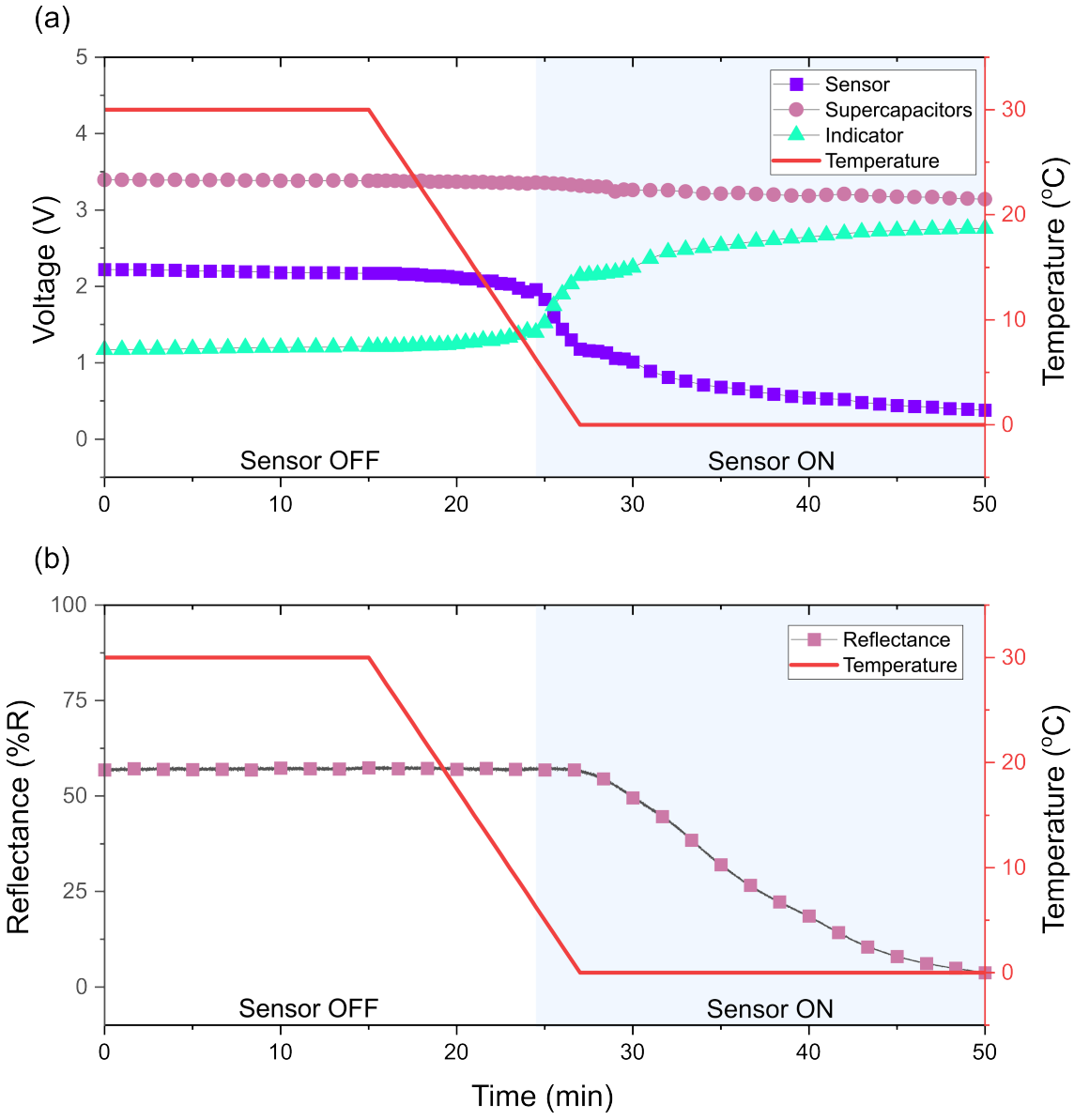

Figure 5.3: (a)Voltages across the sensor, EDOT indicator and SCs, and (b) simultaneous change in reflectance of EDOT indicator when the assembled smart label is exposed to a -2.5 °C min^{-1} ramp rate from 30 °C to 0 °C. Smart label is acclimated at 30 °C for 15 minutes before the start of the ramp. Reflectance is measured at 555 nm.

Previous reports from Behera *et al.* show that the sensor is in its transition state between 6.5 °C and 12.5 °C. In the smart label, a slight decrease in the voltage across the sensor

can be seen around 15 °C, which becomes a sharp decrease in the voltage around 5 °C. As the voltage across the sensor decreases, the voltage across the indicator increases, and a decrease in the reflectance of the indicator is observed. It takes around 18 minutes from when the sharp voltage drop across the sensor is observed until the indicator reaches a reflectance of less than 10%. Digital images of the smart label in the oven before and after the temperature range are shown in Figure 5.4, with insets of the indicator at a range of time points.

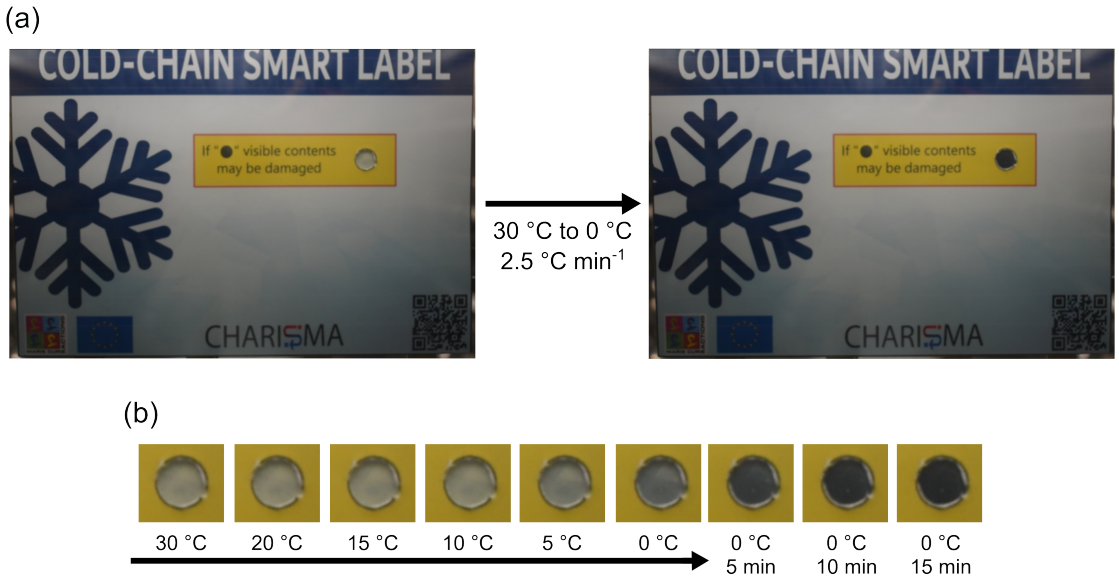

Figure 5.4: (a) Digital images of an assembled smart label inside the climate chamber as it is exposed to a -2.5 °C min^{-1} ramp rate from 30 °C to 0 °C, and (b) images of indicator at various time points during the ramp. Smart label is acclimated at 30 °C for 15 minutes before the start of the ramp. The indicator in the smart label with EDOT monomer in printable electrolyte.

If we compare the rate of activation for the EDOT indicator with three SCsin the integrated circuit to the EDOT indicator activated with three SCs outside of the integrated circuit (Section 5.2.1) we can see that it is substantially slower (20 minutes compared to 1 minute). Even in its more conductive state, the sensor has a resistance in the kilo-ohm range. Since the indicator and the sensor are in series with the SCs, the load is split between the two active elements. When the temperature threshold is reached, the resistance of the sensor decreases, and the voltage shifts to the indicator. However, this process is not instantaneous. The voltage across the indicator never reaches 3 V.

For a smart label assembled with an terthiophene indicator, the voltage across the sensor, SCs, and the indicator during the temperature ramp are shown in Figure 5.5a. The reflectance of the terthiophene indicator during the same ramp is shown in Figure 5.5b. The activation of smart label with terthiophene indicator occurs faster than the activation of the smart label with the with the EDOT indicator. In this case, the indicator drops to a

reflectance of less than 10 %R within three minutes.

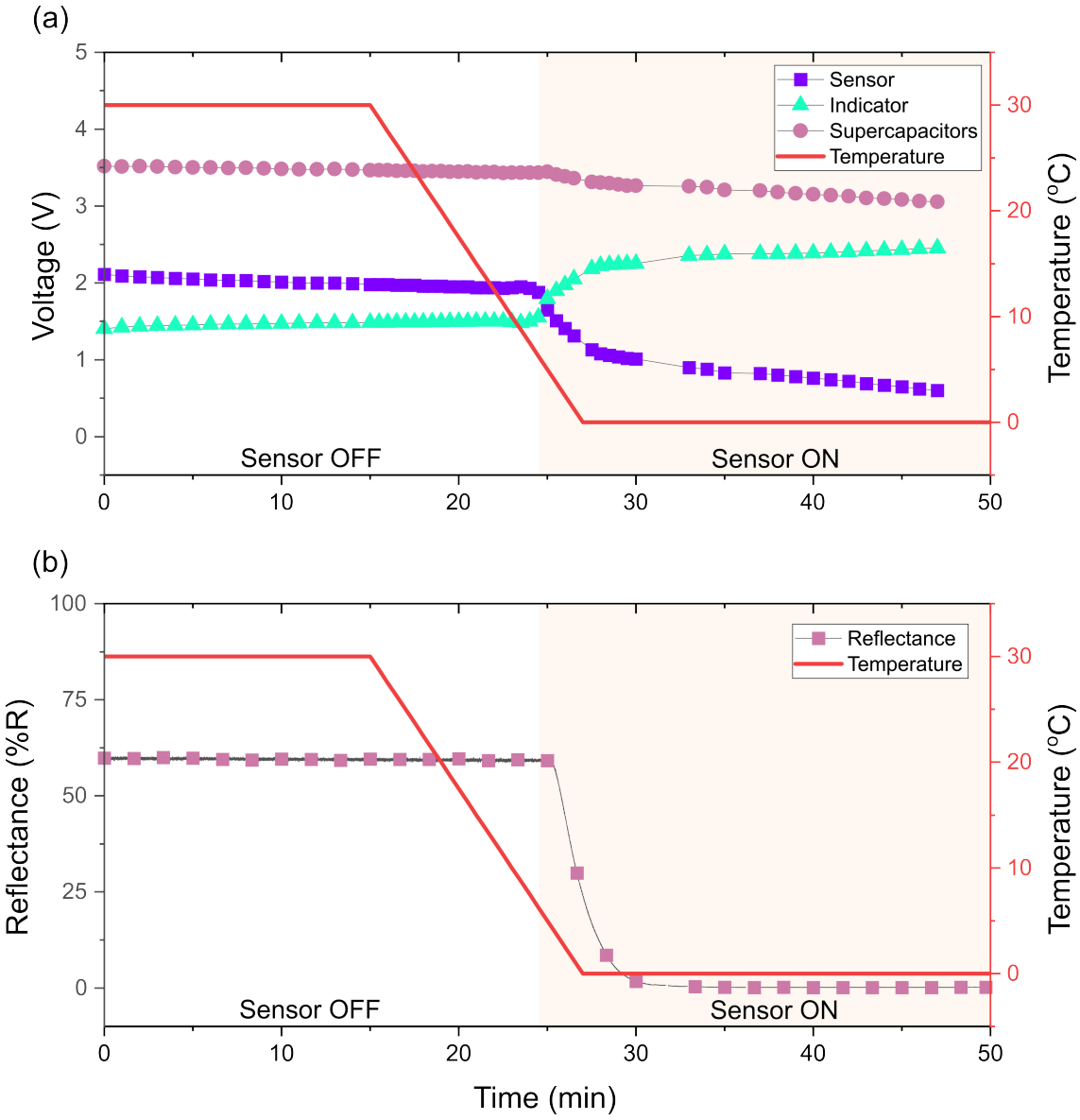

Figure 5.5: (a)Voltages across the sensor, terthiophene indicator and supercapacitors, and (b) simultaneous change in reflectance of terthiophene indicator when the assembled smart label is exposed to a -2.5 °C min^{-1} ramp rate from 30 °C to 0 °C. Smart label is acclimated at 30 °C for 15 minutes prior to the start of the ramp. Reflectance is measured at 555 nm.

5.3 Conclusion

Overall, this study finds that irreversible indicators based on *in situ* polymerization can be effectively activated by printed SCs - showing potential for use in the emerging smart label market. The contrast and the activation speed can be modified by the selection of the monomer precursor used in the indicator, as well as the number of SCs connected

in series. BiEDOT and terthiophene based indicators are particularly promising systems due to their low E_a, and high CE during electropolymerization. Ultimately a flexible smart label, assembled with the same printed SCs and a thermal sensor, was successful in activating both EDOT and terthiophene during a negative temperature ramp. Key limitations to the smart label prototype in its current state are the large size, and the time required to fully activate the irreversible indicator. Further developments would also require improvements to the mechanical durability and environmental stability of the full system.

5.4 Materials and Experimental Methods

Activation of Irreversible Indicators with Printed Supercapacitors

Indicator Electrolyte Composition: A transparent GPE electrolyte was produced as outlined in 2.4. 10 mg ml^{-1} of monomer precursor was mixed into the EC:PC:$LiClO_4$ solution prior to adding the polymer gel.

Indicator Construction: Flexible devices were fabricated using a vertical device architecture composed of two 80 $\Omega\square^{-1}$ PET-ITO electrodes (Eastman, FLEXVUE) and a 220 µm adhesive spacer material (Nitto Denko, D9605). The working area is a 1 cm^2 square. The electrolyte was cured using a LOCTITE 500 W mercury vapor bulb for 120 s. Copper tape was added to improve the electrical contact to the power source.

Supercapacitor Construction: Printed SCs were prepared by the partners at Tampere University of Technology. A double-sided flexible Al/PET substrate was coated with graphite ink (Acheson Electrodag PF-407C) as a current collector on the PET side, while the Al layer served only as a barrier. In order to form an electrode layer, activated carbon ink (Kuraray YP-80F) was applied on the current collector layer using an in-house formulation containing chitosan as a binder. The two layers were achieved using laboratory-scale doctor blade coaters. Afterwards, NaCl:H_2O aqueous electrolyte and a paper separator were added, and the two electrodes were then heat sealed upside down with an annealed adhesive material to form an SC of the electrochemical double-layer capacitor type. The full methodology and characterization of the printed SCs can be found in ref. [232]–[235].

Characterization: The SCs were charged prior to each test by applying 1.2 V across the component for 2 hours. The, the SCs were connected in series using wooden clip to maintain contact between the anode and cathode electrodes. The voltage of the SCs was measured using a FLUKE® 115 handheld multimeter digital CAT III 600 V display (counts): 6000. The indicators were mounted in an Agilent Cary 300 UV-Vis spectrophotometer, where is baseline for the measurement was air. The SCs and indicator were then connected in series using alligator clips, and then the transmittance across the indicator

and the voltage across the SCs were recorded simultaneously. The measurements with the coin cell battery were performed in the same manner, except a 3 V coin cell battery was connected in series with the indicator instead of the SCs.

Integration of Irreversible Indicators into a SMART Label with Chemical Thermal Sensor and Supercapacitors on Flexible Substrate

Indicator Electrolyte Composition: A transparent GPE electrolyte was produced as outlined in Section 2.4. 10 mg ml^{-1} of monomer precursor were mixed into the PC:EC:$LiClO_4$ solution prior to adding the polymer gel.

Indicator Construction: The indicators were constructed using the same printed substrates detailed in Chapter 6. A 220 µm adhesive spacer material (Nitto Denko, D9605) with a 1 cm^2 square working area was added. The electrolyte and precursor mixture were added by drop casting, and then the second substrate was placed and top and sealed with light manual pressure. The electrolyte was cured using a LOCTITE 500 W mercury vapor bulb for 120 s.

Thermal Sensor Construction: The thermal sensors were prepared by the partners at LCR Hallcrest. The full methodology and characterization of the thermal sensor can be found in ref. [231].

Printed Substrate Construction: The silver printed substrate was prepared in an industrial setting (Ynvisible S.A.) using a THIEME LAB1000 sheet-to-sheet screen-printer and according to Ynvisible Industrial Standards and Protocols. The silver was printed on the front of the substrate and cured, and then the substrate was flipped and the silver was printed on the back and cured. The substrates were cut using an Aristomat TL 1310 cutting machine.

Smart Label Assembly: The SCs were charged before each test by applying 1.2 V across the component for 2 hours. The components were connected to the contact pads of the substrate using a double-sided conductive adhesive tape from Laird Performance Materials (DT03B0254R0200). The graphical overlay was printed using an inkjet printer onto a vinyl sticker sheet and then adhered to the back-side of the substrate.

Characterization: The assembled smart labels were placed inside a Binder MKF056-230V Alternating Climate Chamber. The reflectance of the indicator was measured using an Agilent Cary 300 UV-Vis Spectrophotometer with an optical fibre coupler connected to a hand-held UV-Vis reflectance probe with an Ocean fiber optics reflectance probe holder. An image of the optical fiber and the probe holder are shown in Figure 5.6. A labsphere

certified diffuse reflectance standard was used as the baseline for the measurements. Reflectance was measured at 555 nm. The voltage across the indicator and the thermal sensor were measured using a Fluke 115 True RMS Multimeter and a Testboy Digital Multimeter.

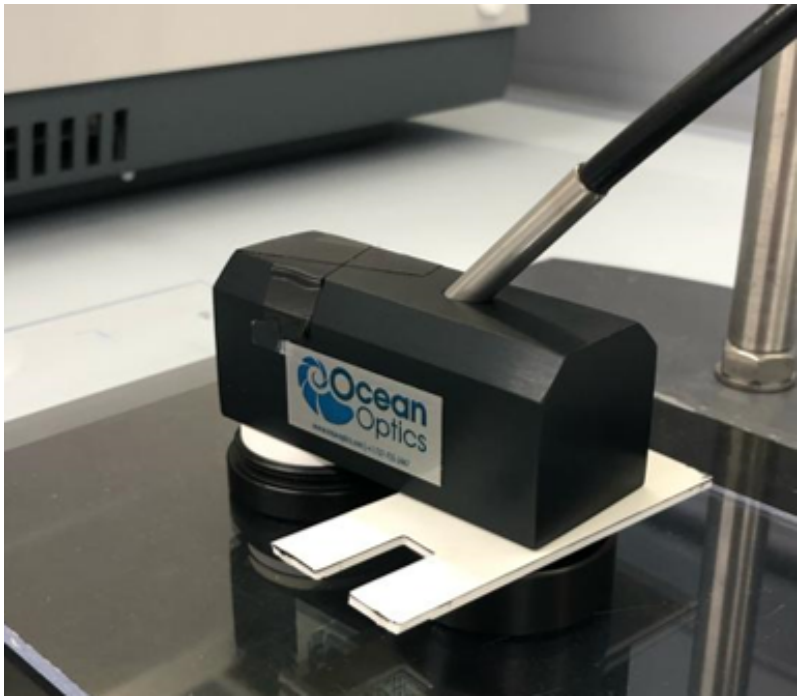

Figure 5.6: Image of optical fiber and probe holder for reflectance measurements. The image is taken while making a blank with the reflectance reference.

6

Fully Printed *In Situ* Polymerized Reversible Indicators

This chapter is based on a manuscript that is in preparation. The work is a result of a collaboration with the Institute of Organic Chemistry at the University of Vienna, the Faculdade de Ciencias e Tecnologia at the Universidade NOVA de Lisboa and Ynvisble. The author contributed to the planning, execution, interpretation, discussion, and preparation of this work. The electrolyte ink used was primarily developed by other collaborators at Ynvisble and the University of Vienna.

6.1 Background and Motivation

In the previous chapters *in situ* electropolymerization has been considered for use in irreversible electrochromic indicators, this chapter focuses on the use of *in situ* electropolymerization for reversible electrochromic indicators. Electrochromic indicators and displays have emerged as a promising candidate to serve as visual interfaces for smart label technologies due to their low-power consumption, and flexible form factor [24], [47], [70]–[73], [142]. However, broad commercialization of electrochromic devices ECDs in smart labels is limited by their high cost compared to non-visual data transmitters such as radio-frequency identification RFID, and near-field communication NFC [209]. Thus, further developments are necessary to lower the manufacturing cost of electrochromic indicators without compromising key operational parameters such as contrast, switching speed, and cycling lifetime.

To this end, *in situ* electropolymerization has been proposed as a simple method to produce electrochromic displays. *In situ* electropolymerization refers to the process of electrochemically depositing a polymer inside a solid-state device [122]. The concept was introduced by the group of Sotzing, and they have reported using a range of different monomer precursors to form the active electrochromic layers in both glass and PET based devices [122]–[127]. They achieve a maximum photopic contrast of 53 % for glass-ITO devices with 2,2-Dimethyl-3,4-propylenedioxythiophene as the monomer precursor [127]. However, a key limitation for *in situ* polymerized ECDs is their low cycling lifetime due to the continued deposition of unreacted monomer on the electrodes. In one report, this was improved by modifying a ProDOT monomer with an acrylate group [123]. The unreacted monomers were UV-crosslinked to the gel electrolyte after the electrochromic film was formed to prevent ongoing electrodeposition on the counter electrode during use. This yielded a lifetime of 10 k cycles with a loss of photopic contrast of only 3%.

Another approach to lowering the manufacturing cost of ECDs is implementing high-volume industrial manufacturing processes, such as screen printing [24], [70], [71]. To the best of our knowledge, there are no reports of using screen printing in conjunction with *in situ* electropolymerization. Combining these two techniques would be beneficial since it can reduce the number of layers that need to be printed during the device assembly process: directly cutting down the production time. Figure 6.1a outlines the manufacturing steps for an ECD using only printing. In this example, there are seven printed layers: silver conductors on both electrodes, an electrolyte layer, a spacer or dielectric separator, an electrochromic layer, and a charge storage layer (in this case, a second electrochromic layer). Figure 6.1b outlines the manufacturing steps for the same ECD using both printing and *in situ* electropolymerization. In this case, two fewer layers need to be printed.

In this work, we employ screen printing in conjunction with *in situ* electropolymerization to optimize the manufacturing of electrochromic indicators. EDOT is used as the precursor monomer to form electrochromic PEDOT films. The thickness of the films is controlled by limiting the charge during the reaction. We use a diffusely reflective, opaque

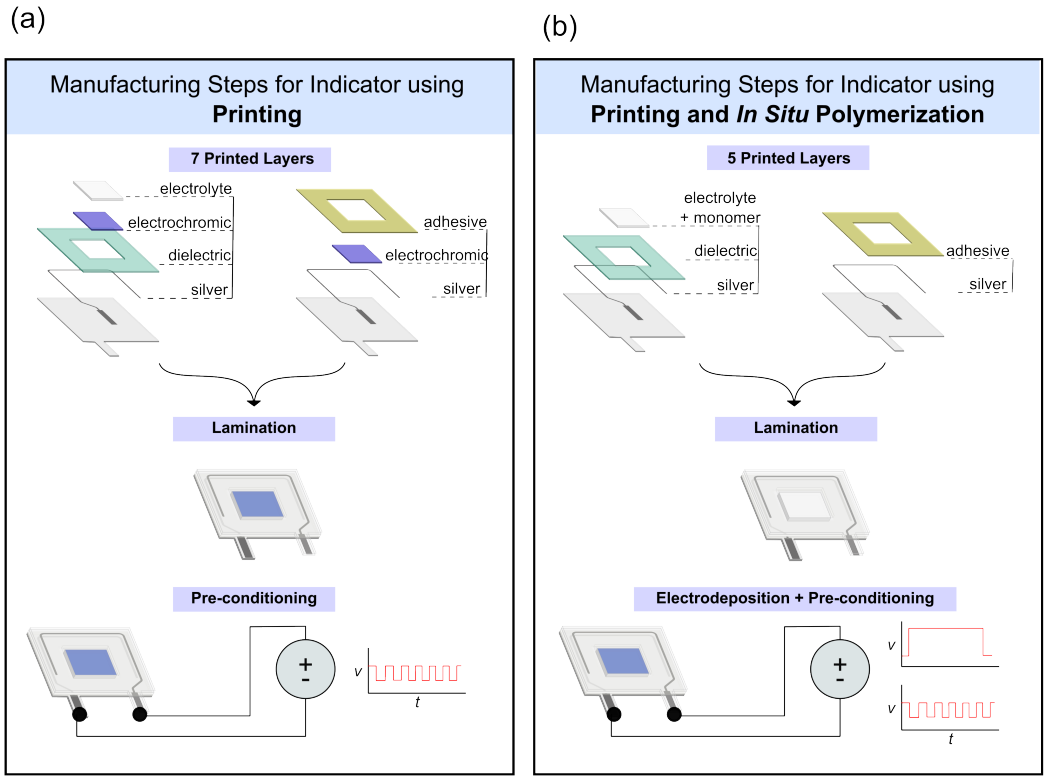

Figure 6.1: Comparison of manufacturing steps for producing an electrochromic indicator using (a) printing, and (b) printing and *in situ* electropolymerization.

electrolyte ink, which is a variation of the electrolyte ink previously reported by Leite *et al.* [236]. One of the key advantages of using an opaque electrolyte, is that an additional electrochromic layer can be deposited on the counter electrode of the device to act as a charge storage material without compromising the overall device contrast (as would be the case with a transparent electrolyte). In this study, we manufacture several variations of electrochromic indicator with different thicknesses of electrochromic film, and with and without a charge storage layer. Then, the performance of the indicators is evaluated based on their optical contrast, switching speed, and cycling lifetime.

6.2 Results and Discussion

6.2.1 Indicator Printing and Construction

The indicators were printed on two separate ITO coated PET substrates and then laminated. The silver, dielectric, and adhesive layers of the indicator were prepared in an industrial setting (Ynvisible S.A.) according to Ynvisible Industrial Standards and Protocols using a THIEME LAB1000 sheet-to-sheet screen-printer. The first substrate was prepared by printing silver paths followed by a layer of adhesive. The second substrate was prepared

by printing silver paths, followed by a layer of dielectric ink. The electrolyte layer was added to the second substrate using a benchtop A4 screen printer with a 100/40 screen. Then, the two substrates were laminated using a weighted roller, and the electrolyte was UV-cured (LOCTITE® UVALOC 97035 with a 1000 W Mercury doped lamp, 1600 mJ s^{-1}). The individual indicators were separated from the sheets using a cutting machine. An image of the screen printing environment, the electrolyte ink after printing, and the configuration of the stack are shown in Figure 6.2.

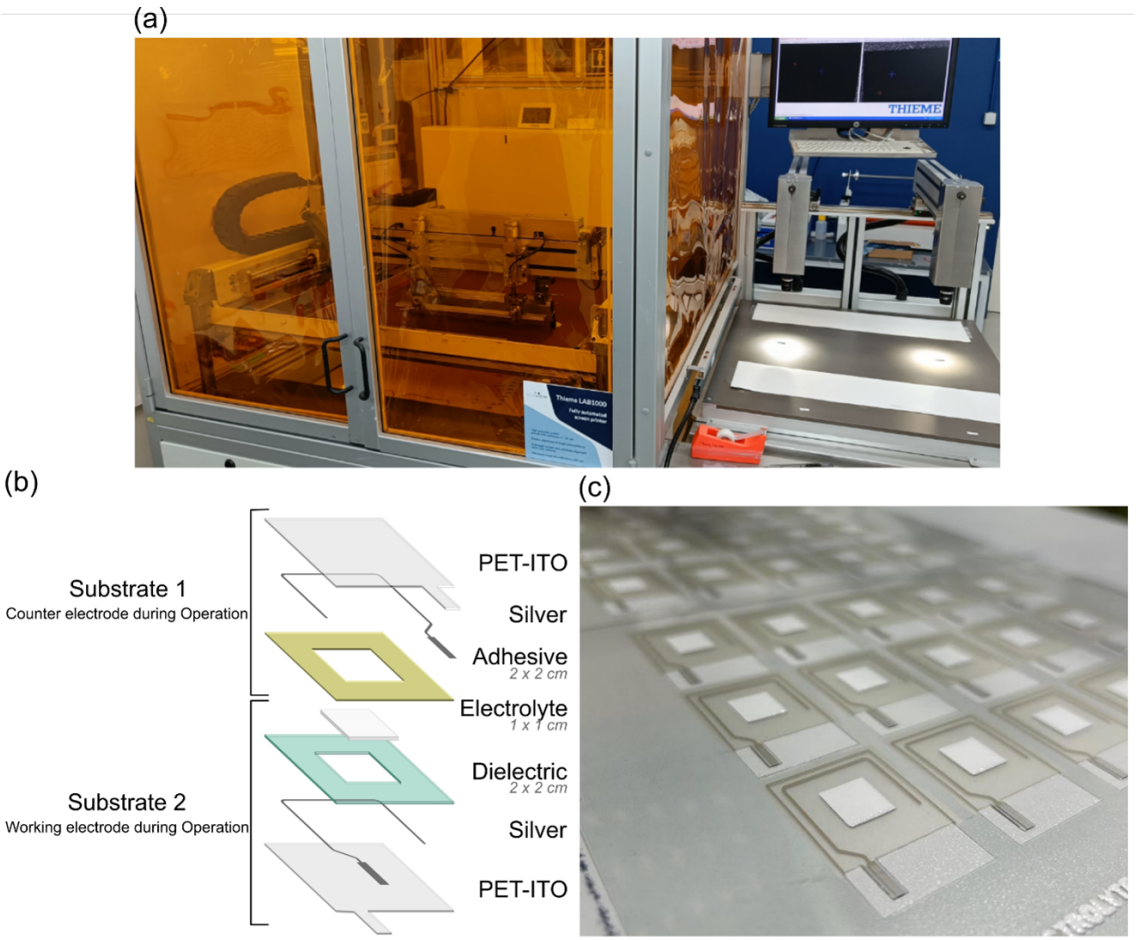

Figure 6.2: (a) Image of industrial screen printer used to print silver, dielectric, and adhesive layers. (b) Design for all the printed layers of the indicator. (c) Image of electrolyte and monomer layer immediately after printing.

6.2.2 Activation of Indicators

The term 'activation' is used here to describe the *in situ* electropolymerization process used to form the electrochromic layers. Two variations of the indicator were manufactured for this study: asymmetrical indicators, and symmetrical indicators. For the asymmetrical indicators, a PEDOT layer is only formed on the working electrode. For the symmetrical indicators, an additional electropolymerization step with a reversed polarity was added

so that PEDOT is formed on both the working electrode and the counter electrode. The difference between the two variations of the indicator is highlighted in Figure 6.3a.

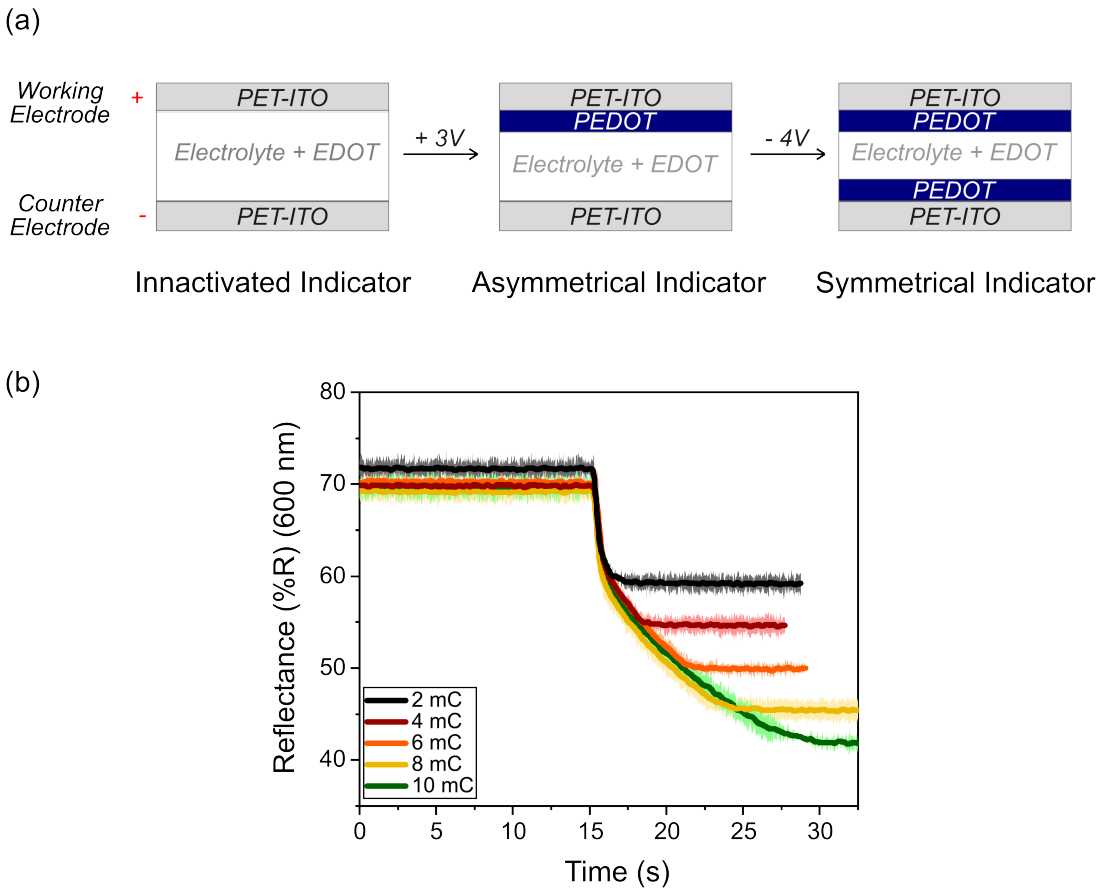

Figure 6.3: (a) Schematic illustrating the difference between the symmetrical and asymmetrical indicators, and (b) reflectance of working electrode of asymmetrical indicators during activation with 3V. Data is shown for indicators activated until they reach 2, 4, 6, 8, and 10 mC.

It was more challenging to obtain a homogenous polymer film on the counter electrode than on the working electrode. We tested multiple voltages and found that the most uniform counter electrode films were formed using – 4.0 V see Appendix C.1. Thus, the indicators are activated with 3.0 V on the working electrode, and then – 4.0 V on the counter electrode (for symmetrical indicators). The indicators are always viewed and evaluated from the side of the working electrode.

The change in reflectance for asymmetrical indicators during activation is shown in Figure 6.3b. As the charge applied increases, a lower reflectance is reached, indicating that more PEDOT was deposited. The time to form the film ranges from less than 2 s for the 2 mC film to around 15 s for the 10 mC film.

6.2.3 Contrast and Switching Time of Indicators

After activation, the contrast and switching time of the indicators were measured using the protocol described in the materials and methods section. Figure 6.4a shows the contrast of the asymmetrical indicators. The results are an average of three indicators, and the voltage used for the switching time protocol was ± 1.5 V. As the amount of charge used during the activation increases, there is a decrease in both the minimum and maximum reflectance values. The highest contrast is achieved in indicators formed with 6 mC of charge. Figure 6.4b shows the contrast of the symmetrical indicators. They show a similar trend to the asymmetrical indicators with a maximum contrast occurring at 6 mC. However, at higher activation charges (8 and 10 mC) some yellowing/browning is observed on the working electrode after activation. This suggests there is a limit to how much PEDOT we can form on the counter electrode without damaging the ITO-PEDOT on the working electrode.

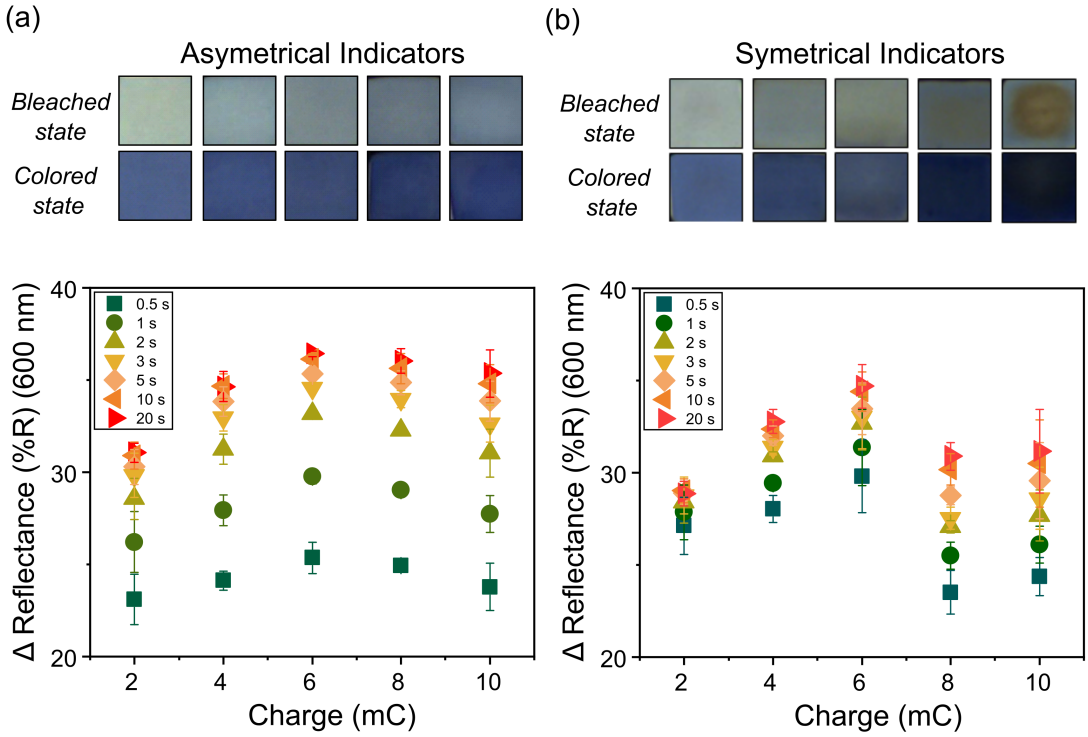

Figure 6.4: Contrast, as measured in Δ Reflectance at 600 nm, for asymmetrical indicators activated with 2, 4, 6, 8 and 10 mC. Color-corrected digital images of their bleached and colored states are above the plot. (b) Contrast, as measured in Δ Reflectance at 600 nm, for symmetrical indicators activated with 2, 4, 6, 8 and 10 mC. Color-corrected digital images of their bleached and colored states are above the plot. Indicators switched with ±1.5 V and data is shown for 0.5, 1, 2, 3, 5, 10, and 20 s pulses.

The switching speed for the 6 mC symmetrical and 6 mC asymmetrical indicators are shown in Figure 6.5 for driving voltages of ± 1.2 V and ± 1.5 V. Three key differences in their switching time and contrast are observed:

- The symmetrical indicators have a lower overall contrast (34.7 Δ%R for symmetrical indicators for 20 s at ± 1.5 V, compared to 36.4 Δ%R for asymmetrical indicators for 20 s at ± 1.5 V). While not visible to the human eye, the electrolyte is not completely opaque (see Appendix C.2). Thus, for the symmetrical indicators, there is a slight contribution of the counter electrode PEDOT film to the color of the indicator as observed from the working electrode. To increase the electrolyte reflectiveness, more TiO_2 could be added to the formulation, but this would change the rheology and reduce the printability.
- The symmetrical indicators exhibit faster switching at both ± 1.2 and ± 1.5 V. With a 0.5 s pulse length, the symmetrical indicators have a 13.2 % higher contrast at ± 1.2 V, and 4.4 % higher contrast at ± 1.5 V.
- At ± 1.2 V, the symmetrical indicators show significantly higher contrast across all pulse lengths.

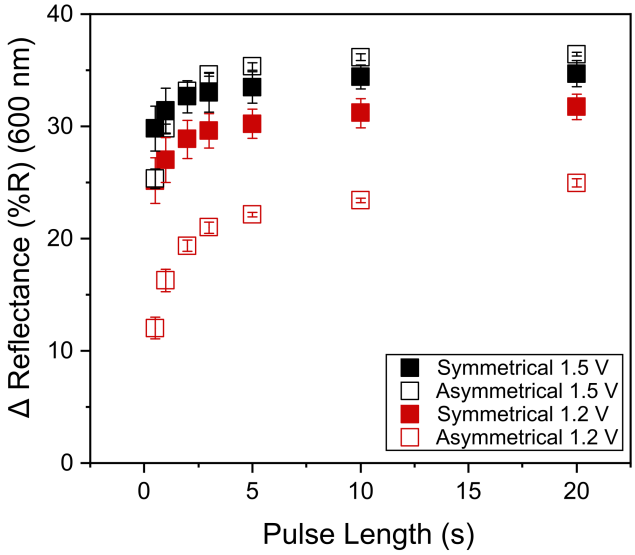

Figure 6.5: Δ Reflectance at different pulse lengths for 6 mC asymmetrical and symmetrical indicators switched with ± 1.2 V and ± 1.5 V.

The difference in the switching times and contrast between the symmetrical and asymmetrical indicators originates from the nature of the charge storage material used. The charge storage material is critical to determining the overall performance of an ECD [93], [95]. As a redox reaction takes place to change the oxidation state of the electrochromic film on the working electrode, a simultaneous complementary redox reaction must take place on the counter electrode.

For the symmetrical indicators a second PEDOT films acts as the charge storage material, whereas for the asymmetrical indicators ITO acts as the charge storage material. Electropolymerized PEDOT films can exhibit coloration efficiencies up to 180-190 cm^2 C^{-1}

[237], [238], which gives rise to redox capacities in the range of 1-10 mC cm^{-2} depending on the film thickness and contrast. In studies of ITO in PC solutions, Bressers and Meulenkamp report an initial charge density for ITO films during cycling of 4 mC cm^{-1}, however this rapidly decreases over 2 k cycles to around 1 mC cm^{-1} [165].

Thus, for the asymmetrical indicators the device is likely to have an unbalanced configuration, where the overall charge passing through the device will be limited by the redox capacity of the ITO. Unbalanced configurations where there is excess charge capacity on the electrochromic layer can result in higher switching voltages and can induce additional reactions at the electrode or in the electrolyte [93], [94]. In ITO, this is often characterized by yellowing or browning and a loss in conductivity due to irreversible reduction [94], [97], [98], [142], [165]. So, while ITO may be a suitable charge storage material for proof-of-concept devices, or when a long cycling lifetime is not required, it is not ideal for applications where long-term stability and performance are a criterion. In the case of the symmetrical indicators, the configuration should be fully balanced since the same material is used on both electrodes and they are polymerized with the same amount of charge.

6.2.4 Lifetime Cycling of Indicators

The previous sections in this study have focused on the activation and then the performance of the indicators after only a brief pre-cycling protocol. However, commercial applications can require that indicators undergo tens of thousands to hundreds of thousands of cycles. Thus, it is critical to understand how the performance of the indicators evolves during use.

Symmetrical and asymmetrical indicators activated with 2, 4 and 6 mC were cycled for 100 k. The driving protocol consists of ± 1.2 V pulses with 1 s at each polarity. The contrast (measured in ΔE), the minimum L* value, and the maximum L* value during this cycling period are shown in Figure 6.6. Almost all of the indicators exhibit an overall increase contrast over 100 k cycles. For example, the 2 mC symmetrical and 2 mC asymmetrical indicators have an increase in contrast of 5.2 and 6.5 ΔE respectively. The increase in contrast is attributed to the continued electrodeposition of PEDOT on the working electrode during the cycling process. This can be observed via the decrease in the minimum and maximum L* values (which indicates a darkening of both the colored and the bleached states over time) and also in the color-corrected digital images of the indicators shown in Figure 6.7a.

The extent to which the color states drift over time is dependent on the initial thickness of the PEDOT film. For example, the 2 mC symmetrical and asymmetrical indicators show a decrease in their maximum L* values of 9.01 and 8.20 respectively, whereas the 6 mC symmetrical and asymmetrical indicators only decrease by 0.38 and 4.67 respectively. Another key difference between the indicators based on their initial film thickness is the reproducibility between the triplicates. For the 2 mC indicators, the triplicates have a

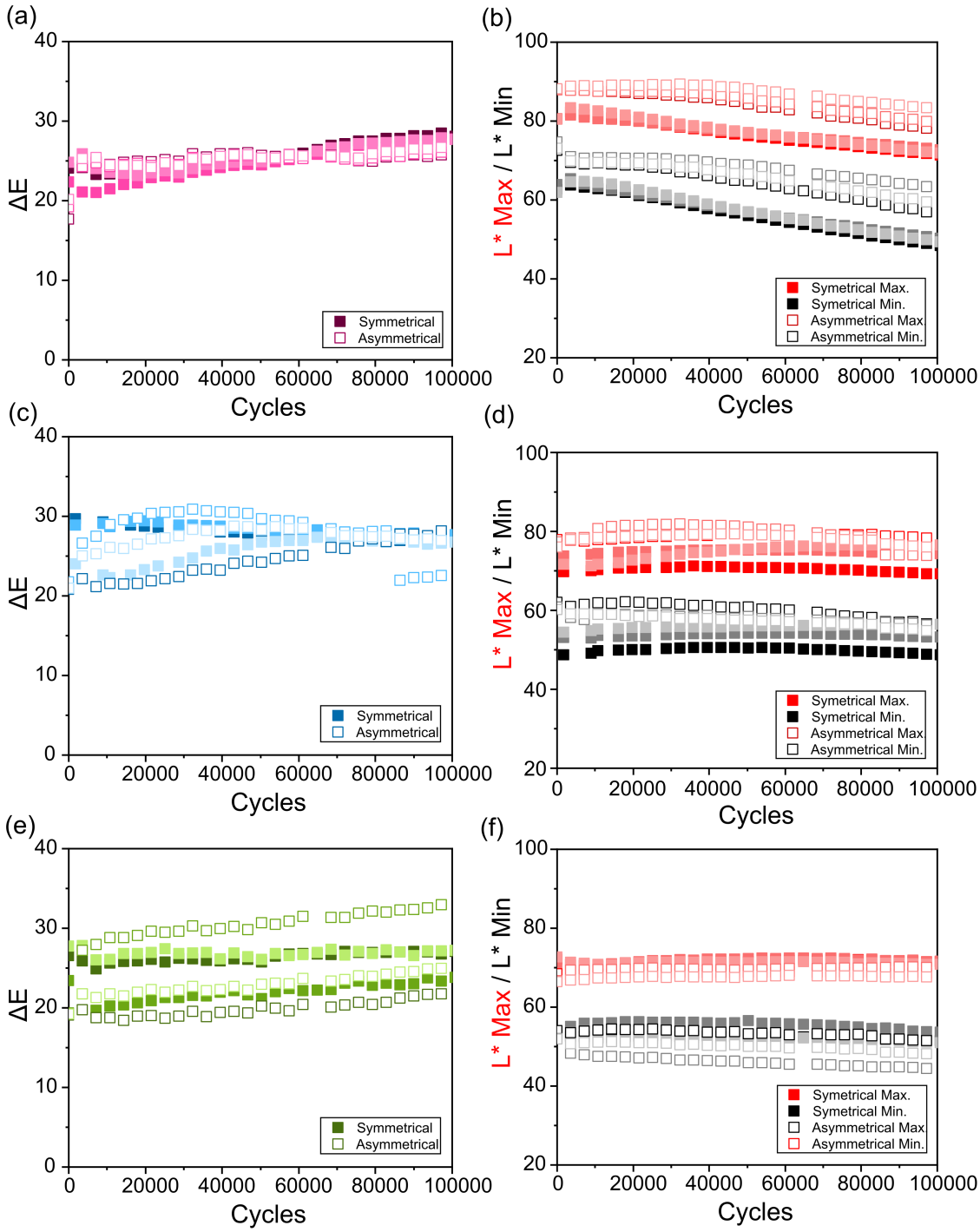

Figure 6.6: ΔE for triplicates of asymmetrical and symmetrical indicators activated with (a) 2 mC, (b) 4 mC, and (c) 6 mC over 100 k cycles of ± 1.2 V applied in 1 s pulses. Minimum and maximum L* values for the same triplicates of asymmetrical and symmetrical indicators activated with (d) 2 mC, (e) 4 mC and (f) 6 mC over 100 k cycles of ± 1.2 V applied in 1 s pulses.

standard deviation of 0.52 ΔE for the symmetrical variation, and 0.31 ΔE for the asymmetrical variation. These values are significantly higher for the 6 mC indicators, which have a standard deviation of 2.15 ΔE for the symmetrical variation, and 5.27 ΔE for the asymmetrical variation. Thus, regarding the starting PEDOT thickness, there is a trade-off between the stability of the color states and the reproducibility of the indicators during cycling. The 2 mC indicators show good reproducibility but have a visible drift in their color states. On the other hand, the 6 mC indicators have a negligible drift in their color state but have poor reproducibility.

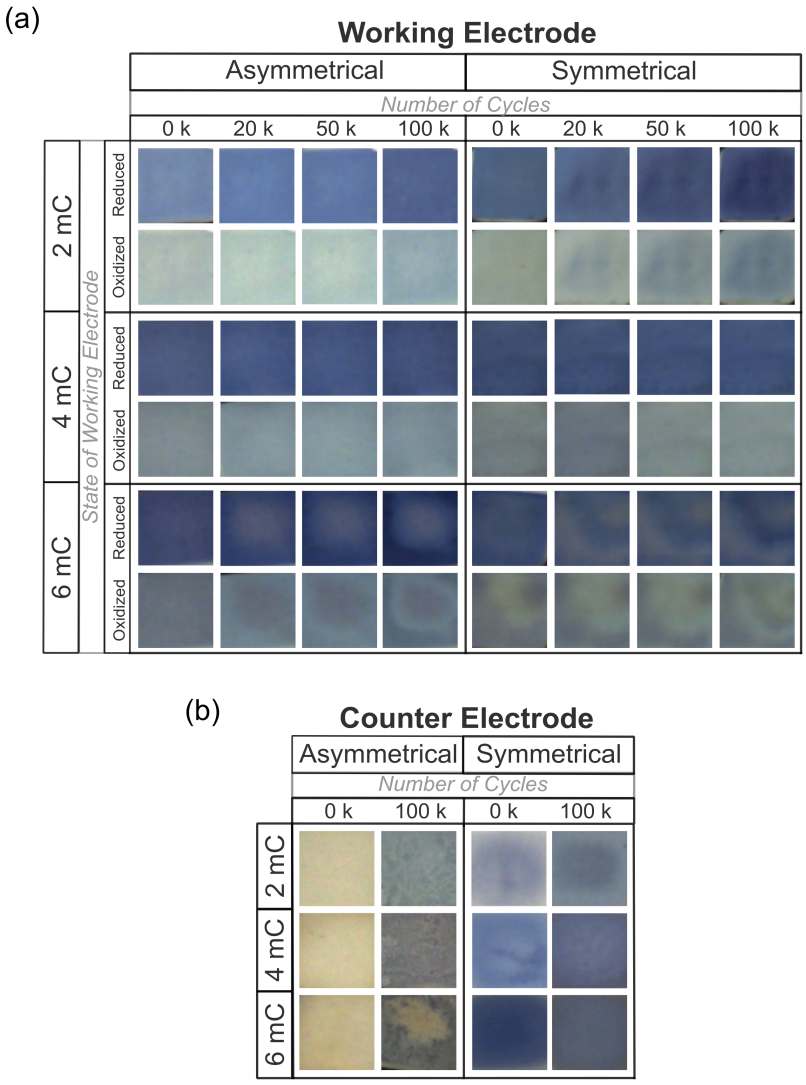

Figure 6.7: Digital images of the (a) working electrode and the (b) counter electrode sides of the indicators over 100 k cycles. Cycling was performed at ± 1.2 V in 1 s pulses.

In addition to the ongoing deposition of PEDOT on the working electrode, there is also ongoing deposition of PEDOT on the counter electrode during cycling. This can be seen in the digital images of the counter electrode, in Figure 6.7b, before and after

the 100 k cycling period. The result of this is that over time the asymmetrical indicators (which begin with only ITO on the counter electrode) turn into symmetrical indicators (which have PEDOT on the counter electrode). This effect is most apparent in the 2 mC asymmetrical indicators where there is an increase in contrast of 5.14 ΔE between the first time point measured at less than 1 k cycles, to the second time point measured at 3.6 k cycles. Using symmetrical indicators from the start avoids this abrupt change in their performance during the early stages of use.

Cycling results for the same set of indicators over 100 k cycles with a driving protocol of ± 1.5 V with 1 s at each polarity are in Appendix C.3. As expected, with a higher driving voltage all of the indicators have a higher ΔE, but the minimum and the maximum L* values drift more significantly over time as the ongoing polymerization reaction is more severe at ± 1.5 V.

6.2.5 Use-Case Prototypes of Indicators

Graphical overlays printed by inkjet were designed to highlight envisioned use-case scenarios for these indicators. Digital images of these prototypes are shown in Figure 6.8. Due to their low-cost manufacturing method, slim profile, fast switching, and long cycling lifetime, they are well suited for integration into visual smart labels. In this case, the indicators are used in smart warning labels, where they could flash on and off to alert the user if there is a problem.

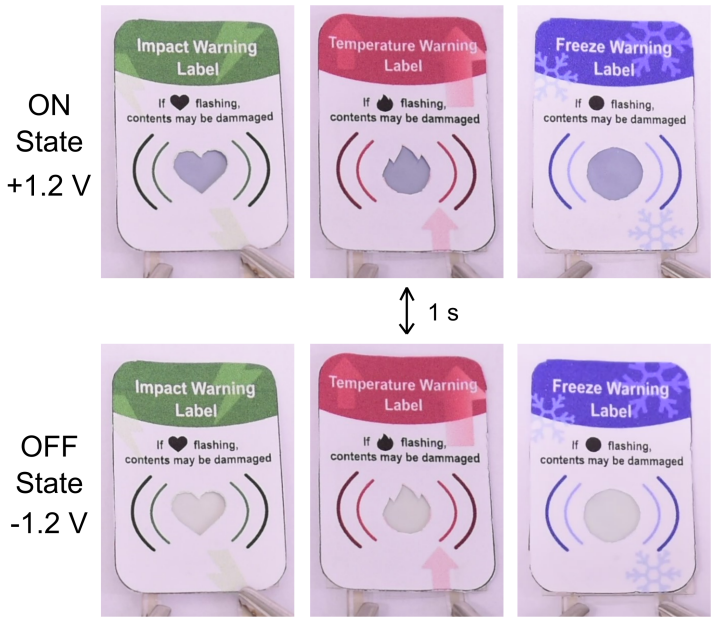

Figure 6.8: Digital images of 2 mC symmetrical indicators with smart label covers demonstrating use cases for impact, high temperature, and freeze warning labels. Indicators are switching with ± 1.5 V in 0.5 s pulses.

6.3 Conclusion

We have successfully reported fully printed electrochromic indicators incorporating an *in situ* electropolymerization technique. To the best of our knowledge, this is the first report on these two techniques being used in conjunction. The proposed method of manufacturing is simple and cost-efficient – only requiring five printed layers – and the final properties of the indicator can be optimized by modifying the voltage and charge used to electrodeposit the electrochromic films. We demonstrate the production of two variations of indicators: symmetrical and asymmetrical. The key difference between them is that symmetrical indicators have PEDOT films electropolymerized on both the working electrode and the counter electrode, whereas the asymmetrical indicators only have a PEDOT film electrodeposited on the working electrode. The use of PEDOT as a charge storage material in the symmetrical indicators lowers the operational voltage and increases the switching speed compared to asymmetrical indicators: further highlighting the importance of balanced electrode configurations in ECDs. In this case, is only possible to produce symmetrical indicators due to the diffusely reflective and opaque nature of the printable electrolyte, which blocks the complementary color transitions of the PEDOT film on the counter electrode from the view of the user.

Compared to previous reports of *in situ* electropolymerized devices, we can achieve a significantly longer cycling lifetime: up to 100 k cycles. This is again attributed to the opaque nature of the electrolyte. Here continued electrodeposition of the unreacted EDOT monomers during cycling results in an increase in contrast rather than a decrease in contrast as previously reported for *in situ* electropolymerized devices [123]. The long cycling lifetime and low-cost proposition of the manufactured indicators make them a promising candidate for use in smart label applications. However, a present limitation of this method of manufacturing is that they have only one pixel. To create displays with more segments, one would either need to pattern the conductive substrate into multiple electrically isolated regions that can be electropolymerized separately or use an array with several indicators.

6.4 Materials and Experimental Methods

Electrolyte Composition: The electrolyte used is a modified version of what was reported in [236]. The printable electrolyte (pQSPEv2) was formulated by adding 47.08 wt% titanium dioxide (TiO_2; ~ 200 nm, rutile pigment with 2.30 % Al_2O_3 surface treatment), to a mixing solution of PC:EC:$LiClO_4$ (0.57:0.26:0.18) with 2.02 wt% of a hyperbranched polyester nanoparticle stabilization agent. The slurry was mixed at high shear rate (1000 rpm) using an overhead stirrer with a dispersing blade for 10 minutes, after which 11.98 wt% glycerol propoxylate-(1PO/OH)-triacrylate (GPTA) was added. After 10 min of mixing, 18.26 wt% PVdF (molecular weight (MW) ~ 534,000 by gel permeation chromatography) was slowly added to the slurry while continuing stirring the formulation

at 1000 rpm. High shear rate mixing was maintained for 24 hours. Finally, 0.50 wt% Irgacure 819 photoinitiator and 2.00 wt% EDOT monomer were added and mixed for 2 hours.

Indicator Activation / In Situ Electropolymerization: *In situ* electropolymerization was performed using a Metrohm Autolab PGSTAT100 potentiostat by controlling the charge consumed while monitoring film formation on the working electrode at 600 nm. The reflectance of the indicator was measured using an Agilent Cary 300 UV-Vis Spectrophotometer with an optical fiber coupler connected to a hand-held UV-Vis reflectance probe with an Ocean fiber optics reflectance probe holder. An image of this set-up is shown in Figure 5.6. A labsphere-certified diffuse reflectance standard was used as the baseline for the measurements. Each indicator was preconditioned by cycling with ±1.0 V in 1 s pulses for 8 minutes before any further tests.

Switching Time Analysis: The switching time of the indicators was measured using an adaptation of the electrical pulse method proposed by Hassab *et al.* [120]. The switching time was evaluated at 1.5 V, and 1.2 V using an electrical protocol containing successive cathodic and anodic pulses with increasing periods. Pulse lengths of 0.5 s, 1 s, 2 s, and 3 s were repeated 10 times. Pulse lengths of 5 s and 10 s were repeated 5 times. The final pulse length of 20 s was repeated twice.

Cycling Analysis: Indicator cycling lifetimes were evaluated by monitoring the color states of the indicators over 100 k cycles. Cycling was performed with both ±1.2 V and ±1.5V (1 s pulse on each electrode). Digital images were captured inside a custom-made cycling chamber with an IDS Imaging UI-3590CP-C-HQ Camera and then color-corrected using an x-rite color checker in the frame of each image to output. The colors were converted from RGB to the CIE L*a*b* color space and then the contrast ΔE was calculated according to Equation 1.5.

7

General Conclusion and Future Outlook

The concept of irreversible electrochromic indicators via *in situ* electropolymerization is still relatively novel. While there are some industrial references in the form of patents and press releases for such devices, there is little scientific literature exploring this topic. The work presented in this dissertation takes several steps to advance the concept and application of *in situ* electropolymerized irreversible electrochromic indicators. This includes a brief discussion on their definition and market potential, a study on the properties of film formation inside of solid-state GPE devices, improvements to the electrical, optical, and environmental stability of the indicators, and the production of a final proof-of-concept smart label.

In an initial investigation, a comparative study on the electrodeposition of EDOT in a UV cross-linkable EO-PO-AGE terpolymer GPE and a liquid electrolyte was performed. This work confirmed some observations that have been reported in previous reports of *in situ* electropolymerization: namely that the use of a GPE not only influences the electrodeposition but can assist in film formation. In this study, this was embodied by a reduction in the overpotential required to deposit the polymer film and an increase in the efficiency of the process. Potential step methods performed in a 3-electrode cell showed a distinctive difference between the current-time transients obtained in the gel media compared to the liquid media for the deposition process. Further, the activation kinetics and CE of EDOT based indications were characterized over a broad range of applied potentials. By delaminating and analyzing the electrodes of the device after activation, it was shown that the reduction reaction on the PET-ITO counter electrode constitutes a significant proportion of the overall color change.

Modifications to the electrical and optical properties of the indicators were achieved by careful selection of the monomer precursor species. Multichromic films were demonstrated in indicators by using mixtures of EDOT and pyrene, as well as EDOT and anthracene. This approach yielded a broad range of colors, including green, yellow, orange, and red. From an electronic perspective, utilizing long-length oligomers as the starting species can

directly lower the E_a and increase the CE. This was effectively demonstrated for EDOT, and its dimer biEDOT, as well as for the dimer and trimer of thiophene, bithiophene and terthiophene. However, there is a trade-off between some of the desired properties. For example, while biEDOT indicators present the lowest E_a from all the monomers tested, it proved to be unstable over time and when exposed to heat.

Thus, one of the key areas identified for further improvement of the irreversible indicators is their environmental stability. For all of the indicators tested, long-term exposure to 60 ^{o}C resulted in a gradual yellowing of both the active area and the inactive area. The best performance was seen with terthiophene-based indicators, although they still exhibited a decrease in both their inactivated transmittance and their contrast after a 147-day exposure period. Testing with commercial antioxidants and stabilizers in EDOT indicators showed limited improvement. It is recommended that future developments to improve the commercial viability of this format of irreversible indicator focus on improving barrier properties and thermal stability of the substrates and encapsulants used.

A demonstration of the application of irreversible electrochromic indicators was made by assembling a smart label with printed SCs and a chemical thermal sensor. This label was successful in activating both EDOT and terthiophene during a negative temperature ramp. The results of this study are promising, but also highlight the need for improvements to all of the components used. Key limitations to the smart label prototype in its current state are its large size, and the time required to fully activate the irreversible indicator. Further advancements should also target the mechanical durability and environmental stability of the full system.

While the primary goal of this dissertation was the development of irreversible electrochromic indicators, many of the findings around *in situ* electropolymerization can also be applied to the manufacturing of reversible electrochromic indicators. The final embodiment of this dissertation focused on developing fully-printed electrochromic indicators, utilizing *in situ* electropolymerization as a simplified technique for depositing the electrochromic and charge storage films. Ultimately the indicators were able to perform 100,000 cycles of reversible switching with minimal degradation to their performance, highlighting the viability of *in situ* electropolymerization for commercial electrochromic device manufacturing. This work is a critical contribution to the field of electrochromics since the manufacturing of fully printable displays remains an ongoing challenge.

Bibliography

[1] J. M. Lourenço, *The NOVAthesis LaTeX Template User's Manual*, NOVA University Lisbon, 2021. [Online]. Available: https://github.com/joaomlourenco/novathesis/raw/main/template.pdf.

[2] "9th OE-A Roadmap White Paper," Organic and Printed Electronics Association, White Paper.

[3] S. Madakam, R. Ramaswamy, and S. Tripathi, "Internet of Things (IoT): A Literature Review," *Journal of Computer and Communications*, vol. 03, no. 05, pp. 164–173, 2015. DOI: 10.4236/jcc.2015.35021.

[4] A. Čolaković and M. Hadžialić, "Internet of Things (IoT): A review of enabling technologies, challenges, and open research issues," *Computer Networks*, vol. 144, pp. 17–39, Oct. 2018. DOI: 10.1016/j.comnet.2018.07.017.

[5] T. K. L. Hui, B. Mohammed, P. Donyai, R. McCrindle, and R. S. Sherratt, "Enhancing Pharmaceutical Packaging through a Technology Ecosystem to Facilitate the Reuse of Medicines and Reduce Medicinal Waste," *Pharmacy*, vol. 8, no. 2, p. 58, Mar. 2020. DOI: 10.3390/pharmacy8020058.

[6] H. Yousefi, H.-M. Su, S. M. Imani, K. Alkhaldi, C. D. M. Filipe, and T. F. Didar, "Intelligent Food Packaging: A Review of Smart Sensing Technologies for Monitoring Food Quality," *ACS Sensors*, vol. 4, no. 4, pp. 808–821, Apr. 2019. DOI: 10.1021/acssensors.9b00440.

[7] C. M. Fernandez, J. Alves, P. D. Gaspar, T. M. Lima, and P. D. Silva, "Innovative processes in smart packaging. A systematic review," *Journal of the Science of Food and Agriculture*, vol. 103, no. 3, pp. 986–1003, Feb. 2023. DOI: 10.1002/jsfa.11863.

[8] "Smart Label Market Size & Share Analysis - Growth Trends & Forecasts (2023 - 2028)," Mordor Intelligence, Tech. Rep. [Online]. Available: https://www.mordorintelligence.com/industry-reports/smart-label-market.

[9] *Smart Packaging Solutions*. [Online]. Available: https://www.faller-packaging.com/en/innovations-and-solutions/smart-packaging/smart-packaging-solutions (visited on 12/27/2023).

[10] "Smart Label Market Size, Share & Industry Analysis, By Technology (Electronic Article Surveillance (EAS) Security, RFID, Sensing Labels, Near Field Communication Tag, and QR Code/2D Barcode), By End-User (Retail, Healthcare & Pharmaceuticals, Food & Beverages, Consumer Electronics, Supply Chain and Logistics, Transportation, and Others) and Regional Forecast, 2019-2026," Fortune Business Insights, Tech. Rep. FBI102419. [Online]. Available: https://www.fortunebusinessinsights.com/smart-label-market-102419.

[11] J. Ajitesh and S. Onkar, "Smart Labels Market by Product Type (RFID, Electronic Article Surveillance Label, Sensing Label, Dynamic Display Label), by Application (Retail Inventory, Perishable Goods), by End User (Retail, Healthcare, Logistics, Others): Global Opportunity Analysis and Industry Forecast, 2022-2031," Allied Market Research, Tech. Rep. A02057. [Online]. Available: https://www.alliedmarketresearch.com/smart-labels-market.

[12] T. M. Fernandez-Carames and P. Fraga-Lamas, "A Review on Human-Centered IoT-Connected Smart Labels for the Industry 4.0," *IEEE Access*, vol. 6, pp. 25 939–25 957, 2018. DOI: 10.1109/ACCESS.2018.2833501.

[13] Q. Cai, H. Yan, R. Yao, *et al.*, "From Traditional to Novel Printed Electrochromic Devices: Material, Structure and Device," *Membranes*, vol. 12, no. 11, p. 1039, Oct. 2022. DOI: 10.3390/membranes12111039.

[14] N. X. Williams, G. Bullard, N. Brooke, M. J. Therien, and A. D. Franklin, "Printable and recyclable carbon electronics using crystalline nanocellulose dielectrics," *Nature Electronics*, vol. 4, no. 4, pp. 261–268, Apr. 2021. DOI: 10.1038/s41928-021-00574-0.

[15] D. Beynon, E. Parvazian, K. Hooper, *et al.*, "All-Printed Roll-to-Roll Perovskite Photovoltaics Enabled by Solution-Processed Carbon Electrode," *Advanced Materials*, vol. 35, no. 16, p. 2 208 561, Apr. 2023. DOI: 10.1002/adma.202208561.

[16] G. Xiao, Z. Zhang, H. Fukutani, Y. Tao, and S. Lang, "Improving the Q -Factor of Printed HF RFID Loop Antennas on Flexible Substrates by Condensing the Microstructures of Conductors," *IEEE Journal of Radio Frequency Identification*, vol. 2, no. 2, pp. 111–116, Jun. 2018. DOI: 10.1109/JRFID.2018.2854264.

[17] D. E. Schwartz, J. Rivnay, G. L. Whiting, *et al.*, "Flexible Hybrid Electronic Circuits and Systems," *IEEE Journal on Emerging and Selected Topics in Circuits and Systems*, vol. 7, no. 1, pp. 27–37, Mar. 2017. DOI: 10.1109/JETCAS.2016.2612623.

[18] P. Lall, K. Goyal, and J. Narangaparambil, "Accuracy, Hysteresis and Extended Time Stability of Additively Printed Temperature and Humidity Sensors," in *2020 IEEE 70th Electronic Components and Technology Conference (ECTC)*, Orlando, FL, USA: IEEE, Jun. 2020, pp. 1070–1080. DOI: 10.1109/ECTC32862.2020.00173.

[19] D. Zymelka, K. Togashi, R. Ohigashi, *et al.*, "Printed strain sensor array for application to structural health monitoring," *Smart Materials and Structures*, vol. 26, no. 10, p. 105 040, Oct. 2017. DOI: 10.1088/1361-665X/aa8831.

[20] A. M. Gaikwad, D. A. Steingart, T. N. Ng, D. E. Schwartz, and G. L. Whiting, "A flexible high potential printed battery for powering printed electronics," *Applied Physics Letters*, vol. 102, no. 23, p. 233 302, Jun. 2013. DOI: 10.1063/1.4810974.

[21] A. M. Gaikwad, G. L. Whiting, D. A. Steingart, and A. C. Arias, "Highly Flexible, Printed Alkaline Batteries Based on Mesh-Embedded Electrodes," *Advanced Materials*, vol. 23, no. 29, pp. 3251–3255, Aug. 2011. DOI: 10.1002/adma.201100894.

[22] C. Costa, R. Gonçalves, and S. Lanceros-Méndez, "Recent advances and future challenges in printed batteries," *Energy Storage Materials*, vol. 28, pp. 216–234, Jun. 2020. DOI: 10.1016/j.ensm.2020.03.012.

[23] A. Ivanov, "A Printed Electroluminescent Matrix Display: Implementation Details and Technical Solutions," in *2018 IMAPS Nordic Conference on Microelectronics Packaging (NordPac)*, Oulu: IEEE, Jun. 2018, pp. 86–94. DOI: 10.23919/NORDPAC.2018.8423861.

[24] K. Freitag, R. Brooke, M. Nilsson, J. Åhlin, V. Beni, and P. Andersson Ersman, "Screen Printed Reflective Electrochromic Displays for Paper and Other Opaque Substrates," *ACS Applied Optical Materials*, vol. 1, no. 2, pp. 578–586, Feb. 2023. DOI: 10.1021/acsaom.2c00140.

[25] E. Dimitriou and N. Michailidis, "Printable conductive inks used for the fabrication of electronics: An overview," *Nanotechnology*, vol. 32, no. 50, p. 502 009, Dec. 2021. DOI: 10.1088/1361-6528/abefff.

[26] R. Venkata Krishna Rao, K. Venkata Abhinav, P. S. Karthik, and S. P. Singh, "Conductive silver inks and their applications in printed and flexible electronics," en, *RSC Advances*, vol. 5, no. 95, pp. 77 760–77 790, 2015. DOI: 10.1039/C5RA12013F.

[27] A. Kamyshny and S. Magdassi, "Conductive Nanomaterials for Printed Electronics," *Small*, vol. 10, no. 17, pp. 3515–3535, Sep. 2014. DOI: 10.1002/smll.201303000.

[28] W. J. Scheideler and V. Subramanian, "How to print high-mobility metal oxide transistors—Recent advances in ink design, processing, and device engineering," *Applied Physics Letters*, vol. 121, no. 22, p. 220 502, Nov. 2022. DOI: 10.1063/5.0125055.

[29] E. K. Lee, M. Y. Lee, C. H. Park, H. R. Lee, and J. H. Oh, "Toward Environmentally Robust Organic Electronics: Approaches and Applications," *Advanced Materials*, vol. 29, no. 44, p. 1 703 638, Nov. 2017. DOI: 10.1002/adma.201703638.

[30] X. Guo, R. P. Ortiz, Y. Zheng, *et al.*, "Thieno[3,4- *c*]pyrrole-4,6-dione-Based Polymer Semiconductors: Toward High-Performance, Air-Stable Organic Thin-Film Transistors," *Journal of the American Chemical Society*, vol. 133, no. 34, pp. 13 685–13 697, Aug. 2011. DOI: 10.1021/ja205398u.

[31] S. Nair, M. Kathiresan, T. Mukundan, and V. Natarajan, "Passivation of organic field effect transistor with photopatterned Parylene to improve environmental stability," *Microelectronic Engineering*, vol. 163, pp. 36–42, Sep. 2016. DOI: 10.1016/j.mee.2016.06.001.

[32] U. Salzner, "Electronic structure of conducting organic polymers: Insights from time-dependent density functional theory," *WIREs Computational Molecular Science*, vol. 4, no. 6, pp. 601–622, Nov. 2014. DOI: 10.1002/wcms.1194.

[33] C. K. Chiang, C. R. Fincher, Y. W. Park, *et al.*, "Electrical Conductivity in Doped Polyacetylene.," *Physical Review Letters*, vol. 40, no. 22, pp. 1472–1472, May 1978. DOI: 10.1103/PhysRevLett.40.1472.

[34] C. K. Chiang, M. A. Druy, S. C. Gau, *et al.*, "Synthesis of highly conducting films of derivatives of polyacetylene, (CH)x," *Journal of the American Chemical Society*, vol. 100, no. 3, pp. 1013–1015, Feb. 1978. DOI: 10.1021/ja00471a081.

[35] T. Ito, H. Shirakawa, and S. Ikeda, "Simultaneous polymerization and formation of polyacetylene film on the surface of concentrated soluble Ziegler-type catalyst solution," *Journal of Polymer Science: Polymer Chemistry Edition*, vol. 12, no. 1, pp. 11–20, Jan. 1974. DOI: 10.1002/pol.1974.170120102.

[36] H. Shirakawa, E. J. Louis, A. G. MacDiarmid, C. K. Chiang, and A. J. Heeger, "Synthesis of electrically conducting organic polymers: Halogen derivatives of polyacetylene, (CH) x," *Journal of the Chemical Society, Chemical Communications*, no. 16, p. 578, 1977. DOI: 10.1039/c39770000578.

[37] E. Da Como and E. von Hauff, "The WSPC Reference on Organic Electronics: Organic Semiconductors. Materials and Energy Series. Volume 1: Basic Concepts, Volume 2: Fundamental Aspects of Materials and Applications. Edited by Jean-Luc Brédas and Seth R. Marder.," *Angewandte Chemie International Edition*, vol. 56, no. 18, pp. 4915–4916, Apr. 2017. DOI: 10.1002/anie.201701913.

[38] H. Van Mullekom, "Developments in the chemistry and band gap engineering of donor–acceptor substituted conjugated polymers," *Materials Science and Engineering: R: Reports*, vol. 32, no. 1, pp. 1–40, Feb. 2001. DOI: 10.1016/S0927-796X(00)00029-2.

[39] U. Salzner, J. Lagowski, P. Pickup, and R. Poirier, "Comparison of geometries and electronic structures of polyacetylene, polyborole, polycyclopentadiene, polypyrrole, polyfuran, polysilole, polyphosphole, polythiophene, polyselenophene and polytellurophene," *Synthetic Metals*, vol. 96, no. 3, pp. 177–189, Aug. 1998. DOI: 10.1016/S0379-6779(98)00084-8.

[40] I. Zozoulenko, A. Singh, S. K. Singh, V. Gueskine, X. Crispin, and M. Berggren, "Polarons, Bipolarons, And Absorption Spectroscopy of PEDOT," *ACS Applied Polymer Materials*, vol. 1, no. 1, pp. 83–94, Jan. 2019. DOI: 10.1021/acsapm.8b00061.

[41] J. L. Bredas and G. B. Street, "Polarons, bipolarons, and solitons in conducting polymers," *Accounts of Chemical Research*, vol. 18, no. 10, pp. 309–315, Oct. 1985. DOI: 10.1021/ar00118a005.

[42] J. L. Brédas, "Relationship between band gap and bond length alternation in organic conjugated polymers," *The Journal of Chemical Physics*, vol. 82, no. 8, pp. 3808–3811, Apr. 1985. DOI: 10.1063/1.448868.

[43] S. Ghosh, V. Gueskine, M. Berggren, and I. V. Zozoulenko, "Electronic Structures and Optical Absorption of N-Type Conducting Polymers at Different Doping Levels," *The Journal of Physical Chemistry C*, vol. 123, no. 25, pp. 15 467–15 476, Jun. 2019. DOI: 10.1021/acs.jpcc.9b04634.

[44] G. Sonmez, H. B. Sonmez, C. K. F. Shen, and F. Wudl, "Red, Green, and Blue Colors in Polymeric Electrochromics," *Advanced Materials*, vol. 16, no. 21, pp. 1905–1908, Nov. 2004. DOI: 10.1002/adma.200400546.

[45] P. M. Beaujuge and J. R. Reynolds, "Color Control in -Conjugated Organic Polymers for Use in Electrochromic Devices," *Chemical Reviews*, vol. 110, no. 1, pp. 268–320, Jan. 2010. DOI: 10.1021/cr900129a.

[46] A. L. Dyer, E. J. Thompson, and J. R. Reynolds, "Completing the Color Palette with Spray-Processable Polymer Electrochromics," *ACS Applied Materials & Interfaces*, vol. 3, no. 6, pp. 1787–1795, Jun. 2011. DOI: 10.1021/am200040p.

[47] E. L. Howard, A. M. Österholm, D. E. Shen, L. P. Panchumarti, C. Pinheiro, and J. R. Reynolds, "Cost-Effective, Flexible, and Colorful Dynamic Displays: Removing Underlying Conducting Layers from Polymer-Based Electrochromic Devices," *ACS Applied Materials & Interfaces*, vol. 13, no. 14, pp. 16 732–16 743, Apr. 2021. DOI: 10.1021/acsami.1c00463.

[48] H. Letheby, "XXIX.—On the production of a blue substance by the electrolysis of sulphate of aniline," *J. Chem. Soc.*, vol. 15, no. 0, pp. 161–163, 1862. DOI: 10.1039/JS8621500161.

[49] S. Asavapiriyanont, G. Chandler, G. Gunawardena, and D. Pletcher, "The electrodeposition of polypyrrole films from aqueous solutions," *Journal of Electroanalytical Chemistry and Interfacial Electrochemistry*, vol. 177, no. 1-2, pp. 229–244, Oct. 1984. DOI: 10.1016/0022-0728(84)80225-9.

[50] R. Córdova, M. Del Valle, A. Arratia, H. Gómez, and R. Schrebler, "Effect of anions on the nucleation and growth mechanism of polyaniline," *Journal of Electroanalytical Chemistry*, vol. 377, no. 1-2, pp. 75–83, Oct. 1994. DOI: 10.1016/0022-0728(94)03425-7.

[51] M. A. Del Valle, M. A. Gacitúa, L. I. Canales, and F. R. Díaz, "Oligomer Chain Length Effect on the Nucleation and Growth Mechanisms (NGM) of Polythiophene," *Journal of the Chilean Chemical Society*, vol. 54, no. 3, 2009. DOI: 10.4067/S0717-97072009000300012.

[52] M. Del Valle, P. Cury, and R. Schrebler, "Solvent effect on the nucleation and growth mechanisms of poly(thiophene)," *Electrochimica Acta*, vol. 48, no. 4, pp. 397–405, Dec. 2002. DOI: 10.1016/S0013-4686(02)00685-0.

[53] M. Del Valle, A. Ramírez, L. Hernández, F. Armijo, F. Díaz, and G. Arteaga, "Influence of the Supporting Electrolyte on the Electrochemical Polymerization of 3,4-Ethylenedioxythiophene. Effect on p- and n-Doping/Undoping, Conductivity and Morphology," *International Journal of Electrochemical Science*, vol. 11, no. 8, pp. 7048–7065, Aug. 2016. DOI: 10.20964/2016.08.46.

[54] A. Downard and D. Pletcher, "A study of the conditions for the electrodeposition of polythiophen in acetonitrile," *Journal of Electroanalytical Chemistry and Interfacial Electrochemistry*, vol. 206, no. 1-2, pp. 147–152, Jul. 1986. DOI: 10.1016/0022-0728(86)90264-0.

[55] A. Hillman and E. F. Mallen, "Nucleation and growtn of polythiophene films on gold electrodes," *Journal of Electroanalytical Chemistry and Interfacial Electrochemistry*, vol. 220, no. 2, pp. 351–367, Apr. 1987. DOI: 10.1016/0022-0728(87)85121-5.

[56] A. Robert Hillman and M. J. Swann, "Spectroscopic studies of the growth and potential cycling of polybithiophene films," *Electrochimica Acta*, vol. 33, no. 10, pp. 1303–1312, Oct. 1988. DOI: 10.1016/0013-4686(88)80119-1.

[57] R. Schrebler, P. Grez, P. Cury, *et al.*, "Nucleation and growth mechanisms of poly(thiophene) Part 1. Effect of electrolyte and monomer concentration in dichloromethane," *Journal of Electroanalytical Chemistry*, vol. 430, no. 1-2, pp. 77–90, Jun. 1997. DOI: 10.1016/S0022-0728(97)00109-5.

[58] E. Ventosa, J. L. Palacios, and P. R. Unwin, "Nucleation and growth of poly(3,4-ethylenedioxythiophene) thin films on highly oriented pyrolytic graphite (HOPG) electrodes," *Electrochemistry Communications*, vol. 10, no. 11, pp. 1752–1755, Nov. 2008. DOI: 10.1016/j.elecom.2008.09.003.

[59] E. Tamburri, S. Orlanducci, F. Toschi, M. L. Terranova, and D. Passeri, "Growth mechanisms, morphology, and electroactivity of PEDOT layers produced by electrochemical routes in aqueous medium," *Synthetic Metals*, vol. 159, no. 5-6, pp. 406–414, Mar. 2009. DOI: 10.1016/j.synthmet.2008.10.014.

[60] J. Heinze, B. A. Frontana-Uribe, and S. Ludwigs, "Electrochemistry of Conducting Polymers—Persistent Models and New Concepts," *Chemical Reviews*, vol. 110, no. 8, pp. 4724–4771, Aug. 2010. DOI: 10.1021/cr900226k.

[61] A. F. Diaz, K. K. Kanazawa, J. I. Castillo, and J. A. Logan, "Electrosynthesis and Study of Conducting Polymeric Films," in *Conductive Polymers*, R. B. Seymour, Ed., Boston, MA: Springer US, 1981, pp. 149–153, ISBN: 978-1-4613-3311-1 978-1-4613-3309-8.

[62] A. Smie, A. Synowczyk, J. Heinze, *et al.*, ",-Disubstituted oligothiophenes, a new oligomeric approach towards the synthesis of conducting polymers," *Journal of Electroanalytical Chemistry*, vol. 452, no. 1, pp. 87–95, Jul. 1998. DOI: 10.1016/S0022-0728(98)00100-4.

[63] R. J. Mortimer, "Electrochromic Materials," *Annual Review of Materials Research*, vol. 41, no. 1, pp. 241–268, Aug. 2011. DOI: 10.1146/annurev-matsci-062910-100344.

[64] A. L.-S. Eh, A. W. M. Tan, X. Cheng, S. Magdassi, and P. S. Lee, "Recent Advances in Flexible Electrochromic Devices: Prerequisites, Challenges, and Prospects," *Energy Technology*, vol. 6, no. 1, pp. 33–45, Jan. 2018. DOI: 10.1002/ente.201700705.

[65] B. J. Miller, "What Will It Take for Smart Windows to Go Mainstream?" *Smithsonian Magazine*, Section: Innovation, Science, , Our Planet, , Energy, , Articles. [Online]. Available: https://www.smithsonianmag.com/innovation/what-will-it-take-for-smart-windows-to-go-mainstream-180980226/ (visited on 12/26/2023).

[66] *Automotive*. [Online]. Available: https://www.gentex.com/products-technology/automotive (visited on 12/26/2023).

[67] *Aerospace*. [Online]. Available: https://www.gentex.com/products-technology/aerospace (visited on 12/26/2023).

[68] *Solar control on demand! - Dynamic Glass*. [Online]. Available: https://chromogenics.com/dynamic-glass/ (visited on 12/26/2023).

[69] *Products - Smart Windows*. [Online]. Available: https://view.com/product (visited on 12/26/2023).

[70] *Printed E-Paper Displays ı The More Cost-Effective E-Paper*. [Online]. Available: https://www.ynvisible.com/segment-displays (visited on 11/09/2023).

[71] R. Brooke, K. Freitag, I. Petsagkourakis, M. Nilsson, and P. Andersson Ersman, "All-Printed Electrochromic Stickers," *Macromolecular Materials and Engineering*, vol. 308, no. 9, p. 2 300 044, Sep. 2023. DOI: 10.1002/mame.202300044.

[72] T. Kololuoma, C. Pinheiro, I. Kaisto, *et al.*, "Adopting Hybrid Integrated Flexible Electronics in Products: Case—Personal Activity Meter," *IEEE Journal of the Electron Devices Society*, vol. 7, pp. 761–768, 2019. DOI: 10.1109/JEDS.2019.2903868.

[73] A. Perera, M. Katz, R. Godaliyadda, J. Hakkinen, and E. Strommer, "Light-based Internet of Things: Implementation of an Optically Connected Energy-autonomous Node," in *2021 IEEE Wireless Communications and Networking Conference (WCNC)*, Nanjing, China: IEEE, Mar. 2021, pp. 1–7. DOI: 10.1109/WCNC49053.2021.9417484.

[74] *Electrochromic systems and displays*, en. [Online]. Available: https://www.ri.se/en/what-we-do/expertises/electrochromic-displays (visited on 01/22/2024).

[75] J. Padilla, A. M. Österholm, A. L. Dyer, and J. R. Reynolds, "Process controlled performance for soluble electrochromic polymers," *Solar Energy Materials and Solar Cells*, vol. 140, pp. 54–60, Sep. 2015. DOI: 10.1016/j.solmat.2015.03.018.

[76] H. Wang, M. Barrett, B. Duane, J. Gu, and F. Zenhausern, "Materials and processing of polymer-based electrochromic devices," *Materials Science and Engineering: B*, vol. 228, pp. 167–174, Feb. 2018. DOI: 10.1016/j.mseb.2017.11.016.

[77] M. Lee, M. Son, D.-m. Chun, and C. S. Lee, "Evaluation of Electrochromic Device Influenced by Various Formulation of Solid Polymer Electrolyte," *International Journal of Precision Engineering and Manufacturing*, vol. 22, no. 1, pp. 189–199, Jan. 2021. DOI: 10.1007/s12541-020-00451-4.

[78] J. Jensen, M. V. Madsen, and F. C. Krebs, "Photochemical stability of electrochromic polymers and devices," *Journal of Materials Chemistry C*, vol. 1, no. 32, p. 4826, 2013. DOI: 10.1039/c3tc30751d.

[79] A. W. Lang, Y. Li, M. De Keersmaecker, *et al.*, "Transparent Wood Smart Windows: Polymer Electrochromic Devices Based on Poly(3,4-Ethylenedioxythiophene):Poly(Styrene Sulfonate) Electrodes," *ChemSusChem*, vol. 11, no. 5, pp. 854–863, Mar. 2018. DOI: 10.1002/cssc.201702026.

[80] C. G. Granqvist, "Transparent conductive electrodes for electrochromic devices: A review," *Applied Physics A Solids and Surfaces*, vol. 57, no. 1, pp. 19–24, Jul. 1993. DOI: 10.1007/BF00331211.

[81] C. I. Bright, "Transparent conductive thin films," in *Optical Thin Films and Coatings*, Elsevier, 2018, pp. 741–788, ISBN: 978-0-08-102073-9.

[82] European Commission. Directorate General for Internal Market, Industry, Entrepreneurship and SMEs., *Critical raw materials for strategic technologies and sectors in the EU: a foresight study*. LU: Publications Office, 2020. [Online]. Available: https://data.europa.eu/doi/10.2873/58081 (visited on 12/26/2023).

[83] European Commission. Directorate General for Internal Market, Industry, Entrepreneurship and SMEs., *Study on the EU's list of critical raw materials (2020): final report*. LU: Publications Office, 2020. [Online]. Available: https://data.europa.eu/doi/10.2873/11619 (visited on 12/26/2023).

[84] M. De Keersmaecker, A. W. Lang, A. M. Österholm, and J. R. Reynolds, "All Polymer Solution Processed Electrochromic Devices: A Future without Indium Tin Oxide?" *ACS Applied Materials & Interfaces*, vol. 10, no. 37, pp. 31 568–31 579, Sep. 2018. DOI: 10.1021/acsami.8b10589.

[85] Y. Ding, M. A. Invernale, and G. A. Sotzing, "Conductivity Trends of PEDOT-PSS Impregnated Fabric and the Effect of Conductivity on Electrochromic Textile," *ACS Applied Materials & Interfaces*, vol. 2, no. 6, pp. 1588–1593, Jun. 2010. DOI: 10.1021/am100036n.

[86] A. Malti, R. Brooke, X. Liu, *et al.*, "Freestanding electrochromic paper," *Journal of Materials Chemistry C*, vol. 4, no. 41, pp. 9680–9686, 2016. DOI: 10.1039/C6TC03542F.

[87] L. Gomes, A. Branco, T. Moreira, F. Feliciano, C. Pinheiro, and C. Costa, "Increasing the electrical conductivity of electrochromic PEDOT:PSS films – A comparative study," *Solar Energy Materials and Solar Cells*, vol. 144, pp. 631–640, Jan. 2016. DOI: 10.1016/j.solmat.2015.10.001.

[88] R. Singh, J. Tharion, S. Murugan, and A. Kumar, "ITO-Free Solution-Processed Flexible Electrochromic Devices Based on PEDOT:PSS as Transparent Conducting Electrode," *ACS Applied Materials & Interfaces*, vol. 9, no. 23, pp. 19 427–19 435, Jun. 2017. DOI: 10.1021/acsami.6b09476.

[89] A. Argun, A. Cirpan, and J. Reynolds, "The First Truly All-Polymer Electrochromic Devices," *Advanced Materials*, vol. 15, no. 16, pp. 1338–1341, Aug. 2003. DOI: 10.1002/adma.200305038.

[90] H. B. Lee, W.-Y. Jin, M. M. Ovhal, N. Kumar, and J.-W. Kang, "Flexible transparent conducting electrodes based on metal meshes for organic optoelectronic device applications: A review," *Journal of Materials Chemistry C*, vol. 7, no. 5, pp. 1087–1110, 2019. DOI: 10.1039/C8TC04423F.

[91] Y. Zhou and R. Azumi, "Carbon nanotube based transparent conductive films: Progress, challenges, and perspectives," *Science and Technology of Advanced Materials*, vol. 17, no. 1, pp. 493–516, Jan. 2016. DOI: 10.1080/14686996.2016.1214526.

[92] M. Costalin, I. Mjejri, N. Penin, O. Viraphong, V. Shanov, and A. Rougier, "Films of directionally oriented carbon nanotubes as counter electrodes for electrochromic devices," *Journal of Physics and Chemistry of Solids*, vol. 154, p. 110 035, Jul. 2021. DOI: 10.1016/j.jpcs.2021.110035.

[93] S. Hassab, D. E. Shen, A. M. Österholm, J. R. Reynolds, and J. Padilla, "Exploring unbalanced electrode configurations for electrochromic devices," *Journal of Materials Chemistry C*, vol. 6, no. 2, pp. 393–400, Jan. 2018, Publisher: The Royal Society of Chemistry. DOI: 10.1039/C7TC04730D.

[94] D. E. Shen, A. M. Österholm, and J. R. Reynolds, "Out of sight but not out of mind: The role of counter electrodes in polymer-based solid-state electrochromic devices," *Journal of Materials Chemistry C*, vol. 3, no. 37, pp. 9715–9725, Sep. 2015, Publisher: The Royal Society of Chemistry. DOI: 10.1039/C5TC01964H.

[95] S. Mondal, S. Roy, Y. Fujii, and M. Higuchi, "Highly Durable Electrochromic Devices for More than 100,000 Cycles with Fe(II)-Based Metallo-Supramolecular Polymer by Optimization of the Device Conditions," *ACS Applied Electronic Materials*, Dec. 2023. DOI: 10.1021/acsaelm.3c01143.

[96] A. Corradini, A. M. Marinangeli, and M. Mastragostino, "Ito as counter-electrode in a polymer based electrochromic device," *Electrochimica Acta*, vol. 35, no. 11, pp. 1757–1760, Nov. 1990. DOI: 10.1016/0013-4686(90)87076-E.

[97] S. Macher, M. Rumpel, M. Schott, U. Posset, G. A. Giffin, and P. Löbmann, "Avoiding Voltage-Induced Degradation in PET-ITO-Based Flexible Electrochromic Devices," *ACS Applied Materials & Interfaces*, vol. 12, no. 32, pp. 36 695–36 705, Aug. 2020. DOI: 10.1021/acsami.0c07860.

[98] R. Ahmad, N. O. Laschuk, I. I. Ebralidze, O. V. Zenkina, and E. B. Easton, "Probing the Influence of Counter Electrode Structure on Electrochromic-Device Operating Potentials and Performance Using Electrochemical Impedance Spectroscopy," *ChemElectroChem*, vol. 8, no. 12, pp. 2193–2204, 2021. DOI: 10.1002/celc.202100195.

[99] Y. Ding, M. Wang, Z. Mei, and X. Diao, "Different ion-based electrolytes for electrochromic devices: A review," *Solar Energy Materials and Solar Cells*, vol. 248, p. 112 037, Dec. 2022. DOI: 10.1016/j.solmat.2022.112037.

[100] Y. Ugata, K. Shigenobu, R. Tatara, K. Ueno, M. Watanabe, and K. Dokko, "Solvate electrolytes for Li and Na batteries: Structures, transport properties, and electrochemistry," en, *Physical Chemistry Chemical Physics*, vol. 23, no. 38, pp. 21 419–21 436, Oct. 2021, Publisher: The Royal Society of Chemistry, ISSN: 1463-9084. DOI: 10.1039/D1CP02946K. [Online]. Available: https://pubs.rsc.org/en/content/articlelanding/2021/cp/d1cp02946k (visited on 10/13/2023).

[101] F. Allebrod, C. Chatzichristodoulou, P. L. Mollerup, and M. B. Mogensen, "Electrical conductivity measurements of aqueous and immobilized potassium hydroxide," *International Journal of Hydrogen Energy*, Advances in Hydrogen Production (Selected papers from ICH2P-2011), vol. 37, no. 21, pp. 16 505–16 514, Nov. 2012. DOI: 10.1016/j.ijhydene.2012.02.088.

[102] H. P. Chen, J. W. Fergus, and B. Z. Jang, "The Effect of Ethylene Carbonate and Salt Concentration on the Conductivity of Propylene Carbonate | Lithium Perchlorate Electrolytes," *Journal of The Electrochemical Society*, vol. 147, no. 2, p. 399, Feb. 2000. DOI: 10.1149/1.1393209.

[103] S. Hess, M. Wohlfahrt-Mehrens, and M. Wachtler, "Flammability of Li-Ion Battery Electrolytes: Flash Point and Self-Extinguishing Time Measurements," *Journal of The Electrochemical Society*, vol. 162, no. 2, A3084, Jan. 2015. DOI: 10.1149/2.0121502jes.

[104] M. Marcinek, J. Syzdek, M. Marczewski, *et al.*, "Electrolytes for Li-ion transport – Review," *Solid State Ionics*, vol. 276, pp. 107–126, Aug. 2015. DOI: 10.1016/j.ssi.2015.02.006.

[105] C. Berthier, W. Gorecki, M. Minier, M. Armand, J. Chabagno, and P. Rigaud, "Microscopic investigation of ionic conductivity in alkali metal salts-poly(ethylene oxide) adducts," *Solid State Ionics*, vol. 11, no. 1, pp. 91–95, Sep. 1983. DOI: 10.1016/0167-2738(83)90068-1.

[106] J. Gurusiddappa, W. Madhuri, R. Padma Suvarna, and K. Priya Dasan, "Studies on the morphology and conductivity of PEO/LiClO4," *Materials Today: Proceedings*, Recent Advances In Nano Science And Technology 2015, vol. 3, no. 6, pp. 1451–1459, Jan. 2016. DOI: 10.1016/j.matpr.2016.04.028.

[107] X. Cheng, J. Pan, Y. Zhao, M. Liao, and H. Peng, "Gel Polymer Electrolytes for Electrochemical Energy Storage," *Advanced Energy Materials*, vol. 8, no. 7, p. 1 702 184, Mar. 2018. DOI: 10.1002/aenm.201702184.

[108] M. Zhu, J. Wu, Y. Wang, *et al.*, "Recent advances in gel polymer electrolyte for high-performance lithium batteries," *Journal of Energy Chemistry*, vol. 37, pp. 126–142, Oct. 2019. DOI: 10.1016/j.jechem.2018.12.013.

[109] H. Niu, L. Wang, P. Guan, *et al.*, "Recent Advances in Application of Ionic Liquids in Electrolyte of Lithium Ion Batteries," *Journal of Energy Storage*, vol. 40, p. 102 659, Aug. 2021. DOI: 10.1016/j.est.2021.102659.

[110] L. Miao, Z. Song, D. Zhu, L. Li, L. Gan, and M. Liu, "Ionic Liquids for Supercapacitive Energy Storage: A Mini-Review," *Energy & Fuels*, vol. 35, no. 10, pp. 8443–8455, May 2021. DOI: 10.1021/acs.energyfuels.1c00321.

[111] J. Zhu, Z. Zhang, S. Zhao, A. S. Westover, I. Belharouak, and P.-F. Cao, "Single-Ion Conducting Polymer Electrolytes for Solid-State Lithium–Metal Batteries: Design, Performance, and Challenges," *Advanced Energy Materials*, vol. 11, no. 14, p. 2 003 836, Apr. 2021. DOI: 10.1002/aenm.202003836.

[112] K. Deng, Q. Zeng, D. Wang, *et al.*, "Single-ion conducting gel polymer electrolytes: Design, preparation and application," *Journal of Materials Chemistry A*, vol. 8, no. 4, pp. 1557–1577, 2020. DOI: 10.1039/C9TA11178F.

[113] S. N. A. M. Johari, N. A. Tajuddin, H. Hanibah, and S. K. Deraman, "A Review: Ionic Conductivity of Solid Polymer Electrolyte Based Polyethylene Oxide," *International Journal of Electrochemical Science*, vol. 16, no. 10, p. 211 049, Oct. 2021. DOI: 10.20964/2021.10.53.

[114] K. Vignarooban, M. Dissanayake, I. Albinsson, and B.-E. Mellander, "Effect of TiO2 nano-filler and EC plasticizer on electrical and thermal properties of poly(ethylene oxide) (PEO) based solid polymer electrolytes," *Solid State Ionics*, vol. 266, pp. 25–28, Nov. 2014. DOI: 10.1016/j.ssi.2014.08.002.

[115] P. Yao, H. Yu, Z. Ding, *et al.*, "Review on Polymer-Based Composite Electrolytes for Lithium Batteries," *Frontiers in Chemistry*, vol. 7, p. 522, Aug. 2019. DOI: 10.3389/fchem.2019.00522.

[116] D. Durmus, "CIELAB color space boundaries under theoretical spectra and 99 test color samples," *Color Research & Application*, vol. 45, no. 5, pp. 796–802, Oct. 2020. DOI: 10.1002/col.22521.

[117] F. W. Billmeyer, "Quantifying color appearance visually and instrumentally," *Color Research & Application*, vol. 13, no. 3, pp. 140–145, Jun. 1988. DOI: 10.1002/col.5080130306.

[118] "ISO/CIE 23539:2023 Photometry — The CIE system of physical photometry," International Commission on Illumination (CIE), Tech. Rep. DOI: 10.25039/IS0.CIE.23539.2023.

[119] R. R. Buckley and E. J. Giorgianni, "CIELAB for Color Image Encoding (CIELAB, 8-Bit; Domain and Range, Uses)," in *Encyclopedia of Color Science and Technology*, M. R. Luo, Ed., New York, NY: Springer New York, 2016, pp. 213–221, ISBN: 978-1-4419-8070-0 978-1-4419-8071-7.

[120] S. Hassab, D. E. Shen, A. M. sterholm, *et al.*, "A new standard method to calculate electrochromic switching time," *Solar Energy Materials and Solar Cells*, vol. 185, pp. 54–60, Oct. 2018. DOI: 10.1016/j.solmat.2018.04.031.

[121] A. Agrawal, J. P. Cronin, L. L. Adams, and J. C. L. Tonazzi, "Flexible and printable electrooptic devices," US20110096388A1, Apr. 2011. [Online]. Available: https://patents.google.com/patent/US20110096388A1/en (visited on 12/02/2023).

[122] Y. Ding, M. A. Invernale, D. M. D. Mamangun, A. Kumar, and G. A. Sotzing, "A simple, low waste and versatile procedure to make polymer electrochromic devices," en, *Journal of Materials Chemistry*, vol. 21, no. 32, p. 11 873, 2011. DOI: 10.1039/c1jm11141h.

[123] M. T. Otley, F. A. Alamer, Y. Zhu, *et al.*, "Acrylated Poly(3,4-propylenedioxythiophene) for Enhancement of Lifetime and Optical Properties for Single-Layer Electrochromic Devices," *ACS Applied Materials & Interfaces*, vol. 6, no. 3, pp. 1734–1739, Feb. 2014. DOI: 10.1021/am404686w.

[124] M. T. Otley, Y. Zhu, X. Zhang, M. Li, and G. A. Sotzing, "Color-Tuning Neutrality for Flexible Electrochromics Via a Single-Layer Dual Conjugated Polymer Approach," *Advanced Materials*, vol. 26, no. 47, pp. 8004–8009, Dec. 2014. DOI: 10.1002/adma.201403370.

[125] F. A. Alamer, M. T. Otley, Y. Zhu, A. Kumar, and G. A. Sotzing, "Dependency of polyelectrolyte solvent composition on electrochromic photopic contrast," *Solar Energy Materials and Solar Cells*, vol. 132, pp. 131–135, Jan. 2015. DOI: 10.1016/j.solmat.2014.08.033.

[126] Y. Zhu, M. T. Otley, F. A. Alamer, *et al.*, "Electrochromic properties as a function of electrolyte on the performance of electrochromic devices consisting of a single-layer polymer," *Organic Electronics*, vol. 15, no. 7, pp. 1378–1386, Jul. 2014. DOI: 10.1016/j.orgel.2014.03.038.

[127] Y. Zhu, M. T. Otley, X. Zhang, *et al.*, "Polyelectrolytes exceeding ITO flexibility in electrochromic devices," *J. Mater. Chem. C*, vol. 2, no. 46, pp. 9874–9881, Oct. 2014. DOI: 10.1039/C4TC01855A.

[128] Y. Tao, K. Zhang, C. Zhang, H. Cheng, C. Jiao, and Y. Zhao, "Electrochemical synthesis of copolymers based on 2-(anthracen-9-yl)thiophene: A facile and efficient route to a series of multicolor electrochromic polymers," *Materials Science in Semiconductor Processing*, vol. 56, pp. 66–75, Dec. 2016. DOI: 10.1016/j.mssp.2016.07.019.

[129] A. Kumar, M. T. Otley, F. A. Alamar, Y. Zhu, B. G. Arden, and G. A. Sotzing, "Solid-state electrochromic devices: Relationship of contrast as a function of device preparation parameters," *J. Mater. Chem. C*, vol. 2, no. 14, pp. 2510–2516, 2014. DOI: 10.1039/C3TC32319F.

[130] J. Y. Lim, H. C. Ko, and H. Lee, "Systematic prediction of maximum electrochromic contrast of an electrochromic material," *Synthetic Metals*, vol. 155, no. 3, pp. 595–598, Dec. 2005. DOI: 10.1016/j.synthmet.2005.09.040.

[131] P. Suppakul, D. Y. Kim, J. H. Yang, S. B. Lee, and S. J. Lee, "Practical design of a diffusion-type time-temperature indicator with intrinsic low temperature dependency," *Journal of Food Engineering*, vol. 223, pp. 22–31, Apr. 2018. DOI: 10.1016/j.jfoodeng.2017.11.026.

[132] K. Sadeghi, J. Kim, and J. Seo, "Packaging 4.0: The threshold of an intelligent approach," *Comprehensive Reviews in Food Science and Food Safety*, vol. 21, no. 3, pp. 2615–2638, May 2022. DOI: 10.1111/1541-4337.12932.

[133] K. Sadeghi, J.-Y. Yoon, and J. Seo, "Chromogenic Polymers and Their Packaging Applications: A Review," *Polymer Reviews*, vol. 60, no. 3, pp. 442–492, Jul. 2020. DOI: 10.1080/15583724.2019.1676775.

[134] E. Mohammadian, M. Alizadeh-Sani, and S. M. Jafari, "Smart monitoring of gas/temperature changes within food packaging based on natural colorants," *Comprehensive Reviews in Food Science and Food Safety*, vol. 19, no. 6, pp. 2885–2931, Nov. 2020. DOI: 10.1111/1541-4337.12635.

[135] *Timestrip PLUS - Temperature Indicators by Timestrip*. [Online]. Available: https://timestrip.com/indicator-labels/temperature-indicators/timestrip-plus (visited on 12/27/2023).

[136] *SpotSee: WarmMark*. [Online]. Available: https://shop.spotsee.io/temperature_indicators/cold_chain_indicators/warmmark_warmmark (visited on 12/27/2023).

[137] *TiltWatch XTR*. [Online]. Available: https://shop.spotsee.io/TiltWatch-XTR (visited on 12/27/2023).

[138] *3BP Inc | Protective, Tamper Prooof & Damage Indicating Packaging*. [Online]. Available: https://www.3bpinc.com/ (visited on 12/27/2023).

[139] *Evigence*. [Online]. Available: https://www.evigence.com/ (visited on 12/27/2023).

[140] *SafeTag*. [Online]. Available: https://buysafetag.com/ (visited on 12/27/2023).

[141] *FreshTag*. [Online]. Available: https://www.insigniatechnologies.com/freshtag (visited on 12/27/2023).

[142] E. L. Howard, C. A. T. Laia, C. Pinheiro, and A. J. Parola, "Influence of a polymeric gel on the in situ electropolymerization of 3,4-ethylenedioxythiophene and application in irreversible electrochemical indicators," *Journal of Applied Electrochemistry*, Sep. 2023. DOI: 10.1007/s10800-023-01991-z.

[143] *TagMatiks Temperature & Humidity RFID Logger Tag*. [Online]. Available: https://rfid4ustore.com/tagmatiks-temperature-humidity-rfid-logger-tag/ (visited on 12/27/2023).

[144] *Molex Tools*. [Online]. Available: https://tools.molex.com/molex/products/family/smart-sensing-labels?parentKey=printed_circuit_products (visited on 12/27/2023).

[145] *Electronic Timestrip Complete- Temperature Indicators*. [Online]. Available: https://timestrip.com/electronic-indicators/electronic-timestrip-complete (visited on 12/27/2023).

[146] *Timestrip Neo - Irreversible Temperature Indicators*. [Online]. Available: https://timestrip.com/electronic-indicators/timestrip-neo (visited on 12/27/2023).

[147] *Tempmate.®-i1 | Temperature Indicator to monitor your goods*, Sep. 2023. [Online]. Available: https://www.tempmate.com/solutions/tempmate-i1/ (visited on 12/27/2023).

[148] *AD TT Sensor Plus 2 | Avery Dennison | RFID*. [Online]. Available: https://rfid.averydennison.com/en/home/product-finder/tt-sensor-plus-2.html (visited on 12/27/2023).

[149] *TagAlert® Indicator*. [Online]. Available: https://www.sensitech.com/en/media/T83000034_TagAlert_RevJ_tcm878-133720.pdf.

[150] J. Kawahara, P. Andersson Ersman, X. Wang, G. Gustafsson, H. Granberg, and M. Berggren, "Reconfigurable sticker label electronics manufactured from nanofibrillated cellulose-based self-adhesive organic electronic materials," *Organic Electronics*, vol. 14, no. 11, pp. 3061–3069, Nov. 2013, ISSN: 15661199. DOI: 10.1016/j.orgel.2013.07.013.

[151] M. A. Baker, A. Shrivastava, and K. S. Chatha, "Smart driver for power reduction in next generation bistable electrophoretic display technology," in *Proceedings of the 5th IEEE/ACM international conference on Hardware/software codesign and system synthesis*, Salzburg Austria: ACM, Sep. 2007, pp. 197–202. DOI: 10.1145/1289816.1289865.

[152] J. C. Jones, "The Zenithal Bistable Display: From concept to consumer," *Journal of the Society for Information Display*, vol. 16, no. 1, pp. 143–154, Jan. 2008. DOI: 10.1889/1.2835021.

[153] *CHARISMA*, en-GB. [Online]. Available: https://charisma.univie.ac.at/ (visited on 01/22/2024).

[154] Y. Tao, K. Zhang, Z. Zhang, H. Cheng, C. Jiao, and Y. Zhao, "Synthesis, characterizations and electrochromic properties of polymers based on functionalized anthracene," *Chemical Engineering Journal*, vol. 293, pp. 34–43, Jun. 2016. DOI: 10.1016/j.cej.2016.02.048.

[155] Y. Wang, "Research progress on a novel conductive polymer–poly(3,4ethylene dioxythiophene) (PEDOT)," *Journal of Physics: Conference Series*, vol. 152, p. 012 023, Mar. 2009. DOI: 10.1088/1742-6596/152/1/012023.

[156] L. Groenendaal, F. Jonas, D. Freitag, H. Pielartzik, and J. R. Reynolds, "Poly(3,4-ethylenedioxythiophene) and Its Derivatives: Past, Present, and Future," *Advanced Materials*, vol. 12, no. 7, pp. 481–494, Apr. 2000. DOI: 10.1002/(SICI)1521-4095(200004)12:7<481::AID-ADMA481>3.0.CO;2-C.

[157] R. Kiebooms, A. Aleshin, K. Hutchison, and F. Wudl, "Thermal and Electromagnetic Behavior of Doped Poly(3,4-ethylenedioxythiophene) Films," *The Journal of Physical Chemistry B*, vol. 101, no. 51, pp. 11 037–11 039, Dec. 1997. DOI: 10.1021/jp9720101.

[158] M. N. Gueye, A. Carella, J. Faure-Vincent, R. Demadrille, and J.-P. Simonato, "Progress in understanding structure and transport properties of PEDOT-based materials: A critical review," *Progress in Materials Science*, vol. 108, p. 100 616, Feb. 2020. DOI: 10.1016/j.pmatsci.2019.100616.

[159] A. C. L. Marques, C. A. P. Baptista, and J. Araujo, "Electrolyte solution, printing method thereof and resulting solid electrolyte," US20140361211A1, Dec. 2014. [Online]. Available: https://patents.google.com/patent/US20140361211A1/en (visited on 10/20/2023).

[160] S. Choi and L. J. Justice, "Water swellable rubber composition having stable swelling property at high temperatures," US20130269787A1, Oct. 2013. [Online]. Available: https://patents.google.com/patent/US20130269787A1/en (visited on 10/20/2023).

[161] T. S. Natarajan, S. Okamoto, K. W. Stöckelhuber, *et al.*, "In Situ Polymorphic Alteration of Filler Structures for Biomimetic Mechanically Adaptive Elastomer Nanocomposites," *ACS Applied Materials & Interfaces*, vol. 10, no. 18, pp. 16 148–16 159, May 2018. DOI: 10.1021/acsami.8b03680.

[162] H. Randriamahazaka, V. Noël, and C. Chevrot, "Nucleation and growth of poly(3,4-ethylenedioxythiophene) in acetonitrile on platinum under potentiostatic conditions," *Journal of Electroanalytical Chemistry*, vol. 472, no. 2, pp. 103–111, Aug. 1999. DOI: 10.1016/S0022-0728(99)00258-2.

[163] J.-P. Hsu, C.-H. Huang, and S. Tseng, "Gel electrophoresis: Importance of concentration-dependent permittivity and double-layer polarization," *Chemical Engineering Science*, vol. 84, pp. 574–579, Dec. 2012. DOI: 10.1016/j.ces.2012.08.032.

[164] L. Liu, S. Yellinek, I. Valdinger, A. Donval, and D. Mandler, "Important Implications of the Electrochemical Reduction of ITO," *Electrochimica Acta*, vol. 176, pp. 1374–1381, Sep. 2015. DOI: 10.1016/j.electacta.2015.07.129.

[165] P. M. M. C. Bressers and E. A. Meulenkamp, "The Electrochromic Behavior of Indium Tin Oxide in Propylene Carbonate Solutions," *Journal of The Electrochemical Society*, vol. 145, no. 7, p. 2225, Jul. 1998. DOI: 10.1149/1.1838624.

[166] D. Wasserberg, S. C. J. Meskers, R. A. J. Janssen, E. Mena-Osteritz, and P. Bäuerle, "High-Resolution Electronic Spectra of Ethylenedioxythiophene Oligomers," *Journal of the American Chemical Society*, vol. 128, no. 51, pp. 17 007–17 017, Dec. 2006, ISSN: 0002-7863, 1520-5126. DOI: 10.1021/ja066920k.

[167] J. J. Apperloo, L. " Groenendaal, H. Verheyen, *et al.*, "Optical and Redox Properties of a Series of 3,4-Ethylenedioxythiophene Oligomers," *Chemistry - A European Journal*, vol. 8, no. 10, p. 2384, May 2002. DOI: 10.1002/1521-3765(20020517)8:10<2384::AID-CHEM2384>3.0.CO;2-L.

[168] J. Guay, P. Kasai, A. Diaz, R. Wu, J. M. Tour, and L. H. Dao, "Chain-length dependence of electrochemical and electronic properties of neutral and oxidized soluble .alpha.,.alpha.-coupled thiophene oligomers," *Chemistry of Materials*, vol. 4, no. 5, pp. 1097–1105, Sep. 1992. DOI: 10.1021/cm00023a031.

[169] L. Laguren-Davidson, C. Van Pham, H. Zimmer, H. B. Mark, and D. J. Ondrus, "Steric Effects on the Controlled Potential Electro-Oxidation of 3-Methylthiophene and Thiophene Oligomers and the Properties of their Polymer Films," *Journal of The Electrochemical Society*, vol. 135, no. 6, pp. 1406–1414, Jun. 1988. DOI: 10.1149/1.2096007.

[170] S. S. Zade, N. Zamoshchik, and M. Bendikov, "From Short Conjugated Oligomers to Conjugated Polymers. Lessons from Studies on Long Conjugated Oligomers," *Accounts of Chemical Research*, vol. 44, no. 1, pp. 14–24, Jan. 2011. DOI: 10.1021/ar1000555.

[171] K. Meerholz and J. Heinze, "Electrochemical solution and solid-state investigations on conjugated oligomers and polymers of the -thiophene and the p-phenylene series," *Electrochimica Acta*, vol. 41, no. 11-12, pp. 1839–1854, Jul. 1996. DOI: 10.1016/0013-4686(95)00503-X.

[172] R. S. Becker, J. Seixas De Melo, A. L. Maçanita, and F. Elisei, "Comprehensive Evaluation of the Absorption, Photophysical, Energy Transfer, Structural, and Theoretical Properties of -Oligothiophenes with One to Seven Rings," *The Journal of Physical Chemistry*, vol. 100, no. 48, pp. 18 683–18 695, Jan. 1996. DOI: 10.1021/jp960852e.

[173] J. M. Tour and R. Wu, "Synthesis and UV-visible properties of soluble -thiophene oligomers. Monomer to octamer," *Macromolecules*, vol. 25, no. 7, pp. 1901–1907, Mar. 1992. DOI: 10.1021/ma00033a010.

[174] G. Zotti and G. Schiavon, "The polythiophene puzzle. Electrochemical and spectroelectrochemical evidence for two oxidation levels," *Synthetic Metals*, vol. 31, no. 3, pp. 347–357, Sep. 1989. DOI: 10.1016/0379-6779(89)90802-3.

[175] S. Jadoun and U. Riaz, "A review on the chemical and electrochemical copolymerization of conducting monomers: Recent advancements and future prospects," *Polymer-Plastics Technology and Materials*, vol. 59, no. 5, pp. 484–504, Mar. 2020. DOI: 10.1080/25740881.2019.1669647.

[176] S. Jadoun, D. S. Rathore, U. Riaz, and N. P. S. Chauhan, "Tailoring of conducting polymers via copolymerization – A review," *European Polymer Journal*, vol. 155, p. 110 561, Jul. 2021. DOI: 10.1016/j.eurpolymj.2021.110561.

[177] C. L. Gaupp and J. R. Reynolds, "Multichromic Copolymers Based on 3,6-Bis(2-(3,4-ethylenedioxythiophene))- *N* -alkylcarbazole Derivatives," *Macromolecules*, vol. 36, no. 17, pp. 6305–6315, Aug. 2003. DOI: 10.1021/ma034493e.

[178] K. Kadac, A. Nowaczyk, and J. Nowaczyk, "Synthesis and characterization of new copolymer of pyrrole and 3,4-ethylenedioxythiophene synthesized by electrochemical route," *Synthetic Metals*, vol. 206, pp. 145–153, Aug. 2015. DOI: 10.1016/j.synthmet.2015.05.021.

[179] T. Yijie, C. Haifeng, Z. Zhaoyang, X. Xiaoqian, and Z. Yongjiang, "Multielectrochromic copolymers of 3,4-ethylenedioxythiophene and naphthalene prepared via electropolymerization in boron trifluoride diethyl etherate," *Journal of Electroanalytical Chemistry*, vol. 689, pp. 142–148, Jan. 2013. DOI: 10.1016/j.jelechem.2012.10.033.

[180] C. Zhang, Y. Xu, N. Wang, *et al.*, "Electrosyntheses and characterizations of novel electrochromic copolymers based on pyrene and 3,4-ethylenedioxythiophene," *Electrochimica Acta*, vol. 55, no. 1, pp. 13–18, Dec. 2009. DOI: 10.1016/j.electacta.2009.05.046.

[181] M. H. Chua, Q. Zhu, T. Tang, K. W. Shah, and J. Xu, "Diversity of electron acceptor groups in donor–acceptor type electrochromic conjugated polymers," *Solar Energy Materials and Solar Cells*, vol. 197, pp. 32–75, Aug. 2019. DOI: 10.1016/j.solmat.2019.04.002.

[182] J. Roncali, M. Lemaire, R. Garreau, and F. Garnier, "Enhancement of the mean conjugation length in conducting polythiophenes," *Synthetic Metals*, vol. 18, no. 1-3, pp. 139–144, Feb. 1987. DOI: 10.1016/0379-6779(87)90868-X.

[183] J. Roncali, F. Garnier, M. Lemaire, and R. Garreau, "Poly mono-, bi- and trithiophene: Effect of oligomer chain length on the polymer properties," *Synthetic Metals*, vol. 15, no. 4, pp. 323–331, Sep. 1986. DOI: 10.1016/0379-6779(86)90081-0.

[184] G. Zotti and G. Schiavon, "Evolution of in situ conductivity of polythiophene deposits by potential cycling," *Synthetic Metals*, vol. 39, no. 2, pp. 183–190, Dec. 1990. DOI: 10.1016/0379-6779(90)90182-K.

[185] B. Rasch and W. Vielstich, "Polythiophenes via thiophene, bithiophene and terthiophene in propylene carbonate: An electrochemical and in-situ FTIR study," *Journal of Electroanalytical Chemistry*, vol. 370, no. 1-2, pp. 109–117, Jun. 1994. DOI: 10.1016/0022-0728(93)03158-L.

[186] A. Yildirim, S. Tarkuc, M. Ak, and L. Toppare, "Syntheses of electroactive layers based on functionalized anthracene for electrochromic applications," en, *Electrochimica Acta*, vol. 53, no. 14, pp. 4875–4882, May 2008. DOI: 10.1016/j.electacta.2008.02.026.

[187] Y.-J. Tao, Z.-Y. Zhang, X.-q. Xu, Y.-J. Zhou, H.-F. Cheng, and W.-W. Zheng, "Facile and economical synthesis of high-contrast multielectrochromic copolymers based on anthracene and 3,4-ethylenedioxythiophene via electrocopolymerization in boron trifluoride diethyl etherate," *Electrochimica Acta*, vol. 77, pp. 157–162, Aug. 2012. DOI: 10.1016/j.electacta.2012.05.087.

[188] B. Fan, L. Qu, and G. Shi, "Electrochemical polymerization of anthracene in boron trifluoride diethyl etherate," *Journal of Electroanalytical Chemistry*, vol. 575, no. 2, pp. 287–292, Feb. 2005. DOI: 10.1016/j.jelechem.2004.10.002.

[189] M. Zhang, W. Zhou, B. Zhuang, Z. Zheng, Q. Zhang, and H. Wang, "Theoretical investigation of electrochromic mechanism in D–A conjugated polymers in visible and infrared bands," *RSC Advances*, vol. 13, no. 17, pp. 11 337–11 345, 2023, Publisher: Royal Society of Chemistry. DOI: 10.1039/D3RA01600E.

[190] J. Zhao, X. Cheng, Y. Fu, and C. Cui, "Electrosynthesis and Characterization of an Electrochromic Material from Poly(1,6-Bis(2-(3,4-Ethylenedioxy)Thienyl)Pyrene) and Its Application in Electrochromic Device," *International Journal of Electrochemical Science*, vol. 8, no. 1, pp. 1002–1015, Jan. 2013. DOI: 10.1016/S1452-3981(23)14075-2.

[191] G. Zotti and G. Schiavon, "The nature of conducting materials by anodic coupling of pyrene," *Synthetic Metals*, vol. 47, no. 2, pp. 193–202, May 1992. DOI: 10.1016/0379-6779(92)90387-X.

[192] D. Leinberger, *Temperature & Humidity in Ocean Containers, Technical Report*. [Online]. Available: https://www.yumpu.com/en/document/read/10676010/temperature-humidity-in-ocean-containers (visited on 10/19/2023).

[193] *Container climate*. [Online]. Available: https://www.tis-gdv.de/tis_e/containe/klima/klima-htm/ (visited on 10/19/2023).

[194] C. Kvarnström, R. Bilger, A. Ivaska, and J. Heinze, "An electrochemical quartz crystal microbalance study on polymerization of oligo-p-phenylenes," *Electrochimica Acta*, vol. 43, no. 3-4, pp. 355–366, Jan. 1998. DOI: 10.1016/S0013-4686(97)00069-8.

[195] G. Sabouraud, S. Sadki, and N. Brodie, "The mechanisms of pyrrole electropolymerization," *Chemical Society Reviews*, vol. 29, no. 5, pp. 283–293, 2000. DOI: 10.1039/a807124a.

[196] S.-C. Luo, J. Sekine, B. Zhu, H. Zhao, A. Nakao, and H.-H. Yu, "Polydioxythiophene Nanodots, Nonowires, Nano-Networks, and Tubular Structures: The Effect of Functional Groups and Temperature in Template-Free Electropolymerization," *ACS Nano*, vol. 6, no. 4, pp. 3018–3026, Apr. 2012. DOI: 10.1021/nn300737e.

[197] Y. Seki, M. Takahashi, and M. Takashiri, "Enhanced thermoelectric properties of electropolymerized poly (3,4-ethylenedioxythiophene) thin films by optimizing electrolyte temperature and thermal annealing temperature," *Organic Electronics*, vol. 55, pp. 112–116, Apr. 2018. DOI: 10.1016/j.orgel.2018.01.028.

[198] J. Remmele, D. E. Shen, T. Mustonen, and N. Fruehauf, "High Performance and Long-Term Stability in Ambiently Fabricated Segmented Solid-State Polymer Electrochromic Displays," *ACS Applied Materials & Interfaces*, vol. 7, no. 22, pp. 12 001–12 008, Jun. 2015. DOI: 10.1021/acsami.5b02090.

[199] J. Roncali, P. Blanchard, and P. Frère, "3,4-Ethylenedioxythiophene (EDOT) as a versatile building block for advanced functional -conjugated systems," *J. Mater. Chem.*, vol. 15, no. 16, pp. 1589–1610, 2005. DOI: 10.1039/B415481A.

[200] K. I. Ritzau-Reid, C. D. Spicer, A. Gelmi, *et al.*, "An Electroactive Oligo-EDOT Platform for Neural Tissue Engineering," *Advanced Functional Materials*, vol. 30, no. 42, p. 2 003 710, Oct. 2020. DOI: 10.1002/adfm.202003710.

[201] G. A. Sotzing, J. R. Reynolds, and P. J. Steel, "Poly(3,4-ethylene dioxythiophene) (PEDOT) prepared via electrochemical polymerization of EDOT, 2,2-Bis(3,4-ethylene dioxythiophene) (BiEDOT), and their TMS derivatives," *Advanced Materials*, vol. 9, no. 10, pp. 795–798, Jan. 1997. DOI: 10.1002/adma.19970091005.

[202] V. Ambrogi, C. Carfagna, P. Cerruti, and V. Marturano, "Additives in Polymers," in *Modification of Polymer Properties*, Elsevier, 2017, pp. 87–108, ISBN: 978-0-323-44353-1.

[203] B. Pelzl, R. Wolf, and B. L. Kaul, "Plastics, Additives," in *Ullmann's Encyclopedia of Industrial Chemistry*, Weinheim, Germany: Wiley-VCH Verlag GmbH & Co. KGaA, Jul. 2018, pp. 1–57, ISBN: 978-3-527-30673-2.

[204] S. Al-Malaika, "Antioxidants: An Overview," in *Plastics Additives*, D. Brewis, D. Briggs, and G. Pritchard, Eds., vol. 1, Dordrecht: Springer Netherlands, 1998, pp. 55–72, ISBN: 978-94-010-6477-4 978-94-011-5862-6.

[205] R. Gensler, C. Plummer, H.-H. Kausch, E. Kramer, J.-R. Pauquet, and H. Zweifel, "Thermo-oxidative degradation of isotactic polypropylene at high temperatures: Phenolic antioxidants versus HAS," *Polymer Degradation and Stability*, vol. 67, no. 2, pp. 195–208, Feb. 2000. DOI: 10.1016/S0141-3910(99)00113-5.

[206] C. J. Emmott, D. Moia, P. Sandwell, *et al.*, "In-situ, long-term operational stability of organic photovoltaics for off-grid applications in Africa," *Solar Energy Materials and Solar Cells*, vol. 149, pp. 284–293, May 2016. DOI: 10.1016/j.solmat.2016.01.036.

[207] Y. Kim, H. Kim, S. Graham, A. Dyer, and J. R. Reynolds, "Durable polyisobutylene edge sealants for organic electronics and electrochemical devices," *Solar Energy Materials and Solar Cells*, vol. 100, pp. 120–125, May 2012. DOI: 10.1016/j.solmat.2011.12.012.

[208] S. Mercier, S. Villeneuve, M. Mondor, and I. Uysal, "Time–Temperature Management Along the Food Cold Chain: A Review of Recent Developments," *Comprehensive Reviews in Food Science and Food Safety*, vol. 16, no. 4, pp. 647–667, Jul. 2017. DOI: 10.1111/1541-4337.12269.

[209] S. Chen, S. Brahma, J. Mackay, C. Cao, and B. Aliakbarian, "The role of smart packaging system in food supply chain," *Journal of Food Science*, vol. 85, no. 3, pp. 517–525, Mar. 2020. DOI: 10.1111/1750-3841.15046.

[210] C. Sykes, "Time- and Temperature-Controlled Transport: Supply Chain Challenges and Solutions," *P & T: A Peer-Reviewed Journal for Formulary Management*, vol. 43, no. 3, pp. 154–170, Mar. 2018, ISSN: 1052-1372.

[211] B. B. Maskey, J. Lee, Y. Majima, *et al.*, "A Smart Food Label Utilizing Roll-to-Roll Gravure Printed NFC Antenna and Thermistor to Replace Existing "Use-By" Date System," *IEEE Sensors Journal*, vol. 20, no. 4, pp. 2106–2116, Feb. 2020. DOI: 10.1109/JSEN.2019.2948752.

[212] M. Bhattacharjee, P. Escobedo, F. Nikbakhtnasrabadi, and R. Dahiya, "Printed Flexible Temperature Sensor with NFC Interface," in *2020 IEEE International Conference on Flexible and Printable Sensors and Systems (FLEPS)*, Manchester, United Kingdom: IEEE, Aug. 2020, pp. 1–4. DOI: 10.1109/FLEPS49123.2020.9239503.

[213] A. V. Quintero, F. Molina-Lopez, E. C. P. Smits, *et al.*, "Smart RFID label with a printed multisensor platform for environmental monitoring," *Flexible and Printed Electronics*, vol. 1, no. 2, p. 025 003, Jun. 2016. DOI: 10.1088/2058-8585/1/2/025003.

[214] *Thinfilm Builds First Stand-Alone Sensor System in Printed Electronics*, Oct. 2013. [Online]. Available: https://www.businesswire.com/news/home/20131016005473/en/Thinfilm-Builds-First-Stand-Alone-Sensor-System-in-Printed-Electronics (visited on 12/28/2023).

[215] A. G. Olabi, Q. Abbas, A. Al Makky, and M. A. Abdelkareem, "Supercapacitors as next generation energy storage devices: Properties and applications," *Energy*, vol. 248, p. 123 617, Jun. 2022. DOI: 10.1016/j.energy.2022.123617.

[216] B. Du, X. Wang, L. Chai, *et al.*, "Fabricating lignin-based carbon nanofibers as versatile supercapacitors from food wastes," *International Journal of Biological Macromolecules*, vol. 194, pp. 632–643, Jan. 2022. DOI: 10.1016/j.ijbiomac.2021.11.107.

[217] X. Chang, M. F. El-Kady, A. Huang, *et al.*, "3D Graphene Network with Covalently Grafted Aniline Tetramer for Ultralong-Life Supercapacitors," *Advanced Functional Materials*, vol. 31, no. 32, p. 2 102 397, Aug. 2021. DOI: 10.1002/adfm.202102397.

[218] S. Satpathy, S. Das, and B. K. Bhattacharyya, "How and where to use supercapacitors effectively, an integration of review of past and new characterization works on super-capacitors," *Journal of Energy Storage*, vol. 27, p. 101 044, Feb. 2020. DOI: 10.1016/j.est.2019.101044.

[219] M. Cakici, R. R. Kakarla, and F. Alonso-Marroquin, "Advanced electrochemical energy storage supercapacitors based on the flexible carbon fiber fabric-coated with uniform coral-like MnO 2 structured electrodes," *Chemical Engineering Journal*, vol. 309, pp. 151–158, Feb. 2017. DOI: 10.1016/j.cej.2016.10.012.

[220] H. Dai, G. Zhang, D. Rawach, *et al.*, "Polymer gel electrolytes for flexible supercapacitors: Recent progress, challenges, and perspectives," *Energy Storage Materials*, vol. 34, pp. 320–355, Jan. 2021. DOI: 10.1016/j.ensm.2020.09.018. (visited on 12/16/2023).

[221] S. Ghosh, S. Yadav, A. Devi, and T. Thomas, "Techno-economic understanding of Indian energy-storage market: A perspective on green materials-based supercapacitor technologies," *Renewable and Sustainable Energy Reviews*, vol. 161, p. 112 412, Jun. 2022. DOI: 10.1016/j.rser.2022.112412.

[222] A. Riaz, M. R. Sarker, M. H. M. Saad, and R. Mohamed, "Review on Comparison of Different Energy Storage Technologies Used in Micro-Energy Harvesting, WSNs, Low-Cost Microelectronic Devices: Challenges and Recommendations," *Sensors*, vol. 21, no. 15, p. 5041, Jul. 2021. DOI: 10.3390/s21155041.

[223] S. Tuukkanen, M. Välimäki, S. Lehtimäki, T. Vuorinen, and D. Lupo, "Behaviour of one-step spray-coated carbon nanotube supercapacitor in ambient light harvester circuit with printed organic solar cell and electrochromic display," *Scientific Reports*, vol. 6, no. 1, p. 22 967, Mar. 2016. DOI: 10.1038/srep22967.

[224] Z. Zhang and B. Cao, "Thermal smart materials with tunable thermal conductivity: Mechanisms, materials, and applications," *Science China Physics, Mechanics & Astronomy*, vol. 65, no. 11, p. 117 003, Nov. 2022. DOI: 10.1007/s11433-022-1925-2.

[225] R. Zheng, J. Gao, J. Wang, and G. Chen, "Reversible temperature regulation of electrical and thermal conductivity using liquid–solid phase transitions," *Nature Communications*, vol. 2, no. 1, p. 289, Apr. 2011. DOI: 10.1038/ncomms1288.

[226] S. A. Angayarkanni and J. Philip, "Thermal conductivity measurements in phase change materials under freezing in presence of nanoinclusions," *Journal of Applied Physics*, vol. 118, no. 9, p. 094 306, Sep. 2015. DOI: 10.1063/1.4929971.

[227] Y. Wang, B. Tang, and S. Zhang, "Single-Walled Carbon Nanotube/Phase Change Material Composites: Sunlight-Driven, Reversible, Form-Stable Phase Transitions for Solar Thermal Energy Storage," *Advanced Functional Materials*, vol. 23, no. 35, pp. 4354–4360, Sep. 2013. DOI: 10.1002/adfm.201203728.

[228] Y. Wu, P. Meng, Q. Zhang, Z. Tan, G. Cheng, and X. Wu, "Room-Temperature Switching Behavior in CNT/Hexadecane Composites," *MRS Advances*, vol. 3, no. 54, pp. 3213–3220, Nov. 2018. DOI: 10.1557/adv.2018.531.

[229] P. C. Sun, Y. L. Wu, J. W. Gao, G. A. Cheng, G. Chen, and R. T. Zheng, "Room Temperature Electrical and Thermal Switching CNT/Hexadecane Composites," *Advanced Materials*, vol. 25, no. 35, pp. 4938–4943, Sep. 2013. DOI: 10.1002/adma.201302165.

[230] R. J. Warzoha and A. S. Fleischer, "Effect of carbon nanotube interfacial geometry on thermal transport in solid–liquid phase change materials," *Applied Energy*, vol. 154, pp. 271–276, Sep. 2015. DOI: 10.1016/j.apenergy.2015.04.121.

[231] S. K. Behera, P. Marrec, A. J. D. Parola, *et al.*, "Functionalized multiwalled carbon nanotube-alkane based resistive thermal sensor for cold chain applications," submitted for publication.

[232] M. Arvani, J. Keskinen, D. Lupo, and M. Honkanen, "Current collectors for low resistance aqueous flexible printed supercapacitors," *Journal of Energy Storage*, vol. 29, p. 101 384, Jun. 2020. DOI: 10.1016/j.est.2020.101384.

[233] J. Keskinen, S. Lehtimäki, A. Dastpak, *et al.*, "Architectural modifications for flexible supercapacitor performance optimization," *Electronic Materials Letters*, vol. 12, no. 6, pp. 795–803, Nov. 2016. DOI: 10.1007/s13391-016-6141-y.

[234] H. Pourkheirollah, J. Keskinen, M. Mäntysalo, and D. Lupo, "An improved exponential model for charge and discharge behavior of printed supercapacitor modules under varying load conditions," *Journal of Power Sources*, vol. 535, p. 231 475, Jul. 2022. DOI: 10.1016/j.jpowsour.2022.231475.

[235] A. Railanmaa, A. Soltani, S. Lehtimäki, *et al.*, "Skin-conformable printed supercapacitors and their performance in wear," *Scientific Reports*, vol. 10, no. 1, p. 15 194, Sep. 2020. DOI: 10.1038/s41598-020-72244-8.

[236] Fabio A S Leite, P. Wierzchowiec, C. Pinheiro, L. Maggini, and D. Bonifazi, "Hybrid Screen-Printable Electrolyte for Large-scale Flexible Electrochromic Display Production," Submitted for Publication.

[237] C. L. Gaupp, D. M. Welsh, R. D. Rauh, and J. R. Reynolds, "Composite Coloration Efficiency Measurements of Electrochromic Polymers Based on 3,4-Alkylenedioxy thiophenes," *Chemistry of Materials*, vol. 14, no. 9, pp. 3964–3970, Sep. 2002. DOI: 10.1021/cm020433w.

[238] E. Poverenov, M. Li, A. Bitler, and M. Bendikov, "Major Effect of Electropolymerization Solvent on Morphology and Electrochromic Properties of PEDOT Films," *Chemistry of Materials*, vol. 22, no. 13, pp. 4019–4025, Jul. 2010. DOI: 10.1021/cm100561d.

A

Appendix - Chapter 2

(a)

(b)

Figure A.1: Digital images of (a) non color corrected, and (b) color corrected irreversible electrochemical indicator with a color checker.

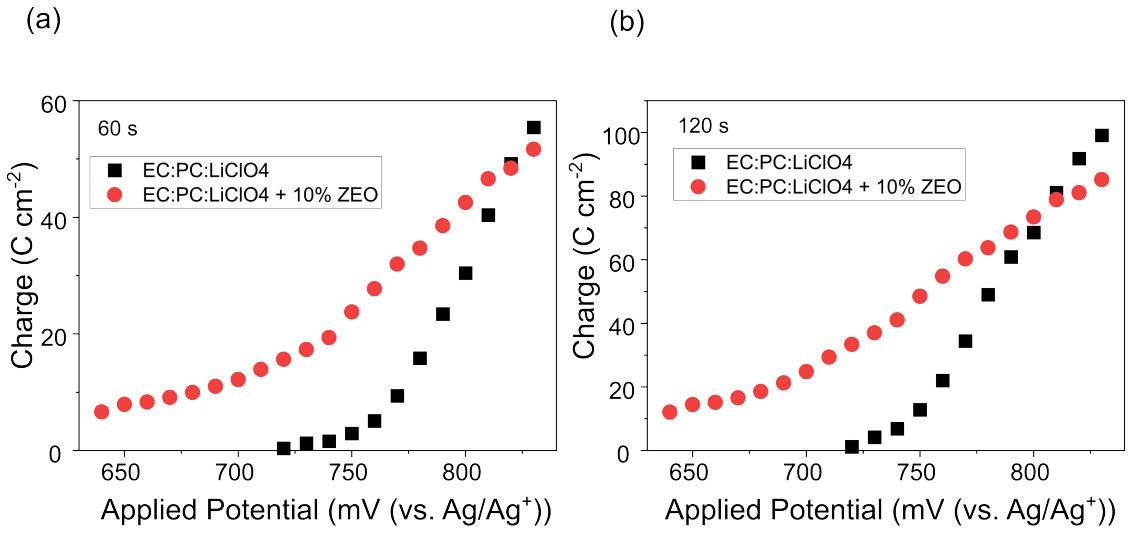

Figure A.2: T(j_{max}) vs. applied potential at (a) 60 s, and (b) 120 s for electropolymerization of 25 mM EDOT in liquid and gel electrolytes.

B

Appendix - Chapter 4

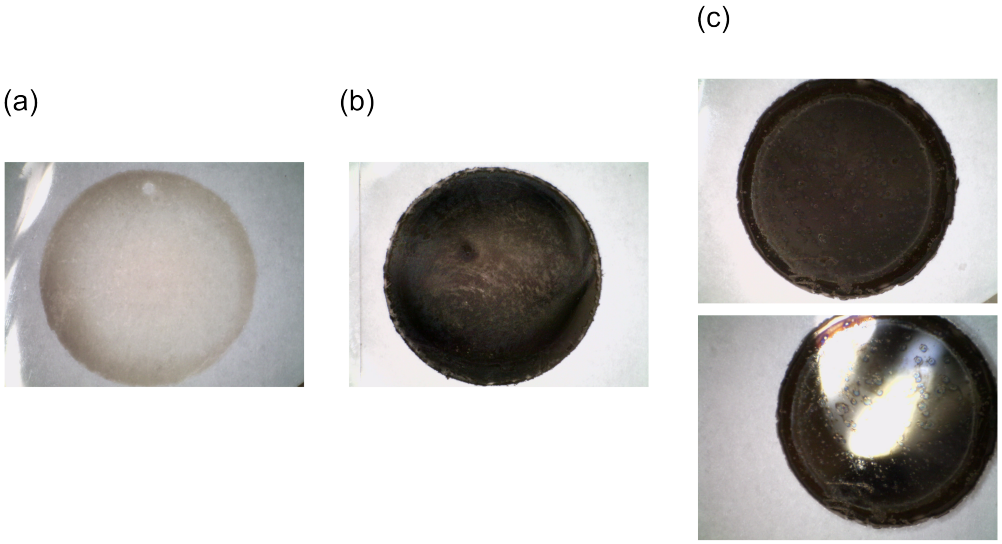

Figure B.1: Digital images of counter electrode from 25 mM EDOT devices activated at (a) -20 ºC, (b) 20 ºC, and (c) 50 ºC.

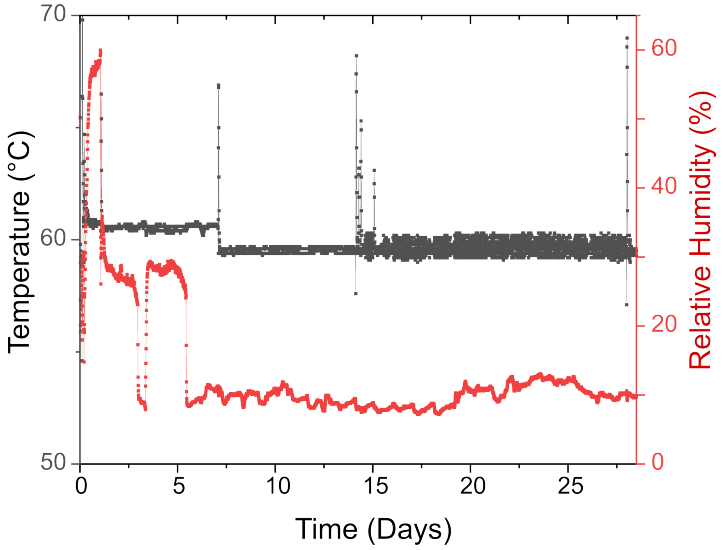

Figure B.2: Temperature and humidity of oven during the first 28 days of the long-term stability testing.

C

Appendix - Chapter 6

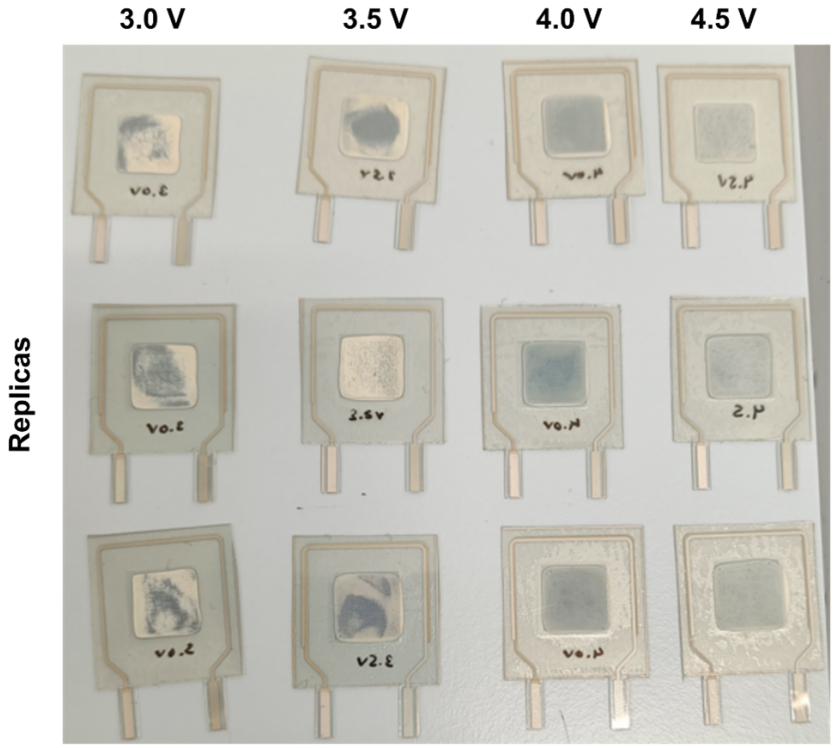

Figure C.1: Images of the counter electrode. of indicators activated at 3.0 V with 6 mC on the working electrode, and then 6 mC on the counter electrode at the specified voltage. The smoothest counter electrode films are observed when - 4.0 V is used.

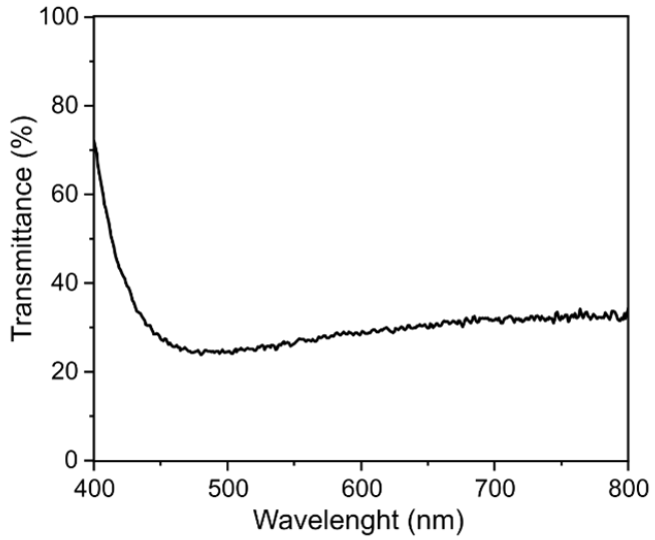

Figure C.2: QSPEv2 electrolyte transmittance spectra. The electrolyte is not 100 % reflective with 20 – 30 % of the light in the 450 – 800 nm range passing through the electrolyte film. Below 450 nm, the amount of light passing through increases.

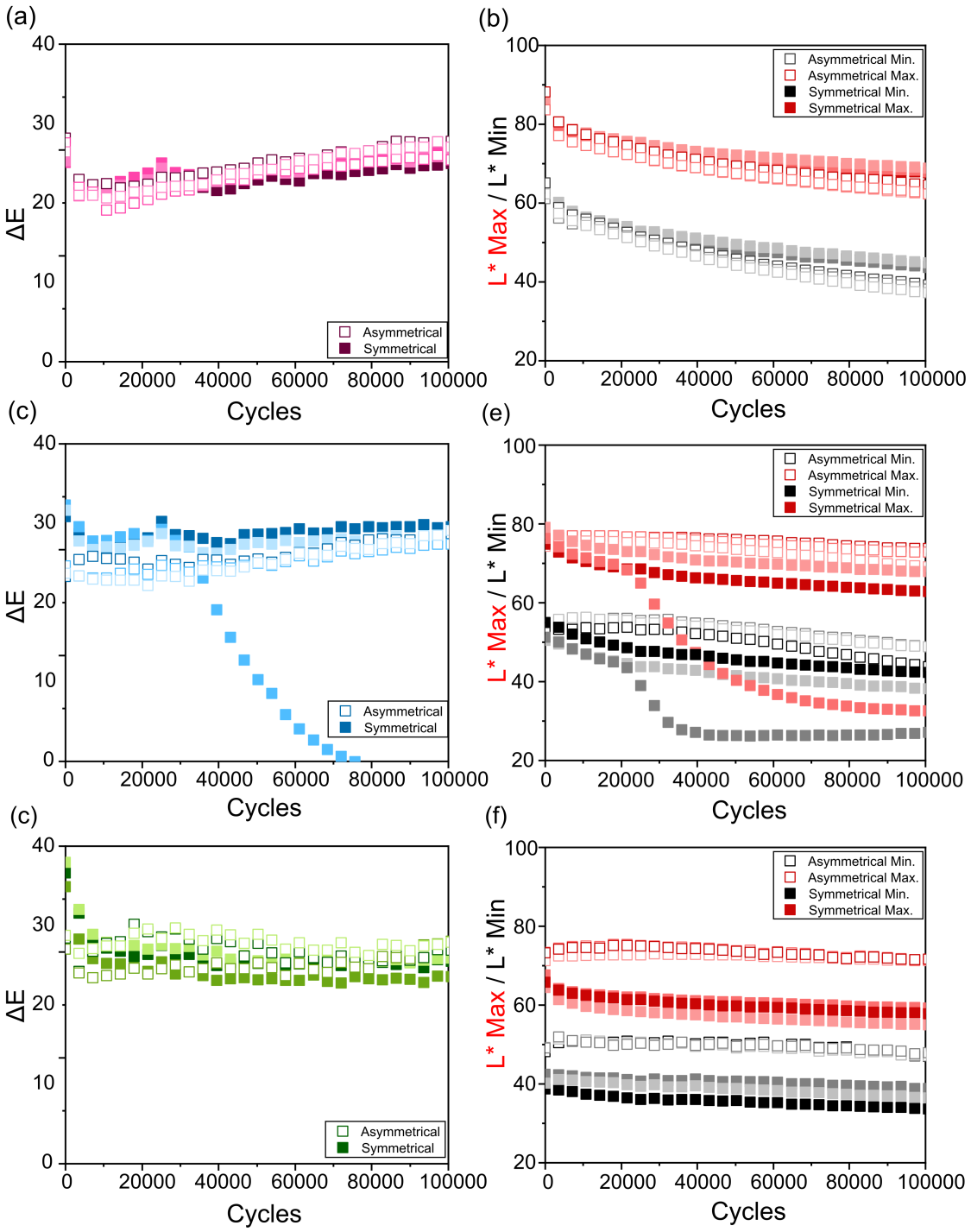

Figure C.3: ΔE for triplicates of asymmetrical and symmetrical indicators activated with (a) 2 mC, (b) 4 mC, and (c) 6 mC over 100 k cycles of ± 1.5 V applied in 1 s pulses. Minimum and maximum L values for the same triplicates of asymmetrical and symmetrical indicators activated with (d) 2 mC, (e) 4 mC, and (f) 6 mC over 100 k cycles of ± 1.5 V applied in 1 s pulses.